HYDROLOGIC PROCESSES ON STEEP HILLSLOPES ACROSS DIFFERENT SCALES: FROM SOIL WATER DYNAMICS TO SPRING WATER CHEMISTRY

Zur Erlangung des akademischen Grades eines

DOKTORS DER NATURWISSENSCHAFTEN (Dr. rer. nat.)

von der KIT-Fakultät für

Bauingenieur-, Geo- und Umweltwissenschaften

des Karlsruher Instituts für Technologie (KIT)

genehmigte

DISSERTATION

von

M.Sc. Markus Merk

aus Mosbach

Tag der mündlichen Prüfung: 16.12.2020

Referent: Prof. Dr. Nico Goldscheider

Korreferent: Prof. Dr. Lucas Menzel

Karlsruhe 2021

We shall, in fact, outlast the stars.

—John Lennox

ABSTRACT

The focus of this work is on near surface flow processes in the unsaturated zone and soil water dynamics on steep hillslopes. It looks at these processes and dynamics across different scales. From the smaller scale of soil water monitoring in lysimeters to the larger scale of a mountainous catchment, where spring water chemistry is studied.

The first study deals with soil moisture dynamics in the unsaturated zone. It is based on depth-resolved soil moisture measurements from a large inclined lysimeter in the top cover of a municipal landfill near Karlsruhe, Germany. Availability of long-term and high-resolution measurements of soil moisture is crucial when it comes to understanding all sorts of changes to past soil moisture variations and the prediction of future dynamics. Aggregated monthly data from two large lysimeters covering a timespan of over 25 years were analyzed. Soil moisture measurements showed a clear seasonal pattern. Lowest values were measured at the end of the vegetation period after a gradual drying out of the soil during spring and summer. Highest values were measured after the vegetation period, following a sharp increase in soil moisture during the winter months. The seasonal response of soil moisture to external influences driving the seasonal dynamics are delayed with depth. A significant decrease in soil moisture levels over the past two decades was observed. This decrease is most pronounced at the start and the end of the vegetation period. Bayesian change point detection revealed, that this decrease is not uniformly distributed over the complete observation period. Largest changes occur at tipping points during years of extreme drought, after which soil moisture levels reach significantly different alternate stable states. These changes affect not only the overall trend in soil moisture, but also the seasonal dynamics. The study highlights the importance of soil moisture measurements for the understanding of moisture fluxes in the vadose zone.

The second study is focused towards spring water chemistry in the Black Forest National Park. Spring water chemistry is influenced by many factors, including geology, climate, vegetation and land use, which determine groundwater residence times and water--rock interaction. We collected water samples at 20 locations during 5 campaigns within the water catchment area of the upper Schönmünz river in the Black Forest National Park, Southwest Germany. Water samples were analyzed hydro-chemically for their contents of inorganic constituents, organic carbon content, fluorescence properties as well as several physico-chemical field parameters. Spring discharge was measured using the salt dilution method and volumetric measurements. Results show, that water chemistry is strongly dependent on geology.

The mineralization of spring waters in the catchment area is generally very low, due to a lack of soluble minerals in the host rocks of the fractured aquifer. Host rocks consist mainly of sandstones, konglomerates and granites. Low mineralization in combination with high contents of dissolved organic carbon lead to low pH. A contribution of dissolved organic carbon to the specific electrical conductivity was observed. Water is only weakly buffered by the ion exchange and silica buffer systems. The aluminum buffer system is also considered to be contributing to the buffer capacity in water with particularly low pH.

In the catchment area, the waters from the sandstone aquifers, the crystalline, and the surface stream can be clearly divided into four groups. Grouping is based on hydro-chemistry and geology. These groups can be clearly distinguished based on Ca^{2+} concentration and oxygen saturation, but other parameters also show clear differences. The response of dissolved organic carbon to changes in hydraulic conditions is highly dynamic. Due to increased flow through the upper soil layer during and after rain events, more organic carbon is extracted from the soil and transported with the water. Measurements of fluorescence excitation-emission matrices indicate an allochthonous source of this organic carbon.

The associated water chemistry data poses a baseline for the springs in the water catchment area. It is a supplement to the ongoing investigations into the flora and fauna in the vicinity of the springs, which will aid the creation of effective protection policies and long term preservation of these valuable ecosystems.

The selection of monitoring points for a paired catchment study comparing the Schönmünz and the Langenbach valleys is presented, along with the initial setup and the measurement probes that are used at each point.

ZUSAMMENFASSUNG

Der Forschungsschwerpunkt dieser Arbeit liegt auf oberflächennahen Abflussprozessen in der ungesättigten Bodenzone und der Bodenwasserdynamik an steilen Hängen. Die Arbeit betrachtet diese Prozesse und Dynamiken auf unterschiedlichen Skalen. Kleinskalig anhand von Bodenfeuchtemessungen in Lysimetern, größer-skalig anhand eines bewaldeten Wassereinzugsgebietes mit steilen Hängen, in dem die Hydrochemie von Quellwasser untersucht wurde.

Die erste Studie befasst sich mit der Bodenfeuchtedynamik in der ungesättigten Bodenzone. Sie basiert auf tiefenaufgelösten Bodenfeuchtemessungen an einem großen geneigten Lysimeter in der Oberflächenabdichtung einer Hausmülldeponie in der Nähe von Karlsruhe, Deutschland. Die Verfügbarkeit von zeitlich hochaufgelösten Langzeitmessungen der Bodenfeuchte ist entscheidend, wenn es darum geht, vergangene Änderungen der Bodenfeuchtedynamik zu verstehen und die zukünftige Entwicklung dieser Dynamik vorherzusagen. Analysiert wurden die zu Monatsdaten aggregierten Messwerte der Bodenfeuchte an zwei Großlysimetern. Die Messungen decken einen Zeitraum von über 25 Jahren ab. Der Verlauf der Bodenfeuchte weist einen klaren Jahresgang auf. Die niedrigsten Werte wurden am Ende der Vegetationsperiode nach einer graduellen Austrocknung des Bodens im Frühling und Sommer gemessen. Die höchsten Werte wurden jeweils nach der Vegetationsperiode in Folge eines raschen Anstiegs der Bodenfeuchte während der Wintermonate gemessen. Die Reaktion der Bodenfeuchte auf die je nach Jahreszeit verschiedenen äußeren Einflüsse setzt sich über die Zeit mit der Tiefe fort. In den letzten zwei Jahrzehnten wurde ein signifikanter Rückgang der Bodenfeuchte beobachtet. Dieser Rückgang ist zu Beginn und am Ende der Vegetationsperiode am stärksten ausgeprägt. Eine Bayes'sche Modellierung ergab, dass dieser Rückgang nicht gleichmäßig über den gesamten Beobachtungszeitraum verteilt ist, sondern Wendepunkte aufweist. Größte Veränderungen treten demnach an diesen Wendepunkten während Jahren extremer Trockenheit auf. Danach befindet sich die Bodenfeuchte auf einem signifikant unterschiedlichen aber dennoch stabilen Niveau. Die Veränderungen beeinflussen nicht nur den übergeordneten Trend der Bodenfeuchte, sondern auch die saisonale Dynamik. Die Studie unterstreicht die Bedeutung von Bodenfeuchtemessungen für das Verständnis der Bodenwasserdynamik in der ungesättigten Bodenzone.

Die zweite Studie befasst sich mit der Quellwasserchemie im Nationalpark Schwarzwald. Die Chemie des Quellwassers wird von vielen Faktoren beeinflusst, darunter Geologie, Klima, Vegetation und Landnutzung, welche die Verweilzeiten des Grundwassers und

die Wasser-Gesteins-Wechselwirkung bestimmen. Wasserproben wurden an 20 Standorten bei 5 Probenahme-Kampagnen im Wassereinzugsgebiet der oberen Schönmünz im Nationalpark Schwarzwald, Südwestdeutschland, genommen. Die Wasserproben wurden hydrochemisch auf ihre Gehalte an gelösten anorganischen Bestandteilen, gelöstem organischem Kohlenstoffgehalt, Fluoreszenzeigenschaften sowie verschiedene physikalisch-chemische Feldparameter untersucht. Die Quellschüttung wurde mit der Salzverdünnungsmethode und volumetrischen Messungen bestimmt. Die Ergebnisse zeigen, dass die Wasserchemie stark von der Geologie abhängig ist. Die Mineralisierung der Quellwässer im Einzugsgebiet ist im Allgemeinen sehr gering, was auf einen Mangel an löslichen Mineralien in den Wirtsgesteinen des geklüfteten Aquifers zurückzuführen ist. Das Wirtsgestein besteht hauptsächlich aus Sandsteinen, Konglomeraten und Graniten. Eine geringe Mineralisierung in Kombination mit hohen Gehalten an gelöstem organischen Kohlenstoff führt zu einem niedrigen pH-Wert. Es wurde ein Beitrag des gelösten organischen Kohlenstoffs zur spezifischen elektrischen Leitfähigkeit beobachtet. Wasser wird durch die Ionenaustausch- und Silika-Puffersysteme nur schwach gepuffert. in Wasser mit besonders niedrigem pH-Wert leistet das Aluminium-Puffersystem auch einen Beitrag zur Pufferkapazität.

Die Gewässer aus dem Sandstein-Aquifer, dem kristallinen Grundgebirge und dem oberflächlich abfließenden Bach lassen sich im Einzugsgebiet klar in vier Gruppen einteilen. Die Gruppierung basiert auf der Hydrochemie und Geologie. Sie lassen sich anhand der Ca^{2+}-Konzentration und der Sauerstoffsättigung klar unterscheiden, aber auch andere Parameter zeigen deutliche Unterschiede. Die Reaktion des gelösten organischen Kohlenstoffs auf Änderungen der hydraulischen Bedingungen geschieht sehr schnell. Aufgrund des erhöhten Durchflusses durch die oberste Bodenschicht während und nach Regenereignissen wird dem Boden mehr organischer Kohlenstoff entzogen und mit dem Wasser abtransportiert. Messungen von Fluoreszenz-Excitations-Emissions-Matrizen weisen auf eine allochthone Quelle dieses organischen Kohlenstoffs hin.

Die zugehörigen wasserchemischen Daten geben den gegenwärtigen Ist-Zustand für die Quellen im Wassereinzugsgebiet wieder. Sie sind eine wichtige Ergänzung zu den laufenden Untersuchungen der Flora und Fauna im unmittelbaren Umfeld der Quellen. Diese Untersuchungen sind unerlässlich bei der Erlassung wirksamer Schutzmaßnahmen und zur langfristigen Erhaltung dieser wertvollen Ökosysteme.

Die Auswahl der Messstellen für eine sogenannte Paired-Catchment-Studie, die das Schönmünz- und das Langenbachtal miteinander vergleicht, wird ebenso vorgestellt wie die Installation und Inbetriebnahme der Messsonden, die an der jeweiligen Stelle eingesetzt werden.

CONTENTS

LIST OF TABLES

INTRODUCTION

*All streams flow into the sea, yet the sea is never full. To
the place the streams come from, there they return again.*

Ecclesiastes 1:7

The existence of the global water cycle has been observed for millennia
and studied for many centuries. It is taught in schools and most
people have at least a general understanding of how it works. Water
evaporates over the oceans, is transported as clouds, falls back down
to the earth's surface in the form of rain and snow, and is transported
back to the oceans in rivers, streams and through groundwater flow.
Once back in the ocean, the cycle begins anew.

Studying the specific intricacies of this global water cycle on much
smaller scales opens up a vast amount of research areas. Numerous
interactions and feedback mechanisms of regional and local water
cycles and the temporal changes and seasonal variations make it
difficult to gain a comprehensive understanding. Among others,
"the hydrological cycle and changing precipitation (rain and snow)
patterns" are assessed by The Intergovernmental Panel on Climate
Change (IPCC), trying to untangle these "into a complete picture of the
climate systems and how it is changing" IPCC (2020). The engagement
of an international body like the IPCC in these areas highlights the
fact, that there is still a lack of a comprehensive understanding of the
water cycle as a whole and its imminent changes.

The study of the dynamics of near surface flow processes on steep
hillslopes, hydrochemistry of springs, and deep desiccation of soils
are only some of these many scientific disciplines. They touch on
hillslope processes, flow processes in the saturated and unsaturated
zones, runoff formation and spring processes. A short theoretical
background and outline of these disciplines is presented below.

1.1 THEORETICAL BACKGROUND ON HILLSLOPE PROCESSES

Many scientific disciplines are contributing to the wide field of re-
search on hillslope processes. These disciplines focus on different
aspects, including but not limited to: geotechnical aspects like stability
of hillslopes and the occurrence of landslides, geomorphologic aspects
like the development and transformation of hillslopes at different
spatial and temporal scales by erosion and denudation, hydrologic
aspects like runoff production and stormflow generation, geochemical
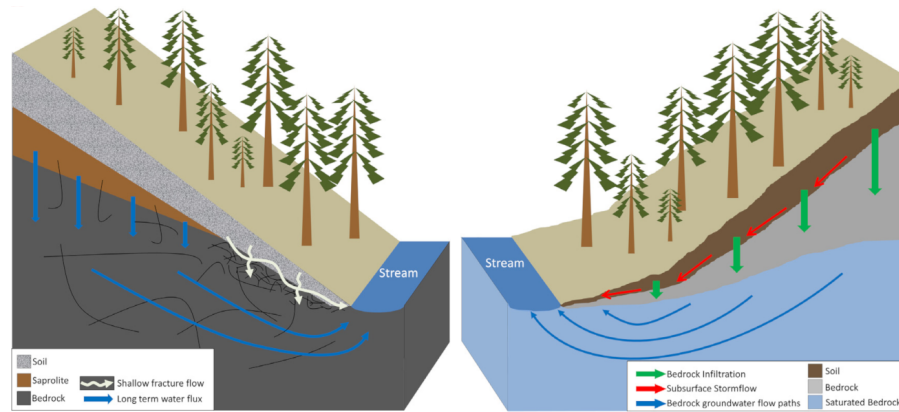
Figure 1.1: Perceptual models of water flow through hillslopes as presented by Gabrielli et al. (2012). In the left model, the majority of the water seeps into the highly fractured bedrock and re-emerges at the stream. In the right model, water moves through shallow fracture pathways, resulting in lateral subsurface stormflow. A proportion of the water flows through longer and more tortuous flow paths in the deeper less fractured bedrock before re-emerging at the stream.

aspects concerning weathering of base rock and formation of soils, hydrogeologic aspects like water movement in the saturated and unsaturated zones in hillslopes, hydrogeochemical aspects concerning solute transport and temporal changes in water chemistry, biological aspects like vegetation and nutrient cycling and many more.

Interdisciplinary approaches discern feedback mechanisms between these disciplines. These include for example surface-water/groundwater interactions or the influence of exposition and inclination angle on vegetation cover like trees, which in turn strongly influence hillslope stability.

The downhill flow of water is neither a new nor a particularly revolutionary concept. It has nonetheless been the focus of more studies than can reasonably be cited here. Waldenmeyer (2003) studied the runoff generation in a catchment area in the northern Black Forest. In addition to this work, dissolved organic carbon (DOC) was used to identify the dominating flow pathway and runoff process (Volkmann, 2002; Casper et al., 2003). Fast and delayed stormflow generation at a hillslope segment was studied by Hangen et al. (2001). A further model shows movement of water through fracture pathways resulting in lateral subsurface stormflow in the shallow highly fractured bedrock and deeper seepage returning as baseflow through longer, more tortuous flow paths in the deeper, less fractured bedrock (Figure 1.1, Gabrielli et al., 2012).

Numerous conceptual models of hillslope flow processes and fracture flow along geologic interfaces as well as their distinction have already been presented in the literature (e.g. Gattinoni and Scesi, 2018; Hangen et al., 2001; Wenninger et al., 2004; Brantley et al., 2017; Sche-

liga et al., 2018; Hinderer et al., 1998; Springer and Stevens, 2008; McGuire and McDonnell, 2006; Volkmann, 2002; Gabrielli et al., 2012; Wisotzky, 2011; Sommer et al., 1997; Asano et al., 2002; Tunaley et al., 2016; Van Tol et al., 2010; Waldenmeyer, 2003; Lin, 2010; Ala-aho et al., 2017; Schenk et al., 2020; Goldscheider et al., 2000). They differ in their scale (local/regional), depiction of groundwater recharge and evapotranspiration, presence of different geologic layers and top soil cover, flow regime (high flow/low flow/storm flow) aquifer type (porous/fractured) and climate domain (arid/humid). They also differ in their use of color (grayscale/color) and dimensionality (2D/2.5D/3D).

1.2 SPRINGS

> *The study of springs is a borderline discipline, because springs are the transition from groundwater to surface water.*
>
> *Brune (1975)*

Scientists from different disciplines do research at springs. As a result, numerous classification schemes exist for springs and the description of processes at springs. These descriptions are often specific to individual localities or disciplines. Any selected spring might be described and classified differently by experts from different scientific communities (hydrogeology, ecology, hydrology, geochemistry, geomorphology). Cantonati et al. (2020) advocate for the integration of different scientific disciplines in the study of groundwater-dependent ecosystems into the unifying, synthetic field of ecohydrogeology (Figure 1.2).

Karst springs, glacial springs, thermal springs, submarine springs or mineral springs are just some example classifications. Historically, the classification of springs "was a verbal recitation of the location, size, temperature, and drinkability of the spring" (Alfaro and Wallace, 1994). The classification has changed over time, based on an increase in scientific knowledge about springs and their origins. Examples of classifications from the early 20th century include the works of Bryan (1919) and Meinzer (1927).

A common classification scheme is helpful to focus research efforts in a more sustainable way towards especially vulnerable ecosystems. A current example for a classification scheme is found in Springer and Stevens (2008), who propose a set of 12 different spheres of discharge of springs to be used across different disciplines.

1.3 FLOW PROCESSES IN THE UNDERGROUND

Many of the feedback mechanisms between groundwater, surface waters (e.g. infiltration) and the atmosphere (e.g. evapotranspiration) involve the critical zone. Thus, understanding soils is crucial in understanding the hydrologic cycle.
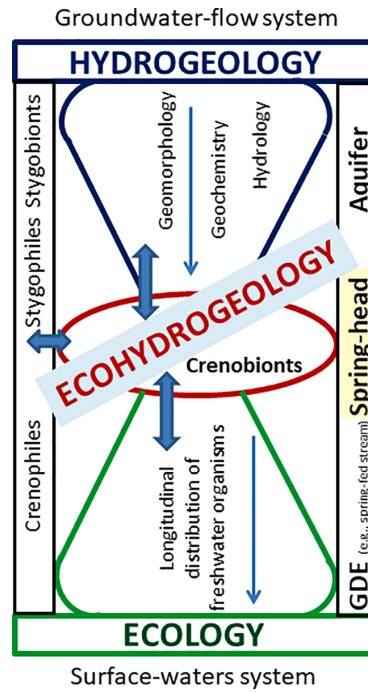
Figure 1.2: Ecohydrogeology is the integrated study of spring ecosystems at the interface between ecology and hydrogeology. Spring ecosystems are at the interface between an aquifer (groundwater) and surface water. The hourglass model of springs presented here is taken from Cantonati et al. (2020).

Flow processes in a saturated aquifer are usually described by Darcy's law given Equation 1.1. Darcy published this well-known equation in the appendix to his 1856 book on the fountains of the city of Dijon (Darcy, 1856). It is valid for laminar flow through porous media.

$$\frac{Q}{A} = K \left(\frac{\Delta h}{L} \right) \tag{1.1}$$

In this equation, the water flux Q per area A is calculated. The hydraulic gradient Δh is the difference in water levels from inlet to outlet. and ΔL is the length of the column. K is a constant defining the water flux for any given hydraulic gradient $(\Delta h/L)$.

The unsaturated zone, often also called the vadose zone, is located at the interface between the groundwater surface and the land surface. The critical zone ranges from the vegetation top to the aquifer bottom (Lin, 2010). Flow processes in the unsaturated zone involve three phases: the solid soil matrix and mass and energy transport in gaseous and liquid phases. This makes them more complicated to describe compared to flow processes in the saturated groundwater zone.

The Richards equation (Richards, 1931), given in Equation 1.2, is used to describe the movement of water in the unsaturated zone. It is an expansion of Darcy's law for unsaturated conditions.

$$\frac{\partial \theta}{\partial t} = \frac{\partial}{\partial z}\left[K\left(\theta\right)\left(\frac{\partial h}{\partial z}+1\right)\right] \tag{1.2}$$

In this equation, θ is the volumetric water content, t is time, z is the vertical elevation, K is the hydraulic conductivity and h is the matric potential induced by capillary forces. The matric potential is caused by adhesive and cohesive forces that bind the water to the particles of the soil matrix. It therefore strongly depends on the soil moisture content and the particle size distribution (Braden, 2012). In effect, the water transport is driven along the gradient of the matric potential, the pressure potential and the gravitational potential. The gravitational potential is dependent on depth z only, multiplied by the gravitational acceleration of 9.81 m/s².

Other effects like the osmotic potential are usually neglected in this context (Braden, 2012). The same is true for hysteresis effects or trapped residual gases that may sometimes influence hydraulic conductivity in an aquifer and lead to different hydraulic conductivities at the same volumetric water content. Furthermore, heterogeneity of the soil determines the distribution of soil moisture and the resulting hydraulic conductivity. Preferential flow in the vadose zone is influenced by macro-pores created by chemical (dissolution of minerals) and biological (plant roots, burrows) processes (Li et al., 2018).

1.4 AIMS AND SCOPE

General aim of this thesis is to gain a deeper understanding of hydrologic processes on steep hillslopes across different scales. This includes soil water dynamics in the unsaturated zone, lateral near surface flow in the soil cover and groundwater flow at the contact between different geologic layers. In reality, these flow processes happen at the same time, there is mixing and often complex influences between these flow processes. Water reaching the surface at a spring can rarely be attributed to only one flow pathway. While most of the spring water might come from a fractured or porous aquifer, lateral water flow parallel to the surface might also contribute to overall discharge dynamics and influence water chemistry in a significant way. Furthermore, processes in the unsaturated zone also influence groundwater recharge, formation of surface- and underground runoff, and the overall discharge behavior.

Weekly, depth resolved time series of soil moisture measurements as well as continuous discharge data from a large inclined lysimeter are the basis for an analysis of flow processes in the unsaturated zone. The

length of the recorded time series covers more than 25 years. Aim was to detect and describe changes to past soil moisture states. What is the overall trend in soil moisture levels? Are there any seasonal influences? Can changes be described by linear models or is there a necessity for more sophisticated models? Are any exceptional hydro-meteorological events that had a lasting impact on subsequent soil moisture levels identifiable? Which parts of the soil are most vulnerable to changes and are therefore affected most by climate change?

Furthermore, water chemistry analyses of spring water from the Black Forest National Park provide insights into groundwater flow dynamics in steep slopes and illuminate underground flow pathways. General aim at this study site was to establish a baseline of spring water chemistry and to gain a fundamental understanding of the flow processes that are relevant in this catchment area. Development of a conceptual model of water flow to the springs was based on this. It is a necessary resource for future assessments of changes in water quality and discharge dynamics following land use variations or climate change. This understanding is also necessary in order to effectively protect the spring habitats and their associated ecosystems. Further research questions to be answered were: What is the overall hydro-chemical composition of the spring water? In what way do springs differ from each other? Which parameters can be used as indicators to characterize these springs? Are there any seasonal patterns observable in discharge behavior or physico-chemical properties? How does the geology influence water chemistry and the discharge dynamics of the springs? What is the influence of land used and vegetation? Can springs be grouped according to geologic layers of discharge and is it possible to use the water chemistry to differentiate between different types of flow?

1.5   STRUCTURE OF THE THESIS

The presented thesis follows a cumulative structure and is mainly based on self-contained, peer-reviewed publications that cover different aspects of hydrologic processes on steep hillslopes across different scales.

Chapter 2 deals with soil water dynamics on steep hillslopes. As such, it is focused towards processes and moisture flux in the unsaturated zone. It is based on soil moisture measurements taken at a large inclined lysimeter near Karlsruhe, Germany. Weekly, depth resolved time series of soil moisture starting in 1994 allowed to identify past changes in soil moisture levels. This chapter underwent a public discussion and peer review in *Hydrology and earth system sciences*.

Chapter 3 focuses on water chemistry and hydrogeology in the catchment area of the Schönmünz stream in the Black Forest National Park. It provides insights into the processes controlling spatial and

temporal dynamics of spring water chemistry within the catchment area. It has been published in *Science of the total environment* following a peer review process.

A comprehensive description of the data collected within the water catchment area of the Schönmünz and the data itself have been published following a peer review process in *Data in Brief*. This publication is reproduced in *Chapter 4*.

Beside the published articles concerning the study site in the Black Forest National Park, a paired catchment study was conceptualized, including the neighboring valley of the Langenbach. The necessary monitoring points were selected and a system for long term monitoring installed at selected springs and measurement points along the surface streams. The general concept and research questions are presented in *Chapter 5*. Selection of monitoring points and initial placement of the measurement equipment is presented in Appendix C.

In *Chapter 6* key findings obtained in the individual studies are summarized in regard to the research objectives stated in Section 1.4. A connection between the individual studies is established. Furthermore, aspects that are important to future research are discussed and approaches to additional research opportunities proposed.

Part I

LARGE INCLINED LYSIMETER

2

DEEP DESICCATION OF SOILS OBSERVED BY LONG-TERM HIGH-RESOLUTION MEASUREMENTS ON A LARGE INCLINED LYSIMETER

ABSTRACT

Availability of long-term and high-resolution measurements of soil moisture is crucial when it comes to understanding all sorts of changes to past soil moisture variations and the prediction of future dynamics. This is particularly true in a world struggling against climate change and its impacts on ecology and the economy. Feedback mechanisms between soil moisture dynamics and meteorological influences are key factors when it comes to understanding the occurrence of drought events. We used long-term high-resolution measurements of soil moisture on a large inclined lysimeter at a test site near Karlsruhe, Germany. The measurements indicate (i) a seasonal evaporation depth of over 2 m. Statistical analysis and linear regressions indicate (ii) a significant decrease in soil moisture levels over the past 2 decades. This decrease is most pronounced at the start and the end of the vegetation period. Furthermore, Bayesian change-point detection revealed (iii) that this decrease is not uniformly distributed over the complete observation period. The largest changes occur at tipping points during years of extreme drought, with significant changes to the subsequent soil moisture levels. This change affects not only the overall trend in soil moisture, but also the seasonal dynamics. A comparison to modeled data showed (iv) that the occurrence of deep desiccation is not merely dependent on the properties of the soil but is spatially heterogeneous. The study highlights the importance of soil moisture measurements for the understanding of moisture fluxes in the vadose zone.

2.1   INTRODUCTION

The understanding of soil moisture dynamics and its coupling to climate and climate change is crucial when it comes to predictions of future variability of soil moisture storage and exchange with the atmosphere and vegetation. Long term data sets of measured soil moisture are of critical importance to achieve a better understanding of how these systems interact and to identify the main drivers for seasonal and long term soil moisture variations. Drought and feedback mechanisms between soil moisture and extreme temperatures are documented in the literature (Lanen et al., 2016; Perkins, 2015; Samaniego et al., 2018). Mass and energy fluxes in soils are coupled processes (Zehe et al., 2019). Due to less evaporative cooling during drought periods, temperatures tend to be higher (Hirschi et al., 2011). A review of soil moisture and climate interactions is given in Seneviratne et al. (2010).

Main drivers of soil moisture dynamics are rainfall (wetting) and the vegetation period (radiation driven drying) (Mälicke et al., 2020). Vegetation can influence the soil water budget through an increase in transpiration, hydraulic lift of water from lower soil layers, reduced runoff on steep slopes and reduced soil evaporation due to shading (Liancourt et al., 2012). Other impact factors include soil type, local groundwater availability, inclination angle and direction of exposition (Schnellmann et al., 2010). Feedback mechanisms between soil moisture and groundwater resources with weather phenomena like El Niño are also described in the literature (Kolusu et al., 2019; Solander et al., 2020). The 2015-2016 El Niño event is associated with extreme drought and groundwater storage declines in Southafrica while at the same time in east African countries south of the equator an increase in precipitation and groundwater recharge was recorded (Kolusu et al., 2019). Similarly, Solander et al. (2020) found evidence for both, increase (eastern Africa) and decrease (northern Amazon basin, the maritime regions of southeastern Asia, Indonesia, New Guinea) in soil moisture storage depending on location. An increase in catchment evapotranspiration was observed during the past decades (Duethmann and Blöschl, 2018). As groundwater recharge is dependent on the availability of excess soil moisture, therefore aquifers respond to climatic periodicities (Liesch and Wunsch, 2019).

Traditionally, soil moisture was determined by taking representative soil samples for gravimetric determination, following oven drying. The main disadvantage of this method, despite being very precise, is its destruction of the sampling location and the sample itself. Achievement of long term data sets is challenging using this method. Non destructive measurement methods include cosmic ray neutrons (Rivera Villarreyes et al., 2011; Kędzior and Zawadzki, 2016), installation of TDR sensors (Li et al., 2019), thermal infrared sensors

(Yang et al., 2015), resistivity measurements like the OhmMapper (Walker and Houser, 2002), capacitance measurements or neutron probes (Hodnett, 1986; Evett and Steiner, 1995). A comparison and discussion of several sensor systems using different measurements principles is given in Jackisch et al. (2020), highlighting also the need for thorough calibration before the use of such systems. During this study two calibrated neutron probes were used. Numeric approaches include modeling of depth-dependent soil moisture based on surface measurements (Qin et al., 2018) or modeling of soil moisture for specific locations based on available weather data (Menzel, 1999). Another modeling approach of soil moisture is based on remote sensing data. This has been done on catchment scale (e.g. Pellenq et al., 2003; Penna et al., 2009), regional scales (e.g. Mahmood et al., 2012; Otkin et al., 2016; Long et al., 2019) and the global scale (eg. Dorigo et al., 2017; Albergel et al., 2019) with various calculation grid sizes and temporal resolutions. Analysis of inherent parameter uncertainty in modeled soil moisture and implications for current discussions about soil moisture dynamics should be considered (Samaniego et al., 2012), as well as upscaling of measurements to different temporal and spatial scales (Mälicke et al., 2019).

Lysimeters are also suitable for gaining in-depth knowledge about water balance and water movements in soil, which is the main reason the lysimeter in this study is operated. It provides a direct measurement of percolation rates through the soil, which makes it suitable for monitoring and demonstration of equivalency of the earthen landfill cover (Abichou et al., 2006). Application of lysimeters, however is not restricted to monitoring of legally acceptable percolation rates, but also allows for studies into water and solute transport in the vadose zone that would not be possible by other means (Singh et al., 2018). Their usage allows for precise determination of evapotranspiration (ET), if soil water storage is accounted for to well below the root zone (Evett et al., 2012) as well asdetermination of incoming water at the land surface due to precipitation and non-rainfall-events like dew or fog (Groh et al., 2018). Furthermore, they are used for determination of preferential flow (Schoen et al., 1999; Allaire et al., 2009), particle transport (Prédélus et al., 2015) and contaminant transport in the vadose zone Goss et al. (2010).

There are about 2500 lysimeters installed at around 200 sites across Europe, around half of them in Germany (Sołtysiak and Rakoczy, 2019). In the present study, we analyze long term soil moisture time series from two large inclined lysimeters located in southern Germany. Data from the monitoring of this test site has previously been evaluated and published concerning the proper function of the landfill cover (Zischak, 1997; Gerlach, 2007) and with regard to flow processes on steep hillslopes (Augenstein et al., 2015) using only much shorter parts of the time series available.

However, a time series analysis of all available soil moisture measurements from this test site to gain insight into long term soil moisture variations has not been done previously and is the main focus of this study. The inclusion of previously unpublished data from the more recent soil moisture measurements allows for a more comprehensive analysis of the time series. Using the available data from this test site, it is possible to identify past events that led to significant changes in the long term dynamics of soil moisture. Main research questions are:

- How did the measured soil moisture levels change over the past decades?

- Can these changes be described by simple linear models, or does it require more sophisticated modeling approaches?

- Can exceptional hydro-meteorological events that had a lasting impact on soil moisture levels be identified as tipping points by statistical methods?

- Are there seasonal differences? During which time of the year did the greatest change in soil moisture level occur?

- Which part of the soil is affected the most?

2.2   STUDY SITE

The study site is located in southern Germany (8.337°N, 49.019°E) near the city of Karlsruhe (Figure 2.2). The climate in the region is classified as warm temperate, fully humid with warm summers or as Cfb according to the Köppen-Geiger Classification scheme (Beck et al., 2018; Kottek et al., 2006). Mean annual precipitation is 760 mm (1990 – 2007, DWD station 2522, Karlsruhe). Annual precipitation and temperatures are shown in Figure 2.1. Exceptionally dry years within the observation period between 1994 and 2019 are 2003 with 566.3 mm and 2018 with 566.7 mm of precipitation. Highest annual precipitation was recorded in 2002 with 981.6 mm, followed by 2013 with 972.4 mm of precipitation. Mean annual temperature was highest in 2018 (12.33 °C) and lowest in 1995 (9.69 °C).

Two large inclined lysimeters are embedded in the municipal landfill site Karlsruhe-West for mandatory monitoring purposes. Cross sections of both lysimters are shown in Figure 2.3. The first lysimeter (Field 1) was built in 1993 and started operation at the end of that year. With a width of 10 m and a length of 40 m, it has a size of 400 m². The mean inclination angle is 23.5° (43.5 %) with a southern exposition. The recultivation layer (RL) in this field has a thickness of 100 cm, it is underlain by a drainage layer (DL) with a thickness of 15 cm followed by a mineral clay liner (MCL) and capillary barrier.

The second lysimeter (Field 2, pictured in Figure 2.4) was built in 2000, with first measurements being taken in December of that year.
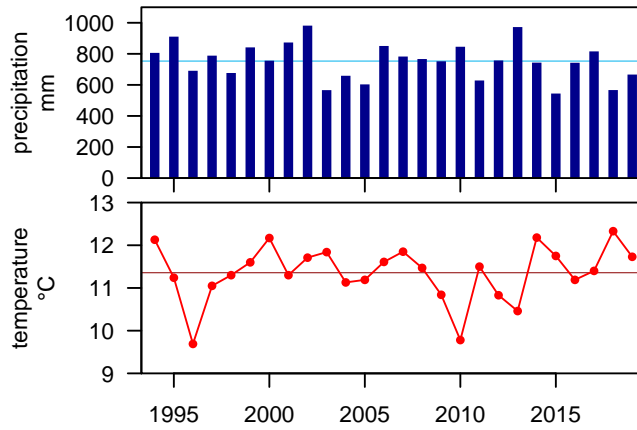
Figure 2.1: Precipitation and Temperature at stations 2522 (Jan 1994 – Oct 2008) and 4177 (Nov 2008 – Dec 2019) (DWD Climate Data Center (CDC), 2020)

It consists of two separate fields with a size of 10 m by 20 m each, resulting in a total size of 400 m². The mean inclination angle is 23.5° (43.5 %) with southern exposition. Results from Field 1 showed, that a thicker RL is necessary in order to protect the MCL from drying out. This insight was considered during the construction of Field 2. The RL in Field 2A has a thickness of 200 cm, in Field 2B it has a thickness of 215 cm. It is underlain by a drainage layer (DL) with a thickness of 15 cm followed by a mineral clay liner and capillary barrier. Depth across the inclined field varies. Additionally, the mineral clay liner is not present in the lower half of Field 2B, reducing the final depth of the lysimeter by 50 cm, affecting measurements taken at NP5 and NP6 below the RL. The RL was constructed by adding layers of soil on top of the compacted surface of the previous layer. Use of different materials in the soil layers can not be ruled out. Further details on the construction of both fields is given in Augenstein et al. (2015). The soil properties of the RL relevant to this study have been modeled by Gerlach (2007) using HELP (Berger, 2015). For the year 2002, the porosity of the RL is 0.4 [-], usable field capacity 0.25 [-] and the wilting point at 0.14 [-]. The permeability was estimated as $k_f = 1.0 \cdot 10^{-6}$ [ms⁻¹]. Formation of preferential flow paths in the lysimeter lead to changes in hydraulic properties over time (Gerlach, 2007).

Both fields are covered by grass and weeds, depending on the current season. The growth of deeply rooted plants that would damage the sealing system is prevented and the grass is cut regularly on the complete landfill cover including both lysimeters. In recent years, sheep have been used to limit the growth of vegetation in a more natural way. Further records on the vegetation cover and plant maintenance are not available.
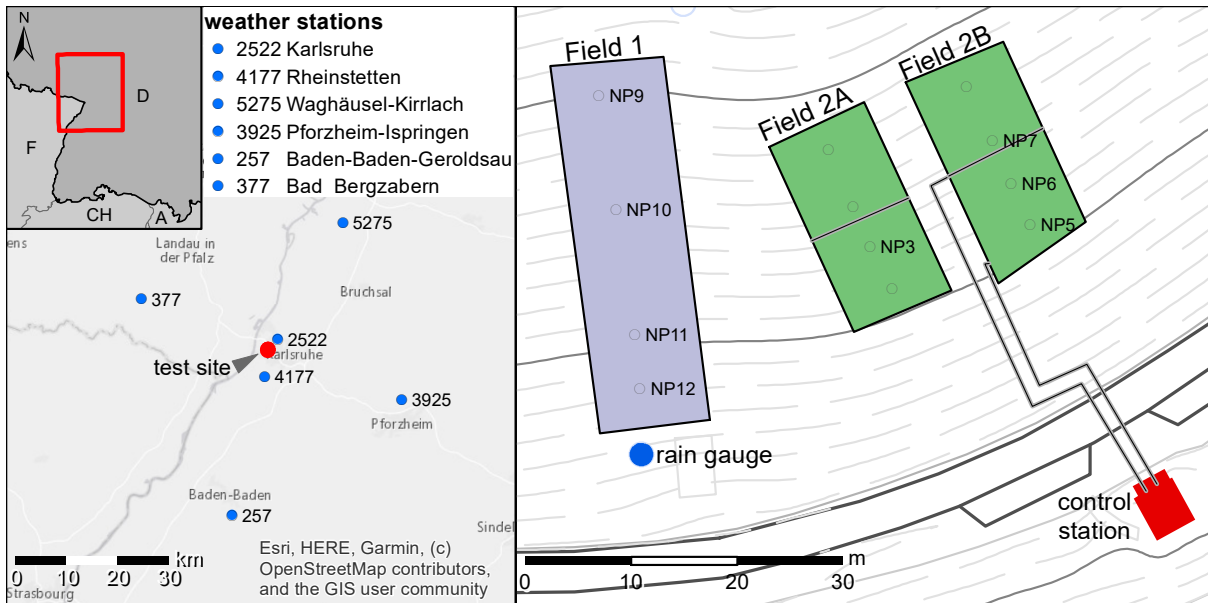
Figure 2.2: Location of the study site on a municipal landfill site in Karlsruhe, Germany, and locations of the weather stations used in this study. Lysimeter 2 consists of two separate fields (Field 2A, Field 2B).
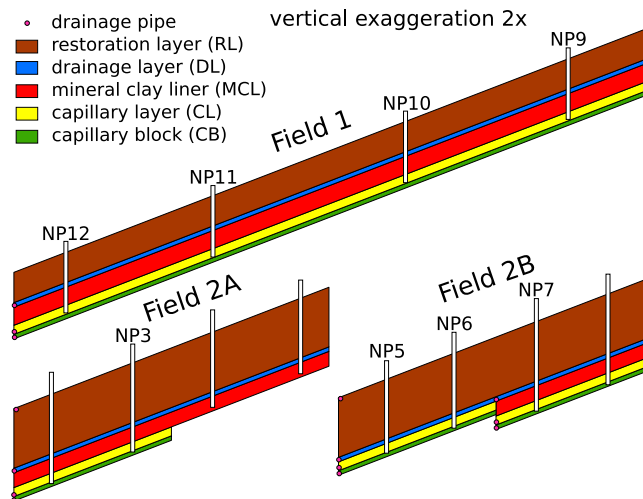
Figure 2.3: Cross sections of lysimeter Field 1 and Field 2 with the different layers and moisture measurement points.

Figure 2.4: Lysimeter Field 2 (visible in the upper part of the image between vertical beams)

2.3 MATERIAL AND METHODS

2.3.1 *Soil moisture and discharge measurements*

Soil moisture measurements were carried out using two different neutron probes. A modified Wallingford IH2 neutron probe was used until 23 August 2012. From 30 November 2012 onward, a modified Troxler 4300 Depth Moisture Gauge was used. Both models used an Am/Be source with activities of 1.85 GBq and 370 MBq respectively (Augenstein et al., 2015). They were modified to fit into the installed measurement tubes. Selected measurement points are shown in Figure 2.2. Neutron probe measurement points (NP) are constructed from steel tubes ($\varnothing$ 40.5 mm) installed vertically in the soil column. At neutron probe measurement point 9 through 12 (NP9, NP10, NP11, NP12) located in lysimeter Field 1, measurements were carried out on a weekly basis until Field 2 was constructed (December 2000). After construction of Field 2, measurements were taken monthly in Field 1. At the same time, weekly measurements in Field 2 at neutron probe measurement points NP3, NP5, NP6 and NP7 started. Measurements were taken in depth increments of 10 cm until the bottom of the lysimeter is reached (final depth Field 1: between 2.1 m and 2.3 m; final depth Field 2: between 2.8 m and 3.4 m). No measurements were taken at the remaining four points in Field 2. During the period of January 2014 to June 2014, no measurements were taken at neither of the two fields due to ongoing construction of new accessibility stairs for Field 2.

Discharge from the drainage pipes (Figure 2.3) is collected in cylindrical tubes equipped with magnetic valves at the bottom. A data logger connected to pressure sensors in each tube records water levels at regular intervals. Additional data points are recorded when the changes in water levels are large. Once the tube is full, the valve at the bottom opens and and closes automatically to empty the tube.

From changes in the recorded water levels, discharge was calculated. The area of the lysimeter field was used to calculate monthly

Table 2.1: Location of weather stations and distances to the test site.

Station name	Station ID	Elevation	Latitude	Longitude	Distance
Karlsruhe	2522	112 m a.s.l.	49.0382°	8.3641°	2.9 km
Rheinstetten	4177	116 m a.s.l.	48.9726°	8.3301°	5.2 km
Bad Bergzabern	377	210 m a.s.l.	49.1070°	7.9967°	26.7 km
Pforzheim-Ispringen	3925	333 m a.s.l.	48.9329°	8.6973°	28.1 km
Waghäusel-Kirrlach	5275	105 m a.s.l.	49.2445°	8.5374°	29.0 km
Baden-Baden-Geroldsau	257	240 m a.s.l.	48.7270°	8.2457°	33.2 km

aggregated discharge per area (mm) from the amount of water that was collected (L).

2.3.2 *Additional data*

Additional data used for this study include daily precipitation and modeled values of usable field capacity (uFC). Daily precipitation data at a station near Karlsruhe is published by the German weather service (DWD) (DWD Climate Data Center (CDC), 2020). Data for this station (Station ID: 2522) is available for the time range until October 2008. Another station, still in operation by the DWD, is located in Rheinstetten (Station ID: 4177), approximately five km south of the test site, providing data from November 2008 onward. Locations of both weather stations are shown in Figure 2.2.

The DWD also publishes derived model results for usable field capacity (uFC) (DWD Climate Data Center, 2020) that can be used for comparison of measured soil moisture time series. They are provided for two different soil types and as depth resolved values for the top 60 cm of the soil column. They are computed by the agrometeorological model AMBAV. For this study the depth resolved values for soil moisture under grass with sandy loam (wilting point 0.13 [-], field capacity 0.37 [-]) were used. Additionally, soil moisture under grass and loamy sand (wilting point of 0.03 [-], field capacity 0.17 [-]) up to 60 cm depth was used. A defined constant water content is used as boundary condition at the bottom of the model. Further model input parameters are hourly values of temperature, dew point, wind speed, precipitation, global radiation and reflected long-wave radiation. Data was used from five stations (Table 2.1: 4177, 377, 3925, 5275, 257, Figure 2.2) and covers a time range from 1 January 1991 until 31 December 2019. Values at station 3925 are available from 2005 onwards. Measured soil moisture data is not directly comparable to uFC, because of a different scale being used. The uFC of 100 % is defined as the soil moisture content that can not be drained by gravity. Nonetheless, both measured soil moisture and usable field capacity have similar temporal distribution patterns.

2.3.3   *Theory and calculations*

Volumetric water content (θ) and uFC are expressed as %. Data analysis and visualization was done in the R system for statistical computing R Core Team (2020).

Time series were transformed into a radial coordinate system, to highlight the asymmetry of the seasonal cycle between gradual drying and fast re-wetting of the soil. New x- and y-coordinates for each measurement were calculated according to Equation 2.1 and Equation 2.2.

$$x = \cos\left(2 \cdot \pi \cdot \frac{d_{year}}{d/a}\right) \cdot \theta \tag{2.1}$$

$$y = \sin\left(2 \cdot \pi \cdot \frac{d_{year}}{d/a}\right) \cdot \theta \tag{2.2}$$

In these two equations, x and y are the new coordinates in a radially transformed coordinate system, θ is the volumetric water content in %. d_{year} is the day of the year. It is divided by the length of the respective year (d/a) in order for 2π to equal one year.

Mean soil moisture of the recultivation layer in Field 2 was calculated as average of NP3 at depths between 10 cm and 180 cm and at NP5, NP6 and NP7 at depths between 10 cm and 220 cm.

For each individual depth, a linear regression was calculated using all measurements for the years 2000 to 2019 (see 2.3.1). Calculations were done using the lm()-function in the R system for statistical computing (R Core Team, 2020). As linear regression can be dependent on the selected start and end times, additional regressions were calculated over the complete available time span, based on time series cut off before 2004 and between 2004 and 2016. The resulting slope of these regression lines represent the mean change of soil moisture in $\%d^{-1}$. A conversion into $\%a^{-1}$ was calculated by using the average length of 365.2425 da^{-1}, according to the Gregorian calendar.

To overcome the limitations of linear regressions when used on data with large seasonal variation compared to a small overall trend, another set of linear trends was calculated based on monthly averages. The monthly values were calculated as averages based on the measured values within each month and depth. No weights were assigned to individual measurements. The time series for all depths were each subdivided into twelve time series, one for each month. For example, application of this subdivision on the time series at a depth of 170 cm at NP3 results in twelve time series (Figure 2.5). Linear regressions were then calculated separately, based on all mean values for each month, giving the average slope for each measurement point, depth
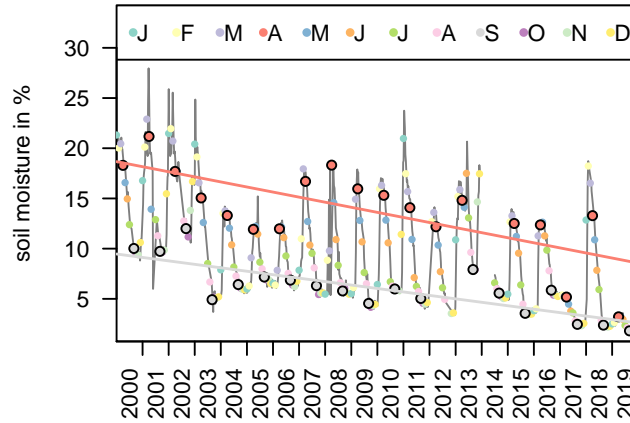
Figure 2.5: Example for the calculation of monthly linear regressions for April and September at NP 3 and at a depth of 170 cm.

and month. An example for these calculations is shown in Figure 2.5 for the months of April and September at NP3 and at a depth of 170 cm.

Measurements at Field 1 were taken weekly at the start of the time series, but the interval changed to monthly measurements later. Therefore, use of all values for regression would lead to an over emphasis of the early part of the time series, due to the higher number of samples during that time span. To avoid this bias and over emphasis, monthly averages were used. The regressions yielded individual values for the change in soil moisture by month and depth. Additionally, further information about the regressions were extracted from the results. These include standard deviations and p values for the slopes. The analysis was done with the time series of uFC in a similar fashion.

Time series analysis are sensitive to the selection of a suitable model. To overcome the paradigm of the single-best model approach in time series decomposition, Zhao et al. (2019b) implemented a Bayesian model averaging scheme to approximate complex relationships by the use of Markov Chain Monte Carlo stochastic sampling. The model space is explored by randomly traversing through combinations of coefficients. The number and location of individual changepoints in seasonality and trend are randomly sampled and all candidate models averaged based on how probable each of them is. Results of the model not only include best estimates for model parameters (e.g. location of changepoints), but also their probability distributions. Bayesian change point detection and time series decomposition was done using the beast()-function from the Rbeast package (Zhao et al., 2019a). This divides the time series into seasonal and trend components, along with change points in both. The period was set to 12 for monthly time series decomposition. The same monthly averaged time series were used as with the previous monthly linear regressions.

2.4 RESULTS

The study represents a very specific case and the interpretation of results is limited to these specific conditions at the landfill.

Measured soil moisture values in the RL at NP5 and NP10 are presented in Figure 2.6 at the corresponding position on the respective soil moisture profiles and before monthly averages were calculated. There is a gap in measurements during the first half of 2014. Field 2 was built in 1999 and no data is available prior to the year 2000. In total, over 140 000 individual soil moisture measurements are shown. Due to grain size and soil properties, the mineral clay liner has a higher moisture content (> 25 %). It is overlain by the gravel drainage layer, which has a very low moisture content. For evaluation, only soil moisture content of the RL is used in this study (n = 91198), because it is thought to be the layer in the lysimeter that reflects best the processes and moisture dynamics found in natural soils.

From this figure, a seasonal pattern is clearly visible. Soil moisture increases relatively quickly in late autumn or winter, especially in the upper parts of the soil. After reaching a critical soil moisture level, discharge from these layers starts more or less instantaneous and is measured as discharge from the DL. This wetting period is followed by a more gradual drying period, starting in late spring and lasting until the consecutive wetting period. The years before 2003 appear to have higher soil moisture content and shorter drying seasons, especially at, but not restricted to, Field 2. This can be seen for example at NP5 in Field 2 where blue colors, indicating soil moisture of over 30 %, alternate with green colors (15 %) before 2003. After 2003, green colors alternate with yellow colors, indicating soil moisture below 10 %. In recent years, the re-wetting of the soil during the winter month repeatedly did not reach the lower parts of the soil, especially in Field 2. For example at NP5 in depths between 100 cm and 200 cm yellow colors indicate soil moisture levels below 5 % for the complete years 2017 and 2019. Measured discharge during these years was significantly lower compared to the prior years. Despite above average precipitation during the second half of 2017, re-wetting was only observed much later in early 2018. Precipitation in 2018 was well below average, and paired with a large atmospheric demand for ET, once again drying out the lower soil and no re-wetting occurring in the winter months.

Soil moisture in Field 1 is higher at the upper slope (NP9) compared to the lower slope (NP12), especially at the start of the measurement series (Figure A.1). As with Field 2, soil moisture levels are lower after 2003. Because the RL is not as thick in Field 1 (100 cm) compared to Field 2 (~215 cm), re-wetting in the lower soil in depths below 100 cm is not observable. However, in years with missing re-wetting (e.g. 2017, 2019), of lower soil in Field 2, a similar gap can be observed in Field 1

below the MCL (~200 cm). In data from Field 2, depth-dependence of soil moisture is clearly evident. Higher soil moisture at depths of around 100 cm sharply decreases over the next 20 cm and downward propagation of the moisture front is also delayed. This effect is caused by differences in soil compaction during construction of the lysimeter and possibly the use of different soil materials. The volume of the lysimeter was filled in several layers and soil consolidated in between each. Porosity and hydraulic conductivity is therefore not uniformly distributed over the complete depth of the lysimeter. Greatest differences are found at the interfaces of two consecutive stages of construction between strongly consolidated top of the underlying layer and the less densely packed bottom of the overlying layer. The consistent and very distinct break of soil moisture over the entire measurement period suggests that there is a distinct change in porosity and hydraulic conductivity between these two layers. Settling down of the soil cover in the years after construction may additionally change soil properties over time.

Values of modeled uFC are also shown in Figure 2.6 for DWD station 4177 under grass and loamy sand.

2.4.1 *Drainage data and discharge behavior*

Discharge from the drainage layer is shown in Figure 2.6 d and e. It follows a seasonal pattern with highest discharges being recorded at the beginning of the year, usually around the months of January or February. During the summer months, discharge is lowest and can be completely absent, especially in recent years. The onset of discharge is usually more or less instantaneous, with highest rates of discharge measured around the time discharge starts. Augenstein et al. (2015) analyzed the discharge behavior as a function of the soil moisture. It usually takes the soil moisture front several weeks to percolate through the soil column and eventually drain. Individual precipitation events during the drier summer months do not lead to an immediate onset of discharge from the lysimeter. However, precipitation events during the discharge period may rapidly increase the amount of discharge. The soil moisture near the bottom of the soil column at the initial onset of discharge is usually lower than the soil moisture when the discharge stops.

Water flow is also influenced by the slope. The soil moisture front on the upper slope usually takes longer to reach equivalent depth on the lower slope. Meaning the lower slope usually gets wet faster, indicating a strong lateral component of sub-surface water flow (Augenstein et al., 2015).

Initially, after construction of the lysimeter, discharge was noticeably higher in comparison to later years. This is more pronounced in Field 2 (Figure 2.6 e). A significant reduction in annual discharge from
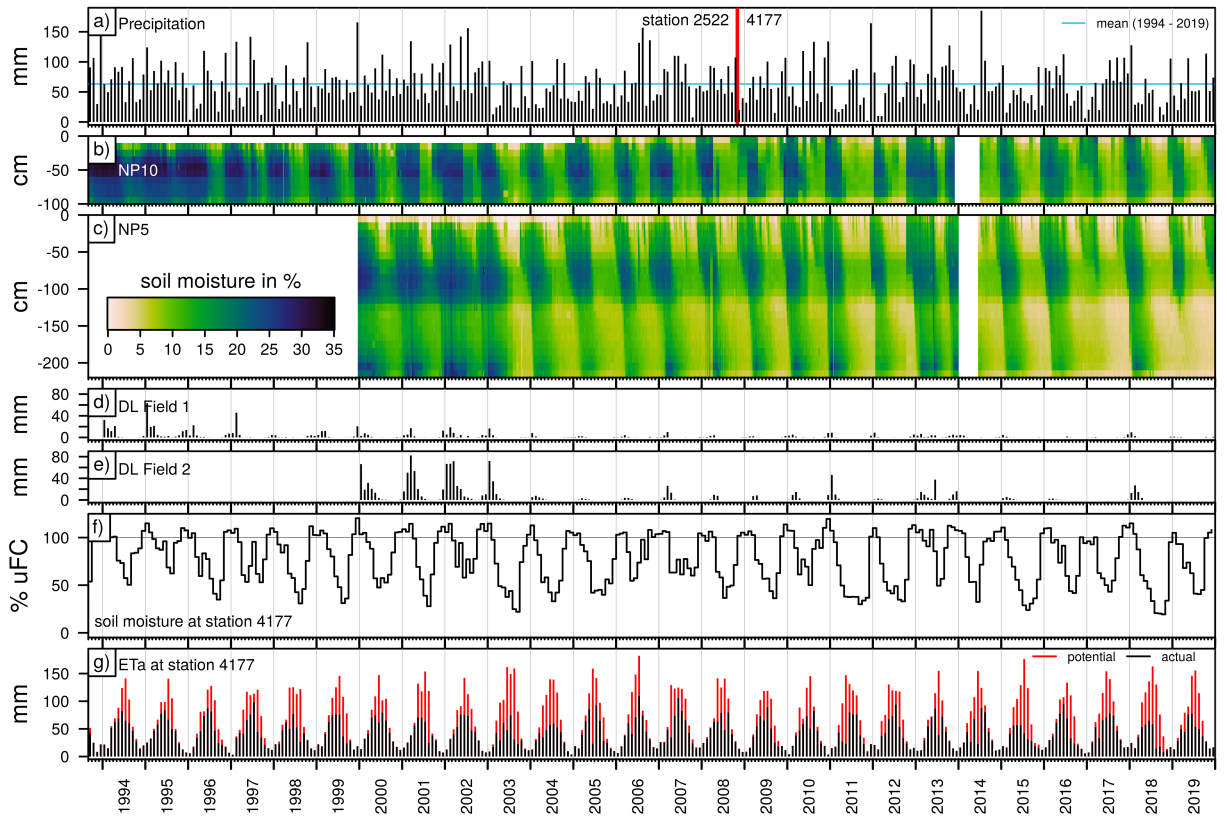
Figure 2.6: a) Monthly precipitation at stations 2522 (Jan 1994 – Oct 2008) and 4177 (Nov 2008 – Dec 2019) (DWD Climate Data Center (CDC), 2020). Blue line represents mean monthly precipitation during 1994 to 2019. b) and c) Time series of selected soil moisture measurements (NP5 and NP10 respectively) at the test site near Karlsruhe, Germany. d) and e) Monthly discharge of the drainage layer (DL) at both lysimeters. f) Simulated monthly averages of usable field capacity (loamy sand), g) Monthly values of simulated potential evapotranspiration (red) and simulated actual evapotranspiration (black) (DWD Climate Data Center, 2020) at station 4177. Measurements on Field 2 are available from 2000 onward. No measurements were taken during the first half of the year 2014.

the DL can be seen around the year 2003. This reduction in drainage coincides with a reduction in soil moisture in both fields. In recent years when the soil moisture front did not reach the lower parts of the soil column, there was no discharge from the DL.

2.4.2 *Asymmetry of drying and re-wetting*

To highlight the asymmetry of the seasonal cycle between gradual drying and fast re-wetting of the soil, two exemplary time series are shown in a polar coordinate system (Figure 2.7). For comparison, the soil moisture time series of NP3 at a depth of 170 cm and a mean time series from all sampling points at Field 2 are shown. The overall trend of both time series is quite similar, however the asymmetry is much more pronounced in the time series of NP3 at 170 cm. The mean of all soil moisture time series in Field 2 was calculated over the complete depth of the recultivation layer (RL). Due to the lag in the downward propagation of soil moisture in the profile, the asymmetry of the seasonal cycle is evened out by calculation of the mean soil moisture over multiple depths and measurement points.

In the two time series shown in polar coordinates, the graph based on mean values describes a circle for each year of observation. In the time series of NP3 at 170 cm on the other hand, the graph describes spirals resembling nautiluses for each year of observation. The decreasing radius over time, apparent from both time series, indicates a decrease in soil moisture. White areas between lines indicate large and sudden changes in soil moisture levels during especially dry years. The opening of the nautilus corresponds to a rapid increase in soil moisture during winter. Depending on precipitation conditions, this increase may occur at the end of the year or the beginning of the consecutive year.

2.4.3 *Overall linear regressions*

In Figure 2.8, results of individual linear regressions of soil moisture measurements are shown for each depth and measurement point. Over the period between 2000 and 2019, soil moisture decreases by $0.34 \pm 0.14\ \%a^{-1}$ within the RL. The observed decrease is lowest in the first 20 cm of the soil column at both lysimeter fields. At the depth of 10 cm there is even a small increase observable in Field 2.

Overall, the decrease in soil moisture is most pronounced at depths of 20 cm to 40 cm in Field 1 (NP9, NP10). Due to the thicker RL compared to Field 1, highest absolute decrease is found at a greater depth of around 100 cm in Field 2. Below 130 cm at Field 2, absolute rate of soil moisture change is slightly lower. Seasonal variations of soil moisture patterns larger than the overall trend lead to a relatively low coefficient of determination (0.20 ± 0.10). However, with exception of
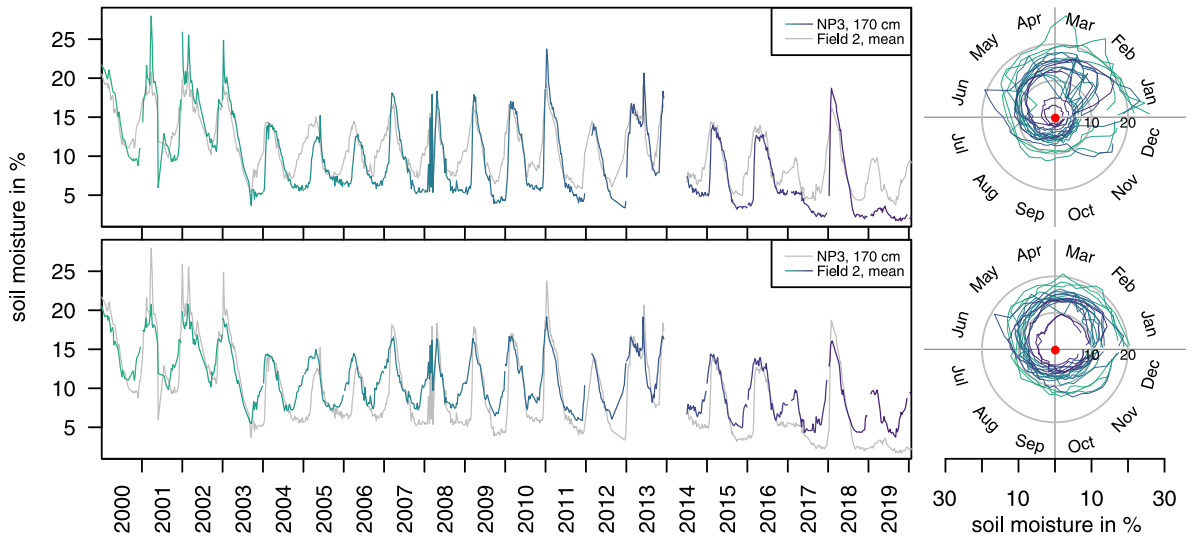
Figure 2.7: Time series of soil moisture at NP3 at 170 cm and mean soil moisture of Field 2 as well as the same data in a polar coordinate system to highlight seasonal asymmetry of gradual drying and fast re-wetting as well as the overall trend of declining soil moisture. Colors indicate the year of the measurement. For context, gray lines showing mean soil moisture of Field 2 and soil moisture at NP3 at 170 cm respectively were added.

two points (NP5 20 cm, NP7 10 cm), all slopes of calculated regression lines are significant ($p < 0.05$, $n = 122$). Coefficients of determination are lowest at the top and increase until a depth of around 100 cm. Precipitation events lead to short term variations in soil moisture. These variations are larger at the surface. Downward movement of the water in the soil column is being dampened with depth. At some depths, soil moisture patterns are more persistent. This might be due to different materials being used or differences in compaction during construction of the lysimeters and landfill cover. Differing soil properties like porosity, hydraulic conductivity and capillary forces determine the water retention capacity of the soil.

2.4.4 *Monthly linear regressions*

The results of linear regressions based on the monthly averages is shown in Figure 2.9. Resulting slopes with $p > 0.05$ (i.e. soil moisture change is not significant) are indicated by a marker.

A statistically significant increase in soil moisture can be observed in the top 10 cm of Field 2 (NP3, NP5, NP6, NP7) during the winter months only. Most other values show a significant decrease in soil moisture. The moisture change in the top 60 cm of the soil does show an increase during summer, but this increase is not statistically significant. The lack of statistical significance might be due to the shorter length of the time series at Field 2 compared to Field 1. As
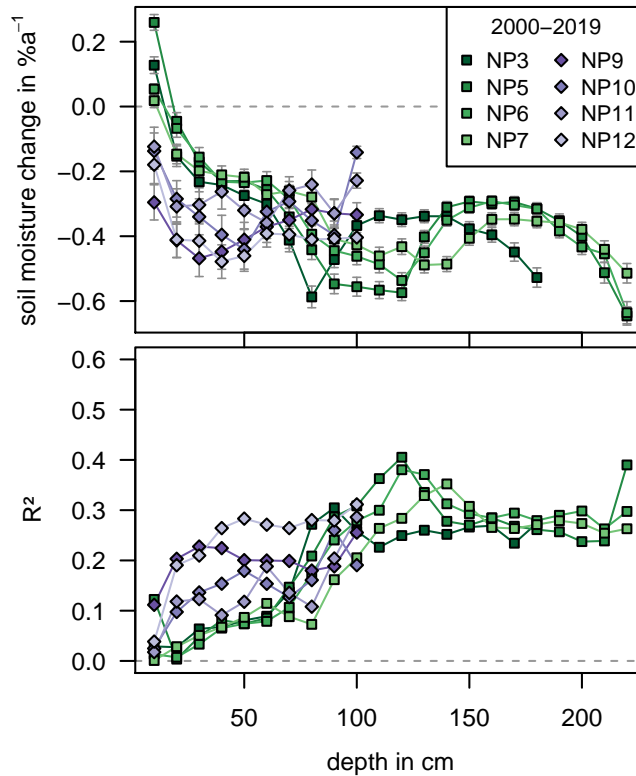
Figure 2.8: Results of individual linear regressions for soil moisture measurements in the recultivation layer, expressed as change in soil moisture content $[\%a^{-1}]$.

previously mentioned, overall soil moisture levels were higher before 2003. Inclusion of additional data before this point, as is the case with Field 1, would push the resulting decrease in soil moisture towards higher absolute values. From depths of around 70 cm to 130 cm (70 cm to 90 cm at NP3), decrease in soil moisture has a semiannual distribution. Highest reductions in soil moisture occurred during November and December as well as during April and May. Below this, decrease in soil moisture is generally lower and does show a weak annual cycle with highest values in December and January and minima during June and July. Highest values are shown in the lowermost 30 cm of the RL directly above the DL between January and May.

In Field 1, a decrease in soil moisture can be observed at all depths. The semiannual distribution of soil moisture change is similar to that of Field 2. It is most pronounced during spring and autumn and less pronounced during winter and summer.

The winter months are usually times of largest groundwater recharge and highest soil moisture in the lower soil. In recent years however, less water percolated through the upper parts of the soil at both lysimeter fields, affecting especially the soil moisture levels in the lower soil. This drying effect is amplified by the DL. It drains excess water and
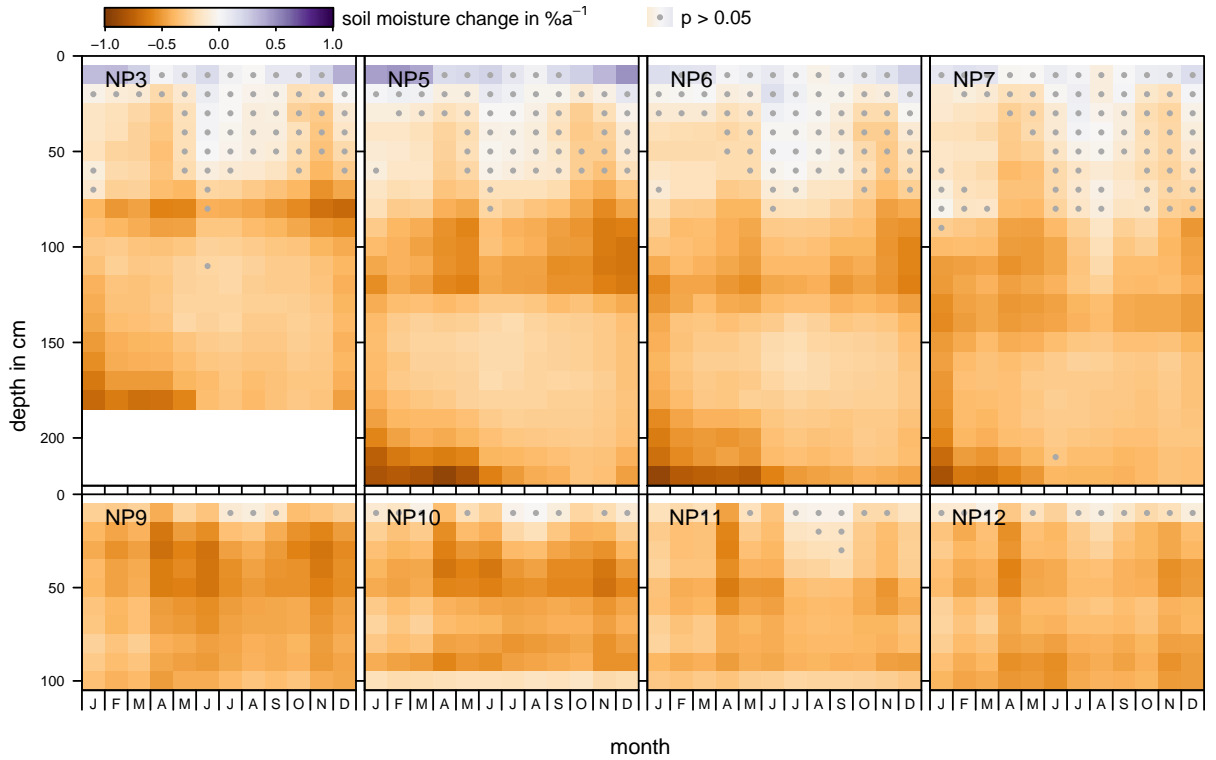
Figure 2.9: Results of individual linear regressions for soil moisture measurements in the recultivation layer, expressed as change in soil moisture content $\left[\%a^{-1}\right]$ calculated over the complete time series for each month based on monthly averages. Upper graphs: Field 2, lower graphs: Field 1. Values for p > 0.05 are indicated by a marker.

inhibits capillary rise. This means the depth of evapotranspiration in the lysimeter is greater than two meters and includes the complete RL.

Results of linear regressions based on monthly averages of uFC are shown in Figure 2.10. Most values indicate a decrease of soil moisture, but at the same time, most linear regressions are not statistically significant (p > 0.05). However, results for station 5275 indicate a clear and significant decrease in soil moisture during most of the year. The decrease in the lower soil layers appears to happen later in the year. Compared to Figure 2.9, the semiannual pattern is not as visible, but some months (August at station 4177, 377, 5275, 257) do show lower annual changes or even an increase in uFC (January at station 3925).

Compared to largest decrease in measured soil moisture at the beginning of the vegetation period in April and at the end of the vegetation period in November, the decline of uFC at the end of the vegetation period appears to happen much earlier (3925, 5275).
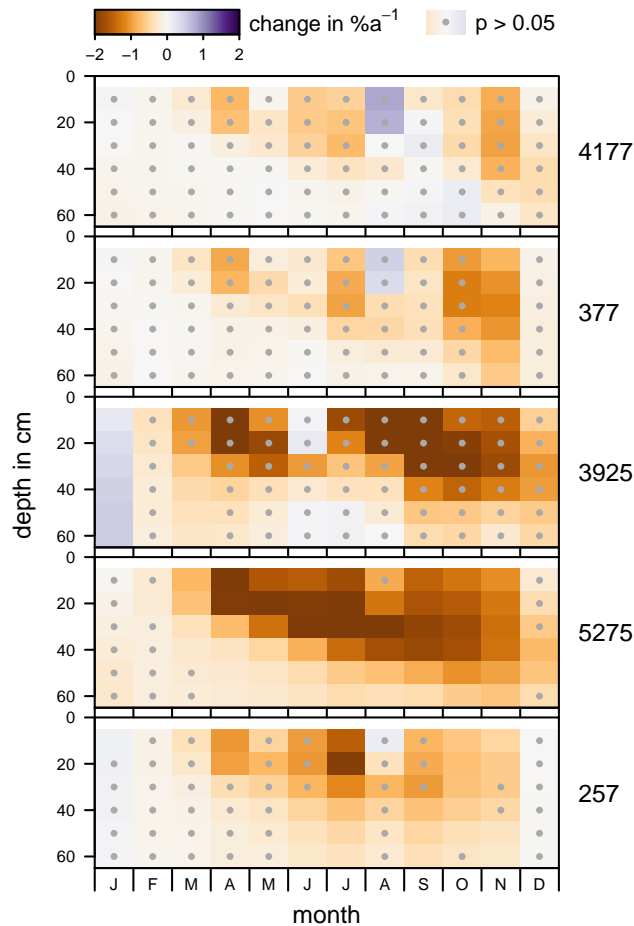
Figure 2.10: Results of individual linear regressions for usable field capacity (uFC) for the top 60 cm (at stations 4177, 377, 3925, 5275, 257), expressed as change in usable field capacity $\left[\%a^{-1}\right]$ calculated over the complete time series for each month based on monthly averages. Statistically non-significant values (p > 0.05) are indicated by a marker.

2.4.5 *Time series decomposition*

During modeling with Rbeast, the time series are decomposed into a trend component and a seasonal component, along with change points in both, seasonality and trend. Individual calculations are done for each depth increment at all measurement points. An example for NP3 at a depth of 170 cm is given in Figure 2.11. The trend component shows a positive slope before 2003. A changepoint in trend with a probability of 68% was discovered in February of 2003. After another changepoint with a lower probability in December 2003 (17%) the soil moisture trend stabilized at a lower level after a significant decrease in soil moisture levels between February and December. Changes in seasonality were detected in 2004 and 2006/2007. In between these, the amplitude of the seasonal variations was lower.
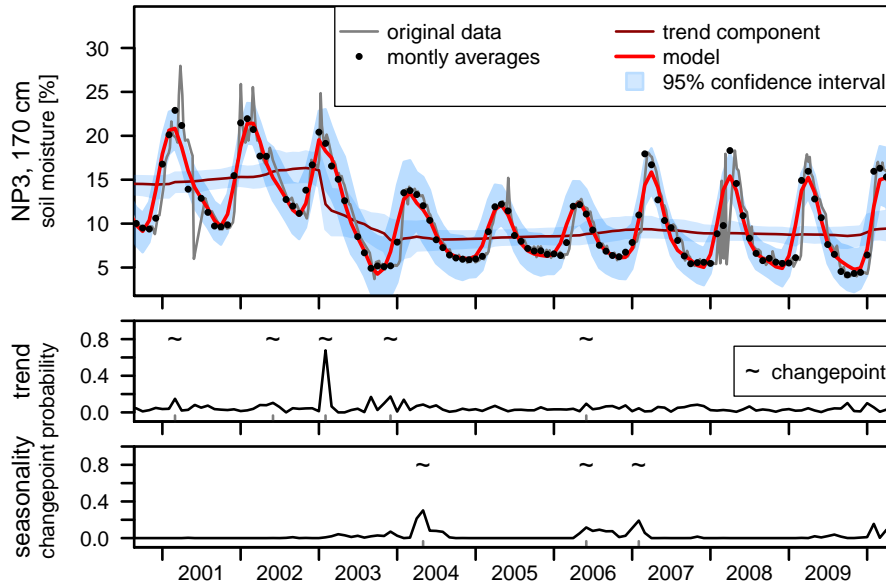
Figure 2.11: Results of time series decomposition for NP3 at a depth of 170 cm. Changepoints and their respective probability distributions are shown also.

In Figure 2.12 the main results of this model are shown for a measurement point in Field 1 (NP5) and Field 2 (NP10). This kind of decomposition allows for easier visual analysis of the underlying trend component (Figure 2.12). Probabilities of change point occurrence indicate times of significant changes in trend and seasonality. Overall, higher soil moisture contents are apparent before 2003 and during a shorter time period in 2013/2014. In the past few years, soil moisture is noticeably lower, especially in depths below 100 cm.

The decomposed time series of NP10 in Field 1 (NP9 - NP12 in Supplement A.5 and A.6) reveal higher initial soil moisture contents, followed by a gradual decrease over time. The decrease is most pronounced at the beginning of the measurement series, until around 1998 a more or less stable level of soil moisture is reached. The amplitude of seasonality at the top of the slope (NP9 and NP10) during this time of high initial soil moisture is lower. This is probably due to the maximum saturation of the soil being reached, leading to an increase in discharge from the soil instead of further increase in soil moisture content and storage. In 2003, a change point in trend is visible. Modeling resulted in high probabilities for this change point. In the following years, the soil moisture is at a lower level. Apart from the elevated soil moisture before 2003, higher soil moisture is also evident in 2013. The distribution of probabilities for a change point in trend does not show a clear cut during this event. Probabilities are elevated over a wider range of time. The amplitude of soil moisture seasonality is more or less stable for the remainder of the time series and does not show high probabilities.
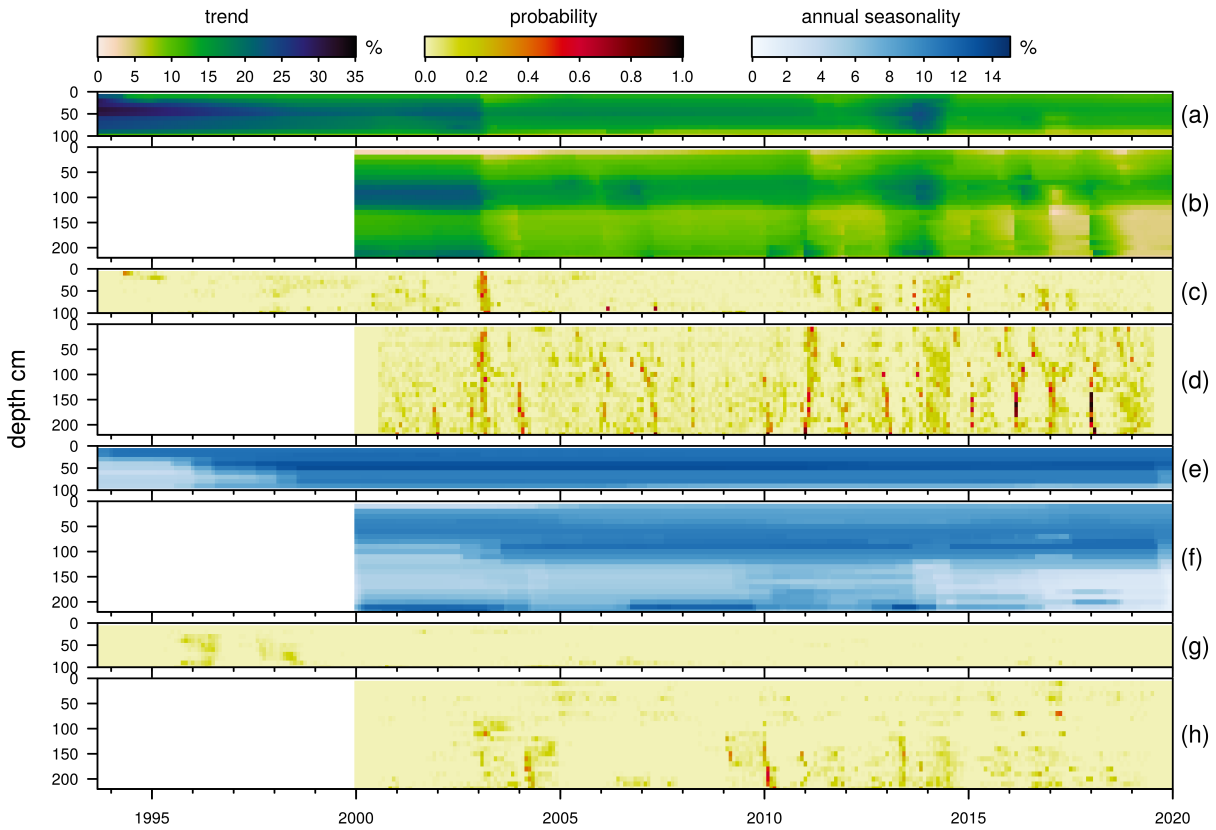
Figure 2.12: Results of modeling soil moisture at NP5 and NP10 with Rbeast. (a) Trend component of soil moisture time series at NP10 in Field 1. (b) Trend component of soil moisture time series at NP5 in Field 2. (c) Probability of change point in trend component at NP10 in Field 1. (d) Probability of change point in trend component at NP5 in Field 2. (e) Amplitude of annual seasonality derived from seasonal component at NP10 in Field 1. (f) Amplitude of annual seasonality derived from seasonal component at NP5 in Field 2. (g) Probability of change point in seasonality component at NP10 in Field 1. (h) Probability of change point in seasonality component at NP5 in Field 2.

Measurements at Field 2 (NP 3, NP5, NP6, NP7) also show higher initial soil moisture contents. As previously mentioned, depth dependence of soil moisture due to lysimeter construction is also visible in the deconstructed time series. No apparent trend is observable until the year 2003. A change point in trend and the corresponding probabilities is then visible around the same time as in Field 1. In the following year (2004) a change point in seasonality with elevated probabilities in the lower half of the RL at Field 2 occurred. Slightly elevated probabilities for this change point were already calculated for the year 2003 itself. In general, amplitudes of seasonal variations are higher towards the top of the RL. After the 2003 change point, higher amplitudes of seasonal variation are found lower in the RL than before (NP3, NP5, NP6). At NP7 (Supplement A.5 and A.6), the amplitude of seasonal variations at a depth of 80 cm increased after this point, but amplitudes in the soil below are significantly lower.

Another visible change point in trend with elevated probabilities is visible at the end of 2011. This change point cannot be seen in Field 1. After 2015, change points with elevated probabilities appear to occur almost every year. At the same time, reduction of soil moisture to a low level not observed previously occurs, mainly in the lower half of the RL. Because of a thinner RL, this effect cannot be observed in Field 1. In recent years from 2015 onward, amplitude of seasonal variation in the lower half of the RL is greatly reduced, because dry soil without the reoccurring annual re-wetting does not show significant seasonality.

Interruption of capillary rise due to lysimeter construction inhibits re-wetting of the lower soil from groundwater. Thus, results of this study might not be applicable to soils with a shallow depth to the groundwater surface or modeled values of usable field capacity. Boundary conditions are different for the modeled usable field capacities analyzed in this study. They are calculated from weather data and standardized soil properties. An additional source of soil moisture is provided by capillary rise due to a constant moisture boundary condition at the bottom of the model. The fact that some stations did show the same patterns as measured soil moisture, while other stations with same soil properties did not, could mean, that there are feedback mechanisms between soil moisture and the input parameters of the uFC model. Future studies should concentrate on these interconnections between soil moisture, groundwater recharge and groundwater level to determine if they amplify or dampen the temporal dynamics of soil moisture.

2.5 DISCUSSION

One possible explanation for the rapid change in soil moisture levels could be a change in soil properties (water retention, preferential flow

paths, hydraulic conductivity, soil structure, etc.) as a result of singular extreme events like the exceptionally dry year 2003. Augenstein et al. (2015) found, that there are hysteresis effects during drying and re-wetting of the soil at this site. Water bound in different states (e.g. adhesive water or water stored in the inter layers of clay minerals) has different migration times. The proportion of water bound in these different states therefore influences the drainage behavior (Šimůnek et al., 2003). During the period of increased soil moisture, water migrates into the inter layers of the clay minerals. (Schnetzer, 2017) This water can not be drained by gravity but still contributes to soil moisture. After discharge from the lysimeter stops, desiccation of these clay minerals may occur by evaporation into the soil air.

Another contribution factor might be changes in soil temperatures (Vanderborght et al., 2017; Schneider et al., 2021). These are usually highest around September and October. Temperature has great effect on viscosity of water and influences surface tension and contact angle. Thus determining how much water can be retained by capillary forces.

Hydraulic conductivity in the vadose zone is dependent on the moisture content. This feedback mechanism might amplify or dampen the hysteresis, depending on the proportions of bound soil moisture in different states (available pore water, pore water in enclosed cavities). Furthermore, extreme drying of the soil might lead to non-reversible desiccation of clay minerals or formation drying cracks as preferential flow paths, both leading to significant changes regarding the overall hydraulic functioning of the whole system. However, though these likely phenomena may occur, changes in soil water dynamics are also visible from the modeled uFC. These are not based on physical measurements which are dependent on time-constant soil properties, but rather use time constant properties of a model soil. The fact that these modeled values also show changes in their temporal soil moisture patterns gives ample evidence that the change points found are not merely a function of soil properties but of the local climate as well, which the modeled values are solely based on.

Changes in measured soil moisture at around the year 2003 could also be the result of the establishment of a vegetation cover after the construction of the lysimeter and over several consecutive years. The soil cover is important to prevent erosion and to lower overall percolation by increasing evapotranspiration. The system is designed with a vegetation cover as an integral part to it's proper functioning. However, Field 1, which has been constructed several years prior to Field 2, shows a similar change at the same time.

A similar change is likewise visible in the modeled data, but a change in vegetation cover is not used as an input to the model. It is still possible that vegetation and evapotranspiration both drive these changes in the model and the measured data, but then it has to be connected through the meteorologic parameters used in the

model (e.g. longer vegetation periods). Ionita et al. (2020) found that prevailing large-scale atmospheric circulation may impact atmospheric blocking over the north sea and central Europe and thus lead to extreme weather to be more persistent. If this is the case, the change towards elevated temperatures would also lead to an extension of the vegetation period. Thus increasing evaporation as a result of higher temperatures, and plant transpiration as a result of the longer vegetation period. If evapotranspiration is limited by the amount of available water, the difference between actual evapotranspiration and potential evapotranspiration will increase. Less evaporative cooling and lower ambient humidity will then increase temperatures even further, increasing the severity of a drought.

Robinson et al. (2016) found evidence for the existence of drought induced alternative stable soil moisture states. They observed a step change that occurred at the beginning of 2004 with an apparent transition to a new stable state in which soil moisture levels never reached saturation again. They found water retention characteristics to change due to a loss of organic material by increased organic matter mineralization under moderate drought conditions. According to their findings, the bottom boundary behavior was modified from a seepage face behavior before 2004, to free drainage after. For arid regions, strong positive feedback between vegetation and soil moisture has been described by D'Odorico et al. (2007). Small changes in environmental variables can lead to rapid and irreversible shifts between two alternate stable states (D'Odorico et al., 2007).

2.6 CONCLUSIONS

Aim of this study was to identify long term variations of soil moisture patterns and to identify the occurrence of particular events that led to tipping points in soil moisture levels. To achieve this, we analyzed high resolution soil moisture measurements from a test site near Karlsruhe, Germany. The data consists of depth-resolved, weekly soil moisture measurements in increments of 10 cm to a final depth of around 200 cm. Additionally, modeled data was used for comparison and interpretation of the results.

Over the investigation period, there is a significant decrease in soil moisture. This decrease is most pronounced at greater depths up to around 200 cm. Comparison of the measured soil moisture with modeled data of uFC for different stations indicates spatial heterogeneity, meaning future changes in soil moisture will vary in severity based on location.

The model depth of 60 cm is sufficient only when looking at the overall dynamics of uFC. Measurements of soil moisture at depths of up to two meters show significant seasonal variations well below the depth of the model. This large seasonal evaporation depth means,

change in soil moisture storage at these depths are an important component in future climate change models that can not be neglected and further real world measurements are needed in order to calibrate these models.

Times of largest changes to the soil moisture levels are the beginning of the vegetation period in April and the the end of the vegetation period in November. This indicates that changes in the vegetation cover might be the large driver of the observed depletion of soil water.

Bayesian modeling of the soil moisture data revealed change points in both trend and seasonality that had high probabilities. It seems reasonable to suggest that specific events of extreme drought had a lasting impact on soil moisture storage and led to deep desiccation of the soil. The most pronounced tipping point being the one during the exceptionally hot drought year 2003. After this point, soil moisture levels were on a lower level. In recent years, soil moisture levels declined even further, accompanied by a decline in the amplitude of seasonal variations. Thus, the impact of a decline in soil moisture is not limited to absolute level of the overall trend, but includes a decrease in seasonality. The overall dynamics are changed without any sign of a return to the previous state. This change in seasonality can not easily be described by simple linear models. Further application of the data and conclusions presented in this study can potentially be used in a much wider context when applied to numeric modeling of soil moisture, vegetation and climate as well as their interactions.

Part II

BLACK FOREST NATIONAL PARK

Chapter 3 is reproduced from: Merk M, Goeppert N, Goldscheider N (2020) "*Processes Controlling Spatial and Temporal Dynamics of Spring Water Chemistry in the Black Forest National Park*", Science of the Total Environment, 723, Article: 137742, doi:10.1016/j.scitotenv.2020.137742.

Chapter 4 is reproduced from: Merk M, Goeppert N, Goldscheider N (2020) "*Physicochemical and major ion data for springs in the Black Forest National Park, Germany*", Data in Brief, Article: 105645, doi:10.1016/j.dib.2020.105645.

Chapter 5 on the ongoing paired-catchment-study has not been published previously.

3

PROCESSES CONTROLLING SPATIAL AND TEMPORAL DYNAMICS OF SPRING WATER CHEMISTRY IN THE BLACK FOREST NATIONAL PARK

ABSTRACT

Spring water chemistry is influenced by many factors, including geology, climate, vegetation and land use, which determine groundwater residence times and water--rock interaction. Changes in water chemistry can have a profound impact on their associated ecosystems. To protect these ecosystems and to evaluate possible changes, knowledge of the underlying processes and dynamics is important. We collected water samples at 20 locations during 5 campaigns within the water catchment area of the upper Schönmünz river in the Black Forest National Park, Southwest Germany and analyzed them hydro-chemically for their contents of inorganic constituents, organic carbon content, fluorescence properties as well as several physico chemical field parameters and spring discharge. Results show that water chemistry is strongly dependent on geology and that the response of dissolved organic carbon to changes in hydraulic conditions is highly dynamic. Due to increased flow through the upper soil layer during and after rain events, more organic carbon is extracted from the soil and transported with the water. Fluorescence EEM measurements indicate an allochthonous source of this organic carbon. This study can be used as baseline to asses future changes and serve as a supplement to ongoing studies of the spring ecosystems.

GRAPHICAL ABSTRACT
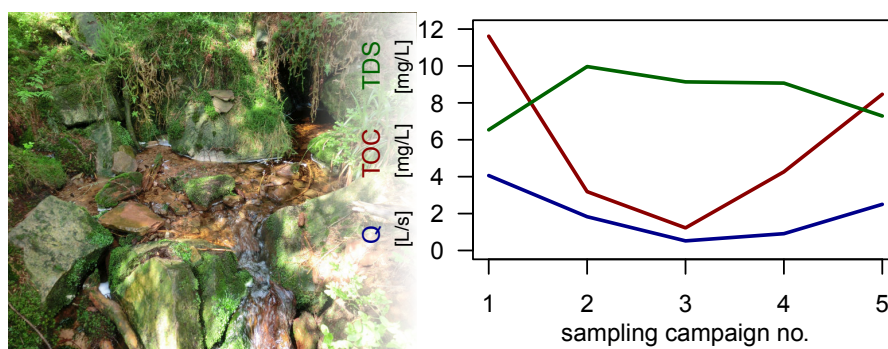
HIGHLIGHTS:

- Generally very low mineralization of spring waters in the Black Forest National Park

- Waters from sandstone aquifers and crystalline distinguished based on hydrochemistry

- High TOC and high TDS in water samples from study area are mutually exclusive

- TOC contributes significantly to conductivity in TOC rich samples

- Baseline for future studies of hydrochemistry in the Black Forest National Park

---

3.1 INTRODUCTION

Non calcareous uplands like the Northern Black Forest with its numerous water catchment areas are vulnerable ecosystems, sensitive to environmental impacts including acidification and climate change (Kløve et al., 2014). Springs are special habitats in that their hydrochemistry has important consequences on the composition of biota (Gerecke et al., 2011; Cantonati et al., 2020), especially at springs from siliceous substrata with very low mineralization (Beierkuhnlein, 1996). In non-acidified, very-low-alkalinity, naturally acidic spring waters emerging from granitoid rocks, even highly diverse and peculiar diatom microalgae communities with stenotopic indicator species could be found (e.g., Cantonati and Lange-Bertalot, 2011 and references therein). However, according to Bertrand et al. (2012), the literature on physical conditions in springs and the groundwater dependent spring ecosystems is relatively scarce. Understanding of principal processes governing the exchange dynamics of solute and water transport at all stages of the water cycle – from precipitation, groundwater recharge, spring discharge and surface runoff – are paramount in establishing effective protection policies. This should also include studies of groundwater–surface water interactions (Conant et al., 2019)

at the spatial and temporal scales relevant for groundwater dependent ecosystems (Kløve et al., 2011).

The deeper groundwater in the crystalline basement of the Black forest has previously been studied (Stober and Bucher, 1999; Stober, 1996), as has been the snowmelt stream water (Feger and Brahmer, 1986) and impact of soils on water chemistry (Feger et al., 1990). Forest influence on surface water chemistry and water yield (Brown et al., 2005), acid precipitation (Probst et al., 1987) and its mitigation by forest liming have been the focus of many publications (Armbruster et al., 2000, 2003; Feger et al., 1995; Hinderer et al., 1998).

Quadflieg (1990) studied the influence of forest, soil type, snowmelt water and amount of precipitation on spring water chemistry in a forested mountainous study area in the Bunter Sandstone formation in Hesse.

Current studies tackle questions regarding formation of surface and near surface runoff. Processes in the unsaturated zone on steep hillslopes play an important part in the transport of solute and particle pollutants. An increasing number of publications deal with climate change and possible impacts on groundwater recharge and quality. Reduction of mean annual precipitation as well as significant increase in numbers of heavy rains have already been reported by Thies (1994). Some case studies into groundwater recharge have already been applied to other catchment areas in the Black Forest (Neukum and Azzam, 2012) and other regions (Tetzlaff et al., 2007; Wang et al., 2018).

However, water chemistry and its impact on the dependent spring ecosystems in the newly established Black Forest National Park have so far not been thoroughly studied. Changes in water chemistry will in turn lead to changes of the spring, stream and lake ecosystems. Establishment of this baseline is important to asses future changes. Understanding the specific processes influencing the water chemistry will aid in their effective protection.

Aim of this study is to:

- characterize spring water according to geologic layer of discharge

- use water chemistry to differentiate between different types of flow (parallel to the slope or along interfaces of geologic formations with differing hydraulic conductivities)

- contribute to the general understanding of spatial and temporal dynamics of spring water chemistry in the newly established Black Forest National Park

- record a current baseline of hydrochemistry at springs located within the catchment area in order to be able to observe future changes due to land use variations or climate change

3.2   STUDY SITE

The study was conducted from May 2016 to May 2017 within the water catchment area of the upper Schönmünz River (16.5 km²) located in the Black Forest National Park, southern Germany (48.6°N, 8.2°E) (Fig. 1). The National Park has been established in 2014 and is the only national park in the state of Baden-Württemberg. A cirque lake (Wildsee) is the source of the main surface stream in the watershed. It is a tributary of the Murg river, which is a tributary of the Rhine.

3.2.1   *Topography and climate*

Elevation at the outflow of the surface is 550 m a.s.l. Higher elevations are found in the west (Seekopf, 1054 m a.s.l). The climate is humid and is characterized by lower average temperatures and higher annual precipitation compared to surrounding landscapes. Mean annual precipitation in the village of Schönmünzach, located a few kilometers down the valley to the east, is 910 mm/a. Mean annual precipitations can reach up to 2700 mm/a on the summit of the Hornisgrinde (1163 m a.s.l.) located to the west of the catchment area. Long term average monthly temperatures in Schönmünzach range from -2 °C in January to 17 °C in July.

Forest liming to improve water chemistry following acid precipitation has been studied in nearby catchment areas in the black forest (Sucker et al., 2009), but no data about forest liming within the current study area were available.

3.2.2   *Geology and hydrogeology*

The geology in the region is characterized by granite and sandstone. The bedrock is composed of two types of chemically similar granites (quartz, feldspar, mica). The western part is dominated by Seebach-granite (GSE), the eastern part by Forbach-granite (GFO). These are overlain by the late Permian sandstones of the tiger sandstone formation (zT) and the lower Triassic sandstones of the Bunter sandstone formation (mainly quartz, mica, clay minerals, iron oxides): the Eck-formation (suE), the building sandstone formation (sVs) and the upper pebble horizon (sVg).

The tiger sandstone formation is composed of well sorted, fluviatile sandstones. Grain sizes are mostly fine, occasionally middle to coarse grained . The base is formed by a layer of conglomerates containing clay and silt. Weathering and oxidation of the contained manganese and iron carbonates formed characteristic dark spots visible in rock samples.

The base of the Bunter sandstone formation is formed by the Eck-formation (suE). It is formed by weakly cemented conglomerates and

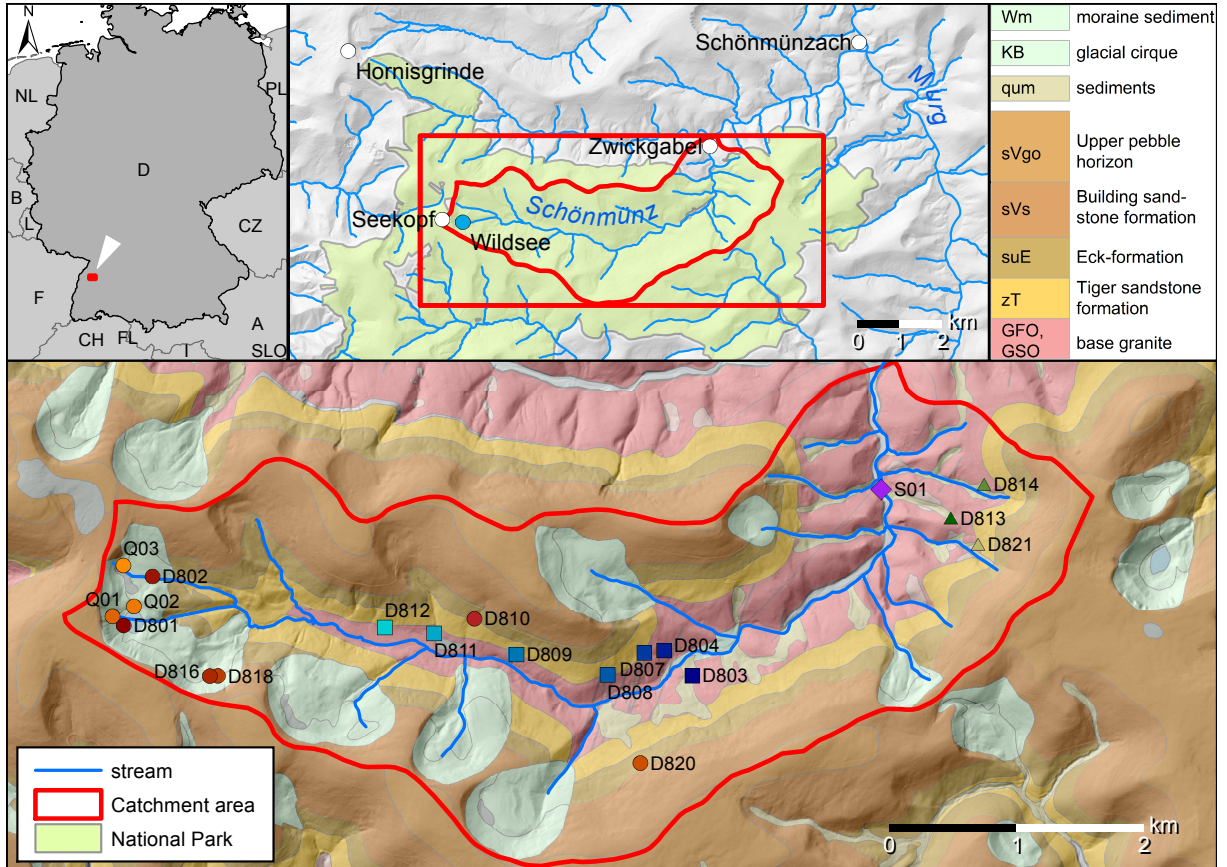Figure 3.1: Map of the Schönmünz water catchment within the Black Forest National Park, southern Germany. Geology: WaBoA. Geobasis-daten © Landesamt für Geoinformation und Landentwicklung Baden-Württemberg, www.lgl-bw.de, Az.: 2851.9-1/19. Symbols indicate the sampling locations at the selected springs based on hydrogeology and topography ($\bigcirc$, $\square$, $\triangle$) and the surface stream ($\diamond$).

coarse red-brown sandstones containing pebbles. Continuing upwards the Eck-formation is followed by the building sandstone formation consisting of coarse red sandstones and the upper pebble horizon. In contrast to the building sandstone formation the upper pebble horizon contains well rounded quartz pebbles.

Colluvium is present at hillslopes with northern exposition in the eastern part of the catchment area. Numerous glacial cirques (KB) with steep slopes, formed during the last glacial period (Würm), are present within the catchment area (Sommer et al., 1997; Thies, 1994). A geologic map of the catchment area is shown in Figure 3.1.

3.2.3 *Spring classification*

Due to the very large number of springs in the catchment area, it was not feasible to take samples at all springs. Therefore a representational selection had to be made in order to reduce the number of springs to include in the sampling program. A number of springs have already been selected prior to our sampling program and were already included in studies of their dependent ecosystems. Springs from differing topographic elevation, geologic layer of discharge, exposure and of spring type were selected. The final selection was based on stratigraphy, spring type as well as flora and fauna in the vicinity of the point of discharge.

Springs were grouped into three clusters based on stratigraphy, topography and hydrogeology. An additional group was formed for the surface stream.

- The Schönmünz River (S01), which is the main surface stream in the study area (surface stream).

- Springs located in the upper part of the catchment area within Building sandstone formation and Eck-formation (sandstone group).

- Springs discharging at the interface of the tiger sandstone formation and the underlying base granite (west granite group).

- Springs (D814, D813, D821) discharging from the granitic base rock in the eastern part of the catchment area (east granite group).

Locations of springs and their respective group memberships are shown in Figure 3.2.
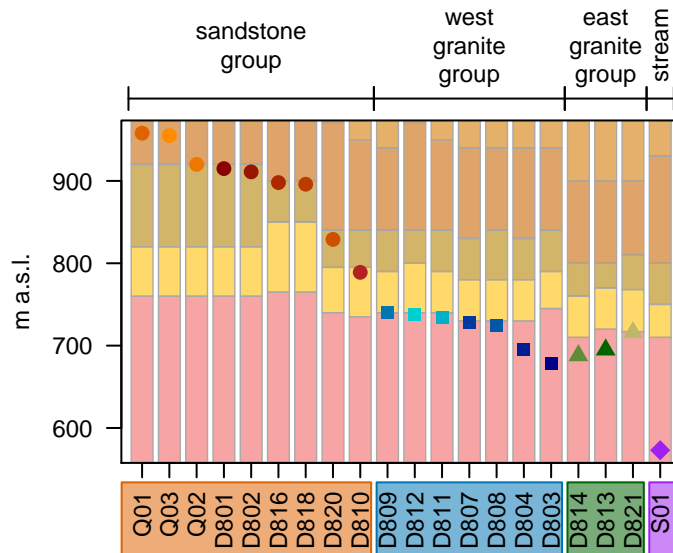
Figure 3.2: Grouping of sampling sites into three groups of springs (based on hydro-stratigraphy and location) and a fourth group representing the surface stream draining the entire catchment.

3.3 MATERIAL AND METHODS

3.3.1 *Field sampling*

Water samples were collected at 20 different locations within the study area during five different field campaigns. The dates of the sampling campaigns 1 to 5 are 25.05.2016 – 06.06.2016, 01.07.2016 – 08.07.2016, 05.09.2016 – 08.09.2016, 02.11.2016 – 07.11.2016 and 08.05. 2017 – 11.05.2017 respectively.

Due to the protection status of the catchment area within the Black Forest National Park, sampling was not possible during winter. Water samples and field measurements at the springs were taken as close to the point of discharge as possible. Differing flow conditions between sampling campaigns led to different locations of discharge at some of the monitored springs. This effect was especially pronounced at spring D810. During high flow conditions, this spring was located several meters further uphill than during low flow. The spring fell completely dry during most of the year. Other springs like Q02 and D802 also dried up in late summer and autumn. Water samples from the stream were taken at the same location during each sampling campaign.

Field measurements of pH, electrical conductivity (EC), dissolved oxygen (DO), the redox potential and temperature were taken using a WTW Multi 3430 connected to the respective probes. During the first sampling campaign, pH was measured using a digital Sentix 82 probe. As this probe is not well suited for waters with low mineralization, these measurements were not used in the data analysis. An analog

Sentix HW probe in combination with an analog TetraCon 325 for temperature compensation and a WTW Multi 340i was used during the second sampling campaign. During the other sampling campaigns a digital Sentix HW-T 900P probe was used, as this type is especially suitable for low mineralization waters. The Sentix HW and Sentig HW-T 900P showed reasonable agreement between sampling campaigns. The probe used for measurement of EC was a TetraCon 925 . An optical probe of type FDO 925 was used to determine DO. Redox potentials were not determined during the first sampling campaign. In the later campaigns, a Sentix ORP-T 900 was used. As redox probes are known to have long equilibration times, the probe was placed in the water at least 20 min before readings were taken. Measured values were converted into standard hydrogen electrode values by adding a temperature dependent reference voltage according to the documentation by the manufacturer. All probes except redox had an integrated temperature sensor. Measured temperatures differed slightly between probes. For correction of redox potentials and data analysis, the mean was used. Alkalinity was determined by titration of 100 mL of sample water with a solution of 0.025 mol/L hydrochloric acid in the field.

Water samples for determination of main anions and cations were filtered using 0.45 μm CA filters and stored in 30 mL PE bottles. For stabilization of samples, 50 μL nitric acid (65%, suprapur) was added to each cation sample in the field. Anions samples were left untreated. Silica samples were filtered using 0.45 μm CA filters and stored in 100 mL PE bottles.

Samples for determination of TOC were collected unfiltered in 50 mL brown glass bottles. Samples for DOC were filtered using glass fiber filters that were heat treated at 450 °C for at least 4 h prior to usage for removal of residual carbon within the filter. DOC samples were mutually stored in 50 mL brown glass bottles. For inhibition of bacterial and algae growth and removal of inorganic carbon, pH of DOC and TOC samples was lowered using 250 mL of hydrochloric acid (37%, suprapur), added to the sample bottle in the field.

Samples for fluorescence spectroscopy were taken unfiltered and stored in 50 mL brown glass bottles without addition of acid or other stabilizing agents. No samples for TOC and fluorescence analysis were taken during the second sampling campaign.

To prevent contamination and remove trace impurities, all sampling equipment (filters, syringes, sample bottles) were rinsed several times with sample water prior to usage. Filled sample bottles were collected in Styrofoam boxes for daily transport to the lab, using cool packs as necessary. All samples were subsequently stored in the dark at +8 °C and usually analyzed within one week.

3.3.2 *Laboratory Analysis*

Element concentrations of Mg^{2+}, K^+ and Na^+ were determined using ion chromatography (ICS-1100, Thermo Fisher Scientific). Ca^{2+} concentrations were determined by flame AAS (Perkin-Elmer 3030 B). Concentrations of Cl^-, SO_4^{2-} and NO_3^- were similarly determined using ion chromatography (ICS-2100, Thermo Fisher Scientific). TOC and DOC concentrations were determined by oxidative combustion at 850 °C and subsequent determination of carbon dioxide (Vario TOC cube, Elementar Analysesysteme GmbH).

Simultaneous measurement of absorbance spectra and fluorescence excitation-emission matrices (EEM) were done by fluorescence spectroscopy (Aqualog, Horiba Scientific). An integration time of 2 s was used for excitation wavelengths from 200 nm to 600 nm in steps of 3 nm. EEMs were corrected for inner filter effects and Raman scattering was removed. Measured intensities were used directly for further analysis without calibrating to any standard.

Measured absorbance spectra have a resolution of 3 nm starting at 201 nm and ending at 600 nm, requiring absorbance at 254 nm to be interpolated linearly between 252 nm and 255 nm.

Dissolved silica was measured using the classical molybdenum blue method.Ammonium molybdate is added to the sample to form a complex of dissolved silica and molybdic acid. This complex is reduced by stannous chloride to molybdenum blue. Absorption measurements were done at 810 nm using a lab photometer (Photolab 6600 UV-Vis, WTW).

Aluminum was determined using a photometer and a sample kit (Spectroquant aluminum test, Merck). Al dissolved by organic complexation with humic substances or other organic molecules (Al(org)) and Al that is dissolved inorganically as Al^{3+} or different Al-hydroxides (Al(inorg)) have not been measured separately.

Total iron ($Fe^{2+/3+}$) was determined using a test kit (Aquaquant iron test, Merck).

3.3.3 *Statistical analysis*

Based on the results of the elemental analysis and the field measurements, ion balances and saturation indices of several mineral phases were derived using PHREEQC Interactive (Version 3.3.7.11094) (Parkhurst and Appelo, 2013) and the WATEQ4 (Ball and Nordstrom, 1991) database. Saturation indices of calcite, quartz, hematite, feldspar and Al-minerals were used for comparison and differentiation of spring waters.

Low pH and a negative saturation index of calcite are possible indicators of acidification within a catchment area. The chemical acidification quotient (AQ) takes into account SO_4^{2-} and NO_3^- as

influencing parameters (Braukmann, 2000). It is calculated by dividing the molar sum of Ca^{2+} and Mg^{2+} by the molar sum of SO_4^{2-} and NO_3^- (Equation 3.1, Quadflieg (1990)). Acidification sensitivity classes were introduced by Hinderer and Einsele (1998). $AQ < 1$ indicate a surplus of the anions SO_4^{2-} and NO_3^- in relation to the cations Ca^{2+} and Mg^{2+}. They are classified as strongly acidified. AQ between 1 and 1.5 are indicator for acidified water. Water with AQ between 1.5 and 3 is classified as very sensitive to acidification.

$$AQ = \frac{(Ca^{2+}) + (Mg^{2+})}{(SO_4^{2-}) + (NO_3^-)} \tag{3.1}$$

Measured fluorescence EEMs for each sample were evaluated by calculation ratios of intensities (I) at different excitation-emission-wavelength pairs in order to obtain derived indices. These indices can be used to differentiate C(org). Humification index (HIX) was calculated according to Equation 3.2 and corrected according to Ohno (2002) to be concentration independent. Biological index (BIX) was calculated according to Equation 3.3 (Zhou et al., 2015).

$$\mathrm{HIX} = \frac{\sum I_{EX(254)}^{EM(435 \to 480)}}{\sum I_{EX(254)}^{EM(300 \to 345)} + \sum I_{EX(254)}^{EM(435 \to 480)}} \tag{3.2}$$

$$\mathrm{BIX} = \frac{I_{EX(310)}^{EM(380)}}{I_{EX(310)}^{EM(430)}} \tag{3.3}$$

HIX values range from 0 to 1 with higher values indicating increasing humification. Low values are expected for fresh autochthonous sources of organic carbon (Ohno, 2002; Garcia et al., 2015). BIX > 0.8 indicate freshly produced DOC by biological or microbial origin. BIX < 0.6 are indication for an allochthonous source of DOC (Garcia et al., 2015).

Hierarchical cluster analysis was done using the `hclust()`-function in the R system for statistical computing (R Core Team, 2017). Parameters were scaled by subtracting the column means and dividing by the column standard deviations prior to analysis. The `hclust()`-function was used with the complete linkage method to find compact, spherical clusters (Murtagh and Legendre, 2014). In hierarchical cluster analysis, distance between all pairs of parameters is calculated. The two parameters with the shortest distance are then combined and the distances to the other parameters recalculated. This is repeated until only one group is left.

Conditional inference trees were computed using the *partykit* add-on package (Hothorn and Zeileis, 2015) in R. The implementation of the conditional inference trees into the `ctree()`-function is described in Hothorn et al. (2006).

3.4 RESULTS AND DISCUSSION

3.4.1 *Field measurements*

Measured temperatures are decreasing with altitude (Figure 3.2 & Figure 3.3). Linear regression between mean water temperatures and elevation of sampling locations reveals a decrease of 0.55 °C ± 0.10 °C for every 100 m increase in elevation (R^2 = 0.64, p < 0.001). The influence of topography on air- and groundwater temperatures is well established knowledge. Seasonal and intra-day variations of temperatures are highest in the surface stream, with observed values ranging from 5.0 °C to 14.1 °C. Water temperatures are strongly influenced by atmospheric temperatures and adapt to changes very rapidly.

Measured electrical conductivities range from 16 µS/cm to 117 µS/cm with a mean of 35 µS/cm (SD = 22 µS/cm). These values indicate that the mineralization of the water in the catchment area is generally very low. At low pH and low mineralization, the contribution of H^+ to conductivity can be significant (pH 4, EC 35 µS/cm) (Braukmann, 2000). Some springs discharging from the sandstone aquifer (sandstone group) tend to exhibit larger variations in electrical conductivities. This is a result of dissolved organic carbon (DOC) contributing to overall conductivity without increasing total mineralization as humic substances may act as anions.

Redox potentials change with altitude (29.8 mV/100m ± 7 mV/100m). DO is lower at springs from the west granite group compared to the sandstone group (Figure 3.3), but a significant relationship with height has not been found (R^2 = 0.10, p = 0.177). A significant change with altitude has neither been found for electrical conductivity (R^2 = 0.05, p = 0.320) or alkalinity (R^2 = 0.29, p = 0.015).

3.4.2 *pH and acidification quotient (AQ)*

pH-values show a clear trend with elevation of sampling location. Linear regression between mean pH and elevation of sampling locations reveals a decrease in pH of 0.77 ± 0.10 for every 100 m increase in elevation (R^2 = 0.76, p < 0.001). Temperature dependence of pH alone does not explain this trend.

Sources of acidity are the cation-exchange capacity in *Sphagnum* moss (release of H^+ in exchange for other cations), dissociation of organic acids from decay of organic material (Siegel et al., 2006). Samples taken at higher altitudes tend to have lower pH-values. These springs discharge from the sandstone aquifer. Samples taken at lower altitudes tend to have higher pH-values. A jump in pH-values occurs between springs from the sandstone aquifer group and the springs discharging from the top of the granitic basement (Figure 3.3). It is
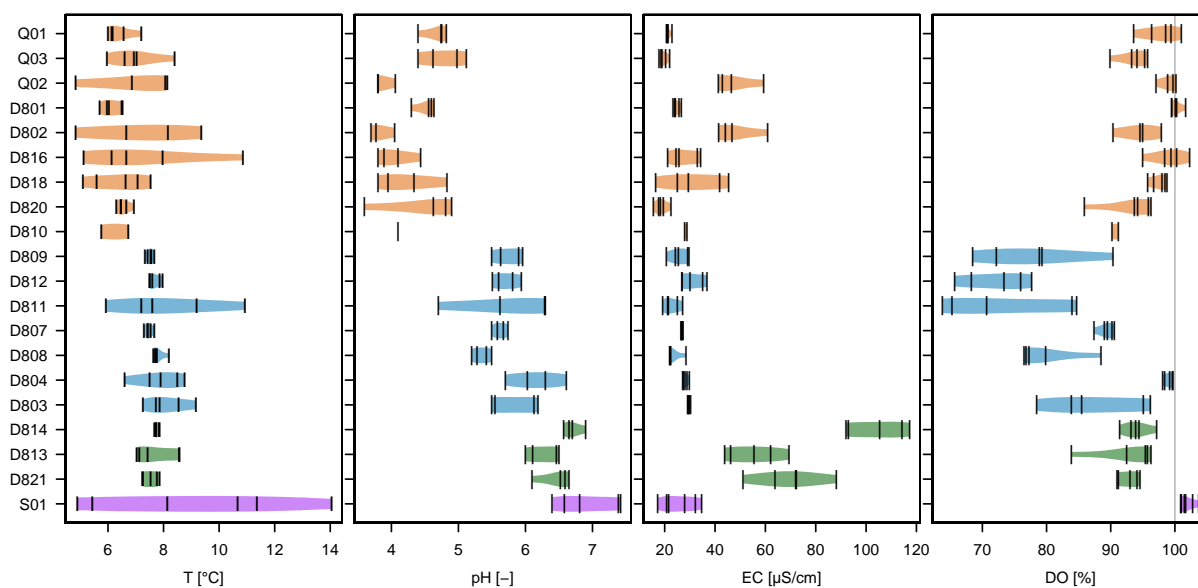
Figure 3.3: Temperature, pH, electrical conductivities and dissolved oxygen measured during the field campaigns ordered by elevation. Individual measurements are shown as black vertical bars. The width of the violins is proportional to the kernel density of the measured values.

concluded that pH is influenced mainly by aquifer type and mean residence times, rather than topographic elevation. Organic acids are thought to be the main cause of the acidity of the springs in the sandstone group. They were the main anion in bog waters from the glacial Lake Agassiz peatlands in Minnesota, US, according to Siegel et al. (2006). Siegel et al. (2006) also suggest, that biosynthesis of organic acids may stabilize discrete ranges of pH found in peat waters.

In Figure 3.4 the acidification quotient and pH are presented. Samples from the sandstone group fall into the Al-buffer and the ion exchange buffer systems. Samples from the west granite group fall mainly into the silicate buffer system. Surface water and samples from the east granite group fall into the carbonate buffer system. Except samples from the east granite group, all samples have an acidification quotient < 3, indicating acidification of these waters. Especially water from the sandstone group with acidification quotients < 1.

3.4.3   *Elemental analysis*

In Figure 3.5 the contents of Ca^{2+}, Na^+, NO_3^- and TOC are shown. Ca^{2+} concentrations are highest for samples from the east granite group (mean = 7.14 mg/L, SD = 2.49 mg/L) and lowest for samples from the sandstone group (mean = 0.35 mg/L, SD = 0.21 mg/L). Samples from the west granite group (mean = 1.66 mg/L, SD = 0.33 mg/L) and the surface stream have intermediate Ca^{2+} concentrations.
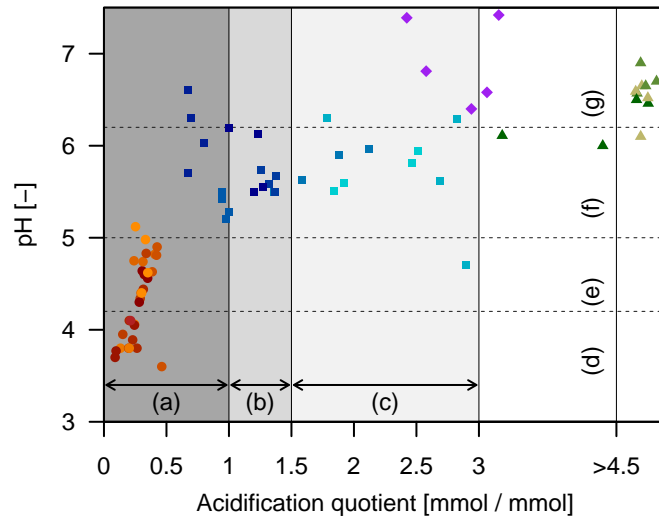
Figure 3.4: Acidification quotient *AQ* and pH of the water samples. The acidification classes a–c are: (a) strongly acidified, (b) acidified, (c) very sensitive to acidification. The different buffer systems d–g are: (d) Al-buffer, (e) ion exchange buffer, (f) silica buffer, (g) carbonate buffer. Water from the sandstone group is strongly acidified and uses the Al buffer and ion exchange buffer systems. Water from the other groups is using the silica buffer and carbonate buffer systems.

The sandstone group, west granite group and east granite group can clearly be distinguished based on their Ca^{2+} concentrations because their ranges of Ca^{2+} concentrations do not overlap.

Na$^+$ concentrations of samples from the sandstone group are similar to those from the west granite group. Exceptions are the two springs D803 and D804. These have significantly higher concentrations of Na$^+$. Their point of discharge is well below the interface between the tiger sandstone formation and the base granite within the base granite itself (Figure 3.2). Springs D813 and D814 from the east granite group also discharge from the base granite, but only show marginally elevated Na$^+$ concentrations. SO_4^{2-} concentrations at these springs are also higher when compared to the other springs within these groups, but differences are not as pronounced as for Na$^+$.

NO_3^- concentrations range from 0.25 mg/L to 3.9 mg/L (0.004 - 0.062 meq/L) with a mean of 1.66 mg/L (SD = 0.79). Concentrations of NO_3^- for samples from the sandstone group determine this range with both minimum and maximum concentrations determined in samples from the sandstone group. NO_3^- concentrations in samples from the sandstone group are very variable. This is true for an inter spring comparison as well as the seasonal variations. NO_3^- concentrations of samples from the west granite group span over a smaller range and seasonal variations are not as pronounced when compared to the sandstone group.

The proportions of NO_3^- in relation to the sum the anions are distinct, depending on group membership. Linear regression over all samples from all four groups does not yield a significant correlation (R^2 = 0.007, p = 0.408). Nitrate concentrations predict the sum of anions best for samples in the sandstone group (a = 0.03 meq/L $\pm$ 0.005 meq/L, b = 1.74 $\pm$ 0.17, R^2 = 0.73, p < 0.001) and the pink group (a = 0.05 $\pm$ 0.06, b = 15.64 $\pm$ 4.68, R^2 = 0.73, p < 0.029). For samples from the west granite group, the linear regression yields a rather similar slope as in the sandstone group, but with different intercept (a = 0.16 $\pm$ 0.03, b = 2.91 $\pm$ 1.00, R^2 = 0.20, p < 0.001). The lowest proportion of NO_3^- is found in samples from the east granite group (a = 0.14$\pm$ 0.13, b = 31.50$\pm$ 5.88, R^2 = 0.69, p < 0.001). The proportion of NO_3^- in the sandstone group is the lowest, even though the highest NO_3^- concentrations were found in samples from this group.

TOC in samples from the sandstone group range from 0.86 mg/L up to 27.54 mg/L and are – compared to NO_3^- – even more variable, considering inter spring comparison and seasonal variations. TOC in samples from the east granite group and west granite group is generally lower and less variable than in samples from the sandstone group.

Organic acids act as anions and contribute to overall charge balance. Unbalanced charge in analysis from similar waters (DOC rich) was reported by Siegel et al. (2006). They used a triprotic analog model for organic acids to calibrate charge balance. Furthermore, organic rich waters do not show clear dissociation endpoints during alkalinity titration (Siegel et al., 2006) leading to greater uncertainties in its determination. At low pH and low mineralization, the contribution of H^+ to the charge balance can be significant. At pH 4, contribution of H^+ to the water solute budget is 0.1 meq. Absolute differences in charge range from -0.2 meq/L to 0.4 meq/L (mean = 0.02 meq/L, SD = 0.12 meq/L). Because of the very low mineralization of the water, these small deviations lead to calculated ion balances ranging from -48% to 63%.

3.4.4 *Major ion chemistry*

The Piper diagram (Piper, 1944) in Figure 3.6 shows the contribution of the major anions and cations to the total ionic charge as percentage of total milliequivalents per litre (meq/L). Color corresponds to group membership. Samples of all field campaigns are shown.

In samples from the sandstone group, the contribution of Ca^{2+} ranges from 3.6% up to 42% (mean = 24.5%, SD = 8.8%), the contribution of Mg^{2+} – due to the Ca^{2+}:Mg^{2+} ratio of 2:1 – is up to 25% (mean = 14.4%, SD = 4.0%). Na^+ and K^+ combined are the main cations in these samples and they contribute the missing 43% to 86% (mean = 61.1%, SD = 9.6%). Individually, Na^+ contributes between 19.5% and
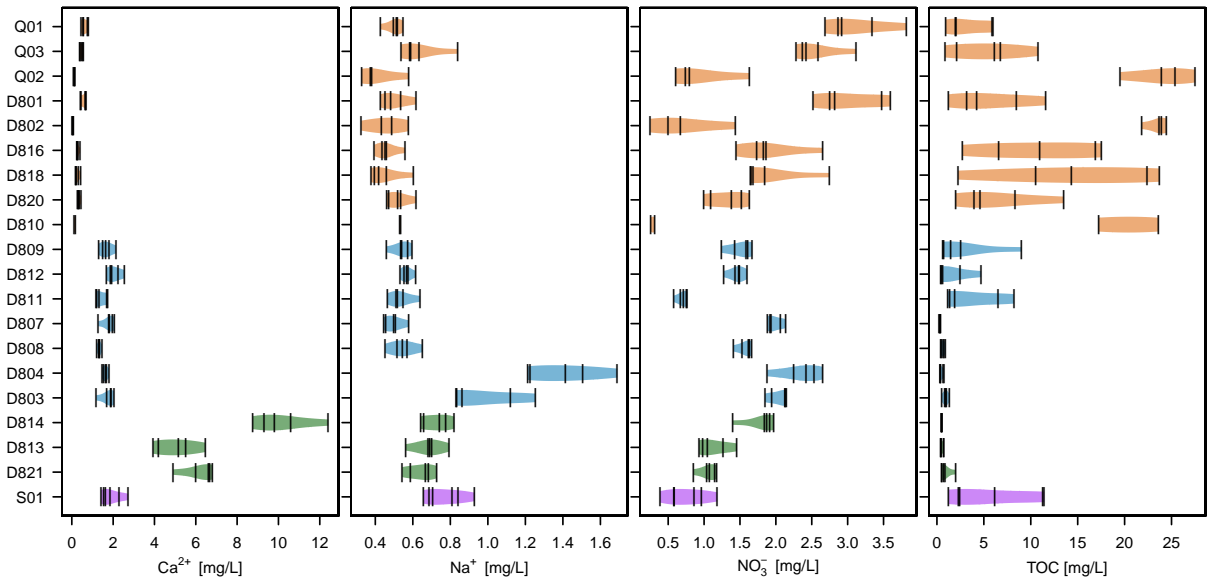
Figure 3.5: Results of inorganic analysis of Ca^{2+}, Na^+ and NO_3^- and TOC.

76.3% (mean = 37.1%, SD = 14.0%) and K^+ contributes between 7.7% and 36.2% (mean = 24.1%, SD = 7.8%). The average amount of Na^+ (mean = 0.021 meq/L, SD = 0.004 meq/L) is higher than the amount of K^+ (mean = 0.017, SD = 0.009 meq/L) in samples from this group (sandstone group).

In samples from the west granite group, contribution of Ca^{2+} is between 28.1% and 50.5% (mean 42.3%, SD = 5.0%) and is therefore higher than in samples from the sandstone group. Similarly, the contribution of Mg^{2+} in samples from the west granite group is larger (min = 16.3%, max = 37.5%, mean = 27.5%, SD = 6.0%) than in samples from the sandstone group. The contribution of Na^+ and K^+ combined in samples from the west granite group is significantly lower (max = 48.3%) than in samples from the sandstone group (min = 43.8%). Contributions of Na^+ (mean = 16.2%, SD = 7.0) and K^+ (mean = 14.0%, SD = 3.6%) are very similar, with contribution of Na^+ reaching a higher maximum (max = 35.3%) compared to K^+ (max = 23.2%). The proportion of Na^+ to K^+ in springs D803 and D804 (west granite group) is higher than in all other samples.

Contribution of Ca^{2+} in samples from the surface stream (S01) (mean = 43.5%, SD = 5.1%) is similar to samples in the west granite group. Contribution of Mg^{2+} is, on average, a little higher (mean = 31.2%, SD = 3.3%), mainly due to a higher minimum (min = 29.9%). Contribution of Na^+ (min = 12.5%, max = 17.9%, mean = 15.7%, SD = 2.5%) is higher than contribution of K^+ (min = 8.3%, max = 11.9%, mean = 9.5%, SD = 1.3%).

Main cation in samples from the east granite group are Ca^{2+} (min = 47.4%, max = 52.8%, mean = 50.1%, SD = 1.3%) and Mg^{2+} (min = 34.8%, max = 42.7%, mean = 39.5%, SD = 2.5%). Contributions of Na^+

(mean = 4.6% SD = 1.3%) and K^+ (mean = 5.8%, SD = 1.5%) are only marginal and reach a combined maximum of 15.1% (mean = 10.4%, SD = 2.6%).

According to Stober and Bucher (1999), plagioclase weathering is the most important process controlling water chemistry in the near surface crystalline rocks of the Black Forest. Ca^{2+} is added to the water by reaction of meteoric water with anorthite under formation of an insoluble Al mineral, usually kaolinite. Na^+ can be added to the water solute budget by dissolution of Na-rich plagioclase or secondary Na-rich mica (Stober and Bucher, 1999). Weathering of biotite and hornblende, both abundant minerals in granites from the Black Forest, contributes to Mg^{2+} and K^+ being added to the solute budget of the waters (Stober and Bucher, 1999). Low Na^+, Mg^{2+} and Ca^{2+} concentrations in waters from Bunter sandstone were found because of a lack of feldspar. More K^+ was found as a result from weathering of mica and illite according to Zöttl et al. (1985).

The ratio of HCO_3^- in samples from the sandstone group is below 33% (mean = 7.3%, SD = 10.5%), some samples with low pH (pH<4.2) contain no HCO_3^-. Cl^- plus NO_3^- contributes over 40% (except in one sample with HCO_3^- equal to zero). SO_4^{2-} contributes 23.5% to 72% of the anions (mean = 35.4%, SD = 9.9%). SO_4^{2-} contribution is higher in samples that contain no HCO_3^-. On average contribution of Cl^- (mean = 11.9%, SD = 6.9%) is lower than that of NO_3^- (mean = 34.4%, SD = 11.0%).

Contribution of Cl^- plus NO_3^- from samples in the west granite group is below 33.8% (mean = 21.4%, SD = 4.8%). Individual contribution of Cl^- (mean = 10.6% SD = 2.6%) and NO_3^- (mean = 11.4%, SD = 3.5%) are very similar. Proportions of SO_4^{2-} (mean = 21.8%, SD = 8.1%) and Cl^- plus NO_3^- (mean = 21.9%, SD = 4.8%) are on average also similar. Compared to the sandstone group, samples from the west granite group have lower proportion of HCO_3^-, lower of Cl^- plus NO_3^- and higher proportion of SO_4^{2-}.

Samples from the east granite group have the lowest proportion of Cl^- plus NO_3^- (mean = 6.5%, SD = 1.2%), lowest proportion of SO_4^{2-} (mean = 9.3%, SD = 2.0%) and the highest proportion of HCO_3^- (mean = 84.2%, SD = 2.9%).

Samples from the surface stream are similar to the samples of the west granite group, but tend to have higher proportions of HCO_3^- and lower proportion of NO_3^-.

One mechanism influencing water chemistry is atmospheric precipitation and the amount of dissolved inorganic constituents (Gibbs, 1970). Contribution of slopes to groundwater recharge is underestimated in traditional models (Pflanz et al., 2014). The mineralization of precipitation is generally very low. Precipitation forms one end member in Figure 3.7. No suitable data of recent and close by precipitation chemistry was available for comparison. Through soil passage
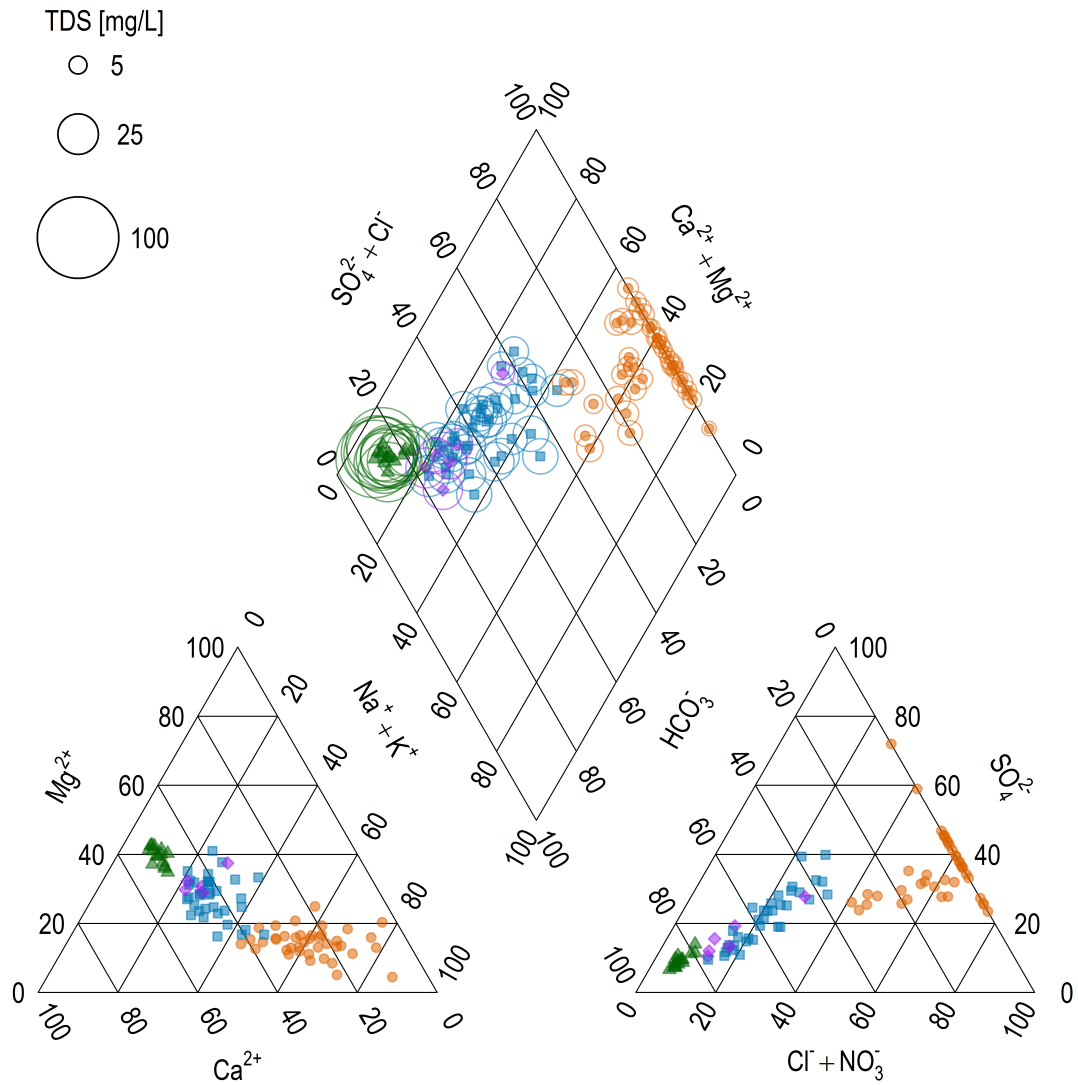
Figure 3.6: Piper diagram of all samples. Colors and shapes correspond to group membership of springs as described in the text. A clear progression of the water composition can be identified from the sandstone group to the surface stream and east granite group via the west granite group.
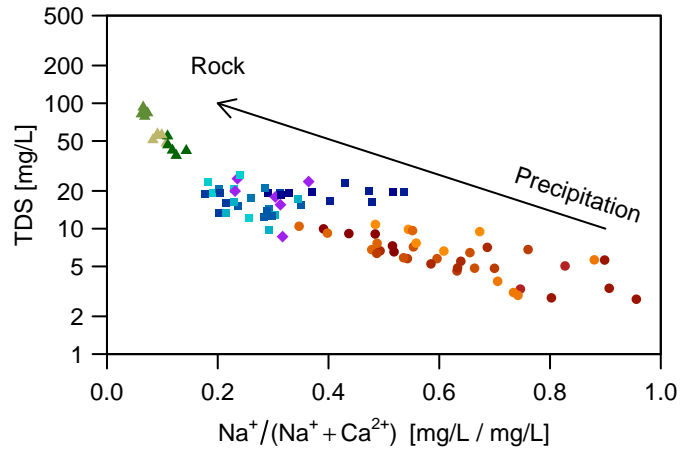
Figure 3.7: Progression of water chemistry from precipitation to rock domi-
nance according to Gibbs (1970). Water from the sandstone group
can be classified as precipitation dominated. Water from the east
granite group can be classified as rock dominated. Water from
the west granite group and the surface stream are intermediate.

and transport to and in the groundwater, mineralization is increasing
by dissolution of surrounding rocks and soil matrix. The dissolution
is controlled by a balance between mean transit time and the mean
effective reaction rates (Maher and Druhan, 2014). The proportion of
Na^+ and Ca^{2+} is shifted towards a lower percentage of Na^+, as more
Ca^{2+} is dissolved over time (Gibbs, 1970).

According to this classification, samples from the sandstone group
fall into the precipitation dominated category. Measured TDS had a
minimum of 2.7 mg/L (mean = 6.4 mg/L, SD = 2.3 mg/L). Variations
of all major ions are listed in Table 3.1. Samples from the east granite
group contain a higher percentage of Ca^{2+} and represent a more
dissolution-dominated water chemistry. Measured TDS reached a
maximum of 93.0 mg/L in samples from the east granite group. This
can still be considered low mineralization and samples are strongly
undersaturated (SI Calcite < -2). Water samples from the west granite
group and the surface stream are located between these two groups.
Notable are the two springs D803 and D804. These springs have
more or less constant amounts of TDS (mean = 19.2 mg/L, SD = 1.9
mg/L) while the proportion of $Na^+/(Na^++Ca^{2+})$ is larger and more
variable (mean = 0.41 , SD = 0.09) than that of the other springs in
the west granite group (mean = 0.25, SD = 0.05). Signs of evaporation
(increasing TDS and increasing $Na^+/(Na^++Ca^{2+})$) were not observed
during this study.

3.4.5 *Organic carbon*

Generally measured content of TOC and DOC in all the samples were
almost the same (a = 0.993 ± 0.004, b = 0 mg/L, R^2 = 0.99, p < 0.001, n

Table 3.1: Summary statistics (minimum, maximum, mean, standard deviation) of major ions.

	min. mg/L	max. mg/L	mean mg/L	SD mg/L
Ca^{2+}	0.02	12.41	1.99	2.52
Mg^{2+}	0.02	6.33	0.89	1.28
Na^+	0.32	1.69	0.63	0.24
K^+	0.07	1.93	0.95	0.42
Cl^-	0.37	1.29	0.79	0.18
NO_3^-	0.25	3.82	1.66	0.79
SO_4^{2-}	0.68	5.87	2.12	1.05

= 96). All samples were clear with some larger particles visible only in a low number of samples. This is also true for samples with elevated levels of DOC as indicative by visible yellow coloration. Therefor POC is of minor importance in the survey area. Willey et al. (2000) found a similar correlation and discontinued filtration of their samples for analysis of organic carbon. Only TOC measurements were used for data evaluation, as these are less likely to be contaminated by filtration equipment during the sample taking process. Furthermore, TOC samples are thought to be more similar to the fluorescence/absorbance samples that were taken unfiltered in a similar fashion.

There is a significant correlation between DOC and absorbance at 254 nm (R^2 = 0.99, p < 0.001, n = 77). Current studies try to link DOC with results of fluorescence measurements. Cumberland and Baker (2007) suggest that in natural environments, this correlation is strongest, with a decrease in correlation strength with anthropogenic influence. In this study, correlation of DOC with fluorescence in peak A was very strong (R^2 = 0.98 , p < 0.001, n = 77). This confirms the low anthropogenic influence on water DOC that was expected in the National Park, thus confirming the earlier findings.

In Figure 3.8 HIX and BIX are shown. Samples from the sandstone group have HIX close to 1 (mean = 0.95, SD = 0.01). Samples from the west granite and east granite group have lower HIX (west granite: mean = 0.77, SD = 0.18, east granite: mean = 0.75, SD = 0.17). Samples from the surface stream have similar HIX and BIX as samples from the sandstone group.

BIX values of samples from the sandstone group are between 0.38 and 0.50 (mean = 0.43, SD = 0.03) and are significantly lower than BIX values of samples from the west granite (mean = 0.73, SD = 0.54) and east granite (mean = 0.68, SD = 0.14) groups. Again samples from the surface stream have similar BIX as samples from the sandstone group.

According to the classification described in subsection 3.3.3, organic carbon in water samples from the sandstone group and the surface
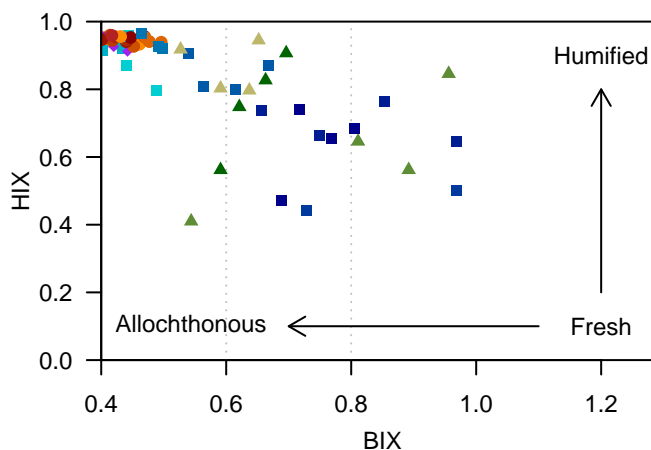
Figure 3.8: Humification Index (HIX) and Biological Index (BIX). Water from the sandstone group has HIX > 0.9, indicating an allochthonous source of DOC. Water from the west granite and east granite groups is less humified, indicating an autochthonous source of DOC.

stream is of allochthonous origin. Organic carbon in samples from the east granite and west granite groups is less humified, indicating a more autochthonous source of organic carbon.

As can be seen in Figure 3.9, high TDS and high TOC are mutually exclusive. Water samples from the sandstone group exhibit large variations in TOC (mean = 11.6 mg/L, SD = 8.8 mg/L) and almost no variation in TDS (mean = 6.4 mg/L, SD = 2.3 mg/L). Water samples from the east granite group exhibit almost no variation in TOC (mean = 0.7 mg/L, SD = 0.4 mg/L) and relatively large variation in TDS (mean = 60.8 mg/L, SD = 18.1 mg/L).

The process by which DOC enters surface stream water depends on precipitation and flow conditions (Terajima and Moriizumi, 2013). Sommer et al. (1997) link high DOC, Fe, Al and P with dominating lateral fluxes in the soil cover. Bernal et al. (2018) found a protein-like character of stream DOC, that they linked to microbial sources and recent biological activity within the stream. They concluded that DOC is not conservatively transported but can be internally produced, transformed and used in the stream water.

3.4.6 *Temporal dynamics*

Temporal development of hydrochemistry is shown in Figure 3.10. TDS at the springs is more or less constant during the different field campaigns. TDS in the surface stream is increasing from sampling one to sampling three – during spring through summer – and decreasing again after summer when discharge is increasing again.

TOC is decreasing with the discharge of the springs until a minimum during sampling campaign three during summer is reached. An event
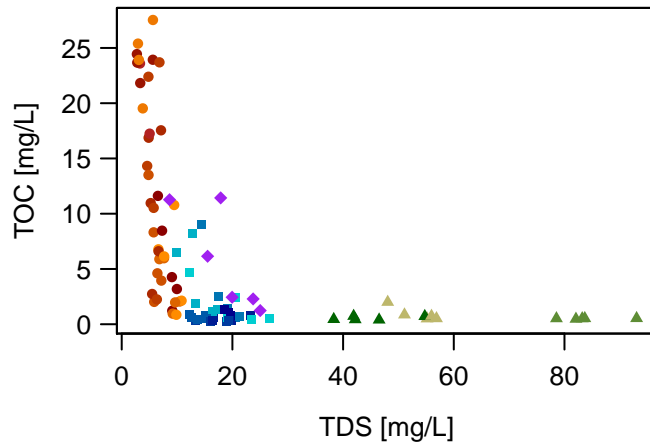
Figure 3.9: Measured TDS and TOC are mutually exclusive. Water from the sandstone group exhibits large variations in TOC and small variations in TDS. Water from the east granite group exhibits large variations in TDS and almost no variation in TDS.

of strong precipitation during the fourth sampling campaign led to a sudden increase of TOC concentrations in water samples from springs in the sandstone group as well as the surface stream and some springs from the west granite group. In a study of a nearby catchment area, Casper et al. (2003) concluded that DOC-rich water forms a rapid lateral runoff component and originates from the upper soil horizons. Dependent on precipitation and flow conditions, DOC is extracted from the forest soil and rapidly transported to the surface stream near the surface.

3.4.7 *Aluminum*

Measured Aluminum concentrations range from the detection limit up to 0.56 mg/L. Over half of the measured Al concentrations were below the detection limit. Concentrations above 0.3 mg/L are only found in samples from the sandstone group with pH < 5. Samples from the Schönmünz river (S01) contained some measurable amount of Al during field campaigns no. 4 and 5. Not all samples with low pH contain high Al concentrations. pH alone does not explain high Al concentrations. The mobilization of Al-species from the soil can not be described by simple cation exchange with H^+ (Ross et al., 2008).

There is a reasonable correlation between Al and TOC concentrations (R^2 = 0.69, $p < 0.001$). This indicates that part of the dissolved aluminum ions form complexes with organic functional groups. In a kinetic study, the release rate of Al was found to increase with concentration of organic acids (Li et al., 2006). A similar correlation of Al and TOC in water samples from surface streams in the Black Forest has already been reported by Zöttl et al. (1985). Therefore, measured Al concentrations represent only part of the total Al contained within
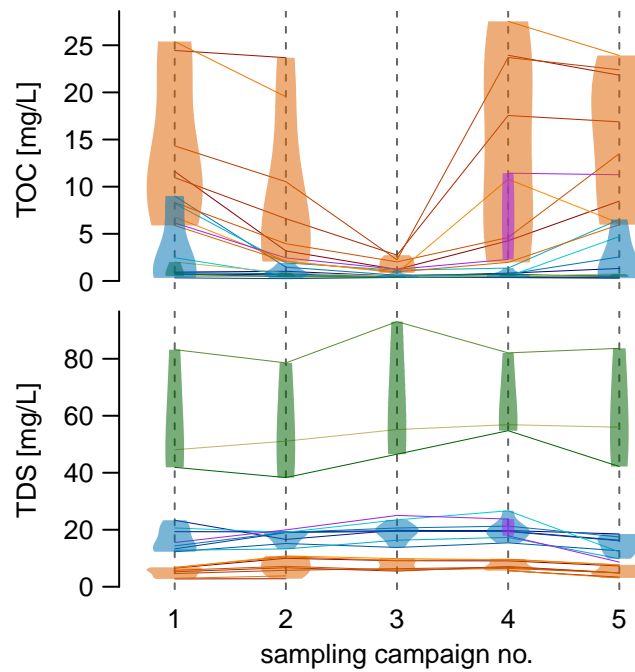
Figure 3.10: Temporal development of TOC and TDS during the five field campaigns. TOC during field campaign no. 3 (low flow conditions) was very low, especially in samples from the sandstone group and in comparison to the other sampling campaigns. Temporal variations of TDS are much lower than variations of TOC.

the water (Siegel et al., 2006). According to Thies (1994), aluminum is on average 60% to 78% organically bound, depending on source of water (groundwater spring – episodic spring) at a nearby lake (Lake Huzenbach).

Al(org) is the dominating Al species in DOC rich waters (Baur et al., 1988). Mobility of Al in the upper soil is mainly controlled by DOC (Baur and Feger, 1992). Seasonal variations in the proportion of organically bound Al species has already been described in the literature (Quadflieg, 1990). The chemical structure of the organic components in the soil is changing with depth. A recent study (Roth et al., 2019) found a decay of plant C(org) in the top most layers and increase of more complex C(org) formed by biological activity. These different organic substances may lead to a change in organically bound Al species and mobilization of Al(org).

Dissolution of Al in soils containing few base cations is an important buffering process (Li et al., 2006) when acidity is added in snow melt waters.

3.4.8 *Silica*

Measured silica ranges from 0.98 mg/L to 4.71 mg/L (mean = 2.65 mg/L, SD = 0.66 mg/L). Mean measured silica in samples from the west granite group (mean = 3.02 mg/L, SD = 0.68 mg/L) is slightly higher than in all other groups (mean = 2.44 mg/L, SD = 0.56 mg/L). Samples from the sandstone group have the lowest average silica (mean = 2.22 mg/L, SD = 0.50 mg/L).

Waters from springs D803 and D804 have positive saturation indices for quartz. Although precipitation of quartz is slow at positive SI, it is no longer dissolved under these conditions. Over saturation of quartz is therefore often attributed to the hydrolysis of alumosilicate minerals and delayed precipitation of quartz (Bennett and Siegel, 1987). Silica in water samples from these two springs must come from additional sources other than quartz, like alumosilicate minerals, feldspar and mica, which are present in the granitic base rock, or amorphous silica. A typical alteration equation of orthoclase is given in Equation 3.4. Weathering of silica minerals is a sink for CO_2 (Hartmann et al., 2009). The other springs discharging from overlying sandstone have lower SI quartz, as few other sources for silica other than quartz are available. In shallow soil, silica concentrations are not dependent on contact time, but are driven by the equilibrium reaction of water with meta-stable amorphous alumosilicates (Asano et al., 2003).

$$2KAlSi_3O_8 + 2CO_2 + 11H_2O \longrightarrow$$
$$2K^+ + 2HCO_3^- + 4H_4SiO_4 + Al_2Si_2O_5(OH)_4 \quad (3.4)$$
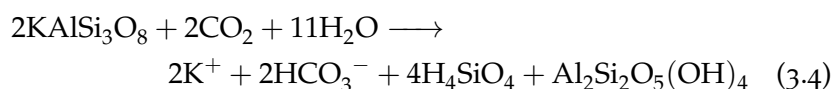
Solubility of quartz is dependent on temperature (Rimstidt, 1997) and pH (Knauss and Wolery, 1988). This may results in a co-dependence on elevation (Drever and Zobrist, 1992). Increased solubility of quartz has been observed in waters from organic rich soils (Bennett and Siegel, 1987). High DOC is available in waters during high flow conditions at springs in the sandstone group and the surface stream. Equilibration times during these periods are thought to be to short to reach an over saturation.

3.4.9   *Cluster analysis*

Results of the hierarchical cluster analysis show proximity of parameters with similar characteristics (Figure 3.11). There are two large groups. The first group contains the components influenced by redox chemistry of the water. The second group contains more conservative components including elements that are not involved in redox reactions.

TOC and DOC have a short distance. As mentioned in subsection 3.4.5 the TOC and DOC are very similar, because there is little to no POC. TOC and DOC are closely related to Fe and Al, both of which are pedogenic metals. Low molecular organic compounds are transported by percolating water. These form organic complexes with Fe and Al, leading to mobilization of these elements during the process of podsolisation (Zöttl et al., 1985). DO is also found within that group, but with a larger distance.

Ca^{2+}, Mg^{2+} and HCO_3^- have a short distance in the cluster tree. A common source for these has already been discussed in subsection 3.4.4. The acidification quotient is also found within the same group, as it is mainly influenced by the Ca^{2+} and Mg^{2+} concentrations (Equation 3.1). EC is found within the same group. Samples from the east granite group with high TDS – especially high Mg^{2+} and Ca^{2+} concentrations – have significantly higher electrical conductivities compared to samples from the other groups. As described in subsection 3.4.5, DOC and TDS are mutually exclusive. They have a longer distance in the cluster tree, despite DOC contributing to electrical conductivity in organic rich samples.

The topographic elevation falls into the same group as redox potential and NO_3^- concentration. Redox potentials in samples from the sandstone group are, on average, higher (mean = 464 mV, SD = 47 mV) than those of the other groups (mean = 403 mV, SD = 60 mV).

Na^+ and silica have a medium distance in the cluster tree. They cluster with temperature and SO_4^{2-} concentration. K^+ and Cl^- concentrations cluster together with pH.

All five groups of parameters described above contain at least one of the parameters measured in the field. As described in subsection 3.4.1, temperature, redox potential and pH are dependent on topographic
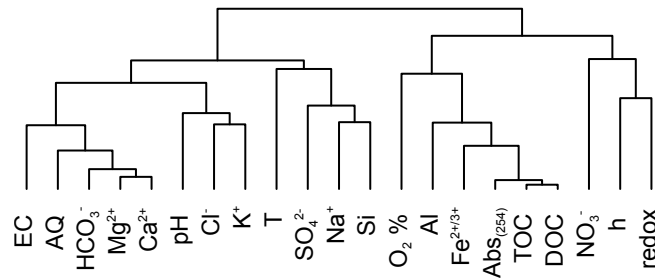
Figure 3.11: Cluster analysis reveals two distinct groups of parameters. A first group containing the parameters influenced by redox chemistry and a second group containing the more conservative components and elements that are not involved in redox reactions.

elevation as a result of geologic stratification and spring discharge from the different formations at different altitudes. Different source rocks provide different availability of solutes (bulk mineral composition) to the water chemistry. Mechanisms of dissolution may be dependent on additional influences like predominant pH, availability of free oxygen, a certain redox state or availability of organic compounds for complexation.

3.4.10 *Conditional inference trees*

A Conditional inference tree is given in Figure 3.12. This confirms that water samples from the different geologic formations can be clearly distinguished, using only two parameters. The classification into the four groups based on geology can be modeled by concentration of Ca^{2+} and DO alone. Distinction of springs D803 and D804 from the rest of the west granite group can be achieved by a third parameter. In this case, a similarly good result with significant p-values can be achieved by use of Ca^{2+} concentration, DO and SO_4^{2-} concentration.

3.5 CONCLUSIONS

The first aim of this study was to characterize spring water according to geologic layer of discharge. There is clear evidence for an influence of geology on spring water chemistry within the catchment area. Water from the sandstone aquifer and water discharging at the interface of the Tiger sandstone formation with the base granite can be distinguished based on their Ca^{2+} and Mg^{2+} concentrations. Springs from the sandstone aquifer at higher altitudes have lower concentrations of these elements than springs at the top of the granitic basement. There is no overlap when comparing the two groups based on the concentration ranges of these two elements. Springs discharging from the granitic basement below the interface to the overlaying
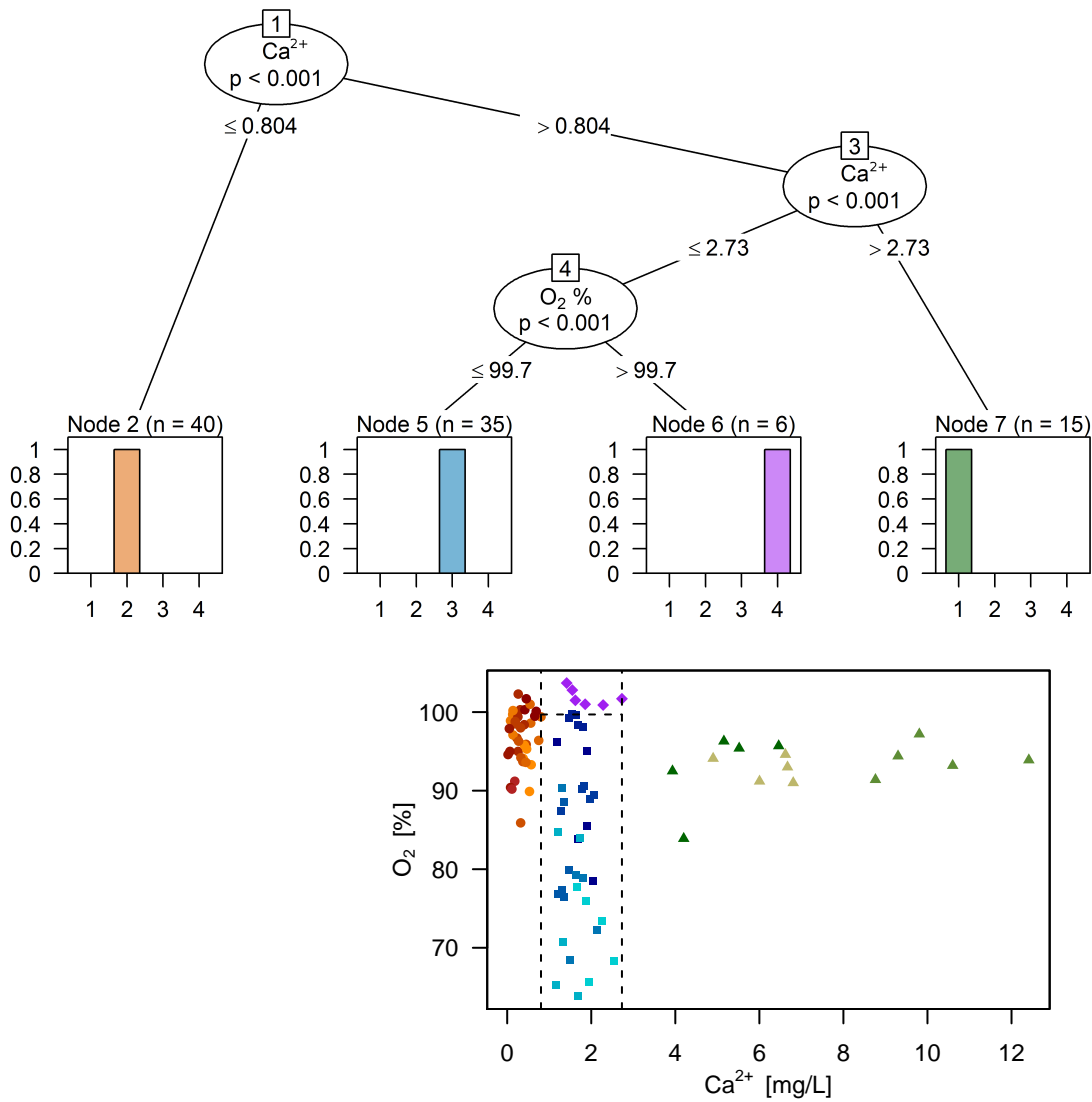
Figure 3.12: Conditional inference tree derived for water samples from the study catchment area. The respective group of an unknown water sample from the catchment area can be determined by use of Ca^{2+} concentration and DO-saturation measurements.

Tiger sandstone formation have higher Na^+ concentrations and high BIX.

A second aim of this study was to use water chemistry to differentiate between different types of flow. The soil organic matter composition is dependent on vegetation type as well as biological and chemical processes within the soil column. Additionally, export of DOC from soil is dependent on soil moisture conditions, hydraulic conductivity and water residence times. On steep slopes, near surface flow and biomat flow are significant flow and transport pathways for DOC. Preferential flow paths and surface flow on steep slopes may lead to rapid runoff into surface streams without containing high DOC. The BIX and HIX were used to differentiate between fresh and humified organic carbon and determine its source. Organic carbon in spring water from the sandstone aquifer was found to be strongly humified and of allochthonous origin. Water from the other springs was less humified, indicating a more autochthonous source. Based on these results, it is concluded that water from the sandstone aquifer is flowing parallel to the slope and extracts organic carbon from the upper soil layers. This flow pattern was observed in the field at some, but not all springs. Water from the top of the granitic basement is flowing along the geologic interface. The autochthonous carbon in this water is extracted from soil in the direct environment of the spring as indicated by the lower level humification. During high flow conditions levels of DOC in water from these springs can also be elevated, but the production of the organic carbon is close to the spring.

The temporal variations of spring water chemistry are highly dynamic. This is especially true for organic carbon contents of the precipitation-dominated springs. Results show that the response of dissolved organic carbon to changes in hydraulic conditions is highly dynamic. Due to increased flow through the upper soil layer during and after rain events, more organic carbon is extracted from the soil and transported with the water. Spatial variations are mainly caused by geologic formation along with topography.

This study recorded a baseline of hydrochemistry at the springs located within the catchment area. Future changes due to land use variations or climate change as well as their influence on water chemistry can be assessed by comparison against this baseline. Further research work is needed in order to elucidate the influence of forest use and climate change on spring water chemistry within the catchment area of this study to effectively protect and conserve these invaluable groundwater dependent ecosystems.

4

PHYSICOCHEMICAL AND MAJOR ION DATA FOR SPRINGS IN THE BLACK FOREST NATIONAL PARK, GERMANY

ABSTRACT

The dataset in this article consists of the general physicochemical parameters (temperature, pH, specific electrical conductivity, dissolved oxygen, redox potential, alkalinity) and concentrations of major ions (Ca^{2+}, Mg^{2+}, K^+, Na^+, Cl^-, SO_4^{2-}, NO_3^-) of water samples collected at 19 springs and the surface stream in the water catchment area of the upper Schönmünz river in the Black Forest National Park, Germany. Data on concentrations of dissolved organic carbon (DOC), total organic carbon (TOC), spectral absorbance at different wavelengths and fluorescence as well as microbiological indicators (*E. coli*, total coliforms, enterococci) are also reported. Sampling was conducted during five field campaigns between spring 2016 and spring 2017.

Knowledge of the current physicochemical parameters and concentrations of dissolved organic and inorganic constituents provides a baseline to assess future changes and serves as a supplement to ongoing studies of the spring ecosystems. Understanding the specific processes influencing the water chemistry will aid in their effective protection.

For more details and further discussion on this dataset, the reader is referred to the associated research article "Processes controlling spatial and temporal dynamics of spring water chemistry in the Black Forest National Park" (Merk et al., 2020).

SPECIFICATIONS TABLE

Subject	Environmental Science (General)
Specific subject area	Spring water chemistry
Type of data	Tables
How data were acquired	Mg^{2+}, K^+, Na^+: ion chromatography, ICS-1100, Thermo Fisher Scientific Ca^{2+}: flame AAS, Perkin-Elmer 3030 B Cl^-, SO_4^{2-}, NO_3-: ion chromatography, ICS-2100, Thermo Fisher Scientific TOC, DOC: oxidative combustion, Vario TOC cube, Elementar Analysesysteme GmbH absorbance spectra, fluorescence excitation-emission matrices: Aqualog, Horiba Scientific Silica: classical molybdenum blue method, Photolab 6600 UV-Vis, WTW Al: Spectroquant aluminum test, Merck total iron: Aquaquant iron test, Merck Coliforms/*E. coli*: Idexx Colisure, Quanti-Tray/2000 Enterococci: Idexx Enterolert, Quanti-Tray/2000
Data format	Raw (water chemistry data) Processed [Humification index (HIX) and biological index (BIX), derived from fluorescence measurements] Shapefile (all selected sampling locations)
Parameters for data collection	Water samples were collected at 19 springs and the surface stream during five different field campaigns in different seasons. Selection of springs was based on stratigraphy, spring type as well as flora and fauna in the vicinity of the point of discharge.
Description of data collection	Physicochemical parameters were determined in the field. Samples for anions and cations were filtered using 0.45 μm CA filters and stored in 30 mL PE bottles. Cation samples were acidified with nitric acid. Samples for DOC (filtered, glass fibre filter 0.45 μm) and TOC were stored in 50 mL brown glass bottles and acidified with hydrochloric acid. Samples for fluorescence measurements were stored in 50 mL brown glass bottles. Silica samples were filtered using 0.45 μm CA filters and stored in 100 mL PE bottles.
Data source location	Water catchment area of the upper Schönmünz river, Black Forest National Park, southern Germany (48.55 - 48.59°N, 8.23 – 8.34°E)
Data accessibility	With the article

VALUE OF THE DATA

- The data can be used as a baseline for water chemistry of the springs and their respective ecosystems within the water catchment area.

- The dataset is a helpful and necessary supplement to ongoing investigations into the spring ecosystems, especially research of flora and fauna in the vicinity of the spring.

- Knowledge of the processes controlling spatial and temporal dynamics of spring water chemistry is important for creation of effective protection policies.

4.1 DATA DESCRIPTION

Water samples were collected at 20 different locations within the study area during five different field campaigns. The dates of the sampling campaigns one to five are 25 May 2016 – 6 June 2016, 1 July 2016 – 8 July 2016, 5 September 2016 – 8 September 2016, 2 November 2016 – 7 November 2016 and 8 May 2017 – 11 May 2017, respectively. The locations of the sampling points are listed in Table 4.1 and shown in Figure 4.1. Because it was not possible to take samples at all of the numerous springs in the catchment area, a selection had to be made. Sampling points were chosen to include springs of differing elevation, geology and spring type in order to get a diverse overview of the hydrochemistry in the catchment area. Some sampling points were included in the sampling programme as they were already part of ongoing studies of the associated spring ecosystems. The final selection was based on stratigraphy, spring type as well as flora and fauna in the vicinity of the point of discharge. (Merk et al., 2020)

Springs were grouped into the three clusters listed in Table 4.1, based on topography, geology and water chemistry. A summary of major ion chemistry is listed in Table 4.2.

Absorbance data files (*.abs) (B) are comma separated files containing measured absorbance spectra. Files are named by sampling station, sampling campaign and sampling date, separated by an underscore. Data columns in the files are: Wavelength (nm); I1 (µA) Abs Detector Raw; I1 dark (µA) Dark Offset for Abs Detector; R1 (µA) Ref Detector raw; R1dark (µA) Dark Offset for Ref Detector, XCorrect (-) Linear interp; I1c (µA Dark subtracted Abs Detector); R1c (µA) Corrected Ref Detector, I1c/R1c (µA/µA) Corrected Intensity; Abs (OD) –Log(T); Percent T (T*100) % Transmittance.
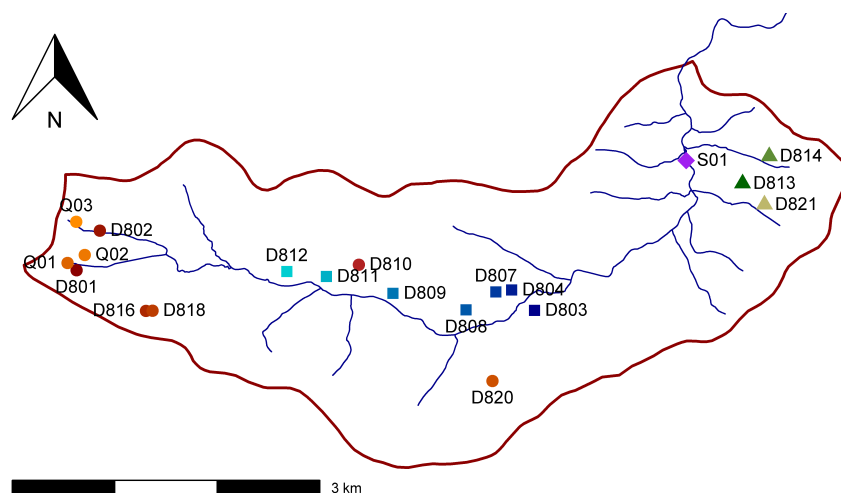
Figure 4.1: Map of the Schönmünz water catchment within the Black Forest National Park, southern Germany. Symbols indicate the sampling locations at the selected springs based on hydrogeology and topography ($\bigcirc$, $\square$, $\triangle$) and the surface stream ($\diamondsuit$).

Fluorescence data files (*.csv) (B) are comma separated files containing measured fluorescence excitation-emission matrices (EEM) in counts per second, as measured by the device. Files are named by sampling station, sampling campaign and sampling date, separated by an underscore. The first data column contains the emission wavelengths (nm) and the first data row contains the excitation wavelengths (nm).

The shapefile (B) contains the locations of all sampling stations within the water catchment area. Coordinate reference system is the German DHDN GK3, based on the Bessel 1984 spheroid.

The spreadsheet in the appendix (B) contains individual values of measured data: Location, Date, Time, campaign number, specific electrical conductivity (SEC), pH, O_2, HCO_3^-, measured redox potential, corrected standard redox potential (EH), Temperature (T), concentrations of: Cl^-, SO_4^{2-}, NO_3^-, PO_4^{3-}, Na^+, K^+, Mg^{2+}, Ca^{2+}, Fe_{tot}, aluminium (Al), silica (Si), total dissolved solids (TDS), acidification quotient (AQ), most probable numbers (MPN/100 mL) for Coliforms, *E. coli* and Enterococci, concentrations of total organic carbon (TOC) and dissolved organic carbon (DOC), biological index (BIX) (Zhou et al., 2015), humification index (HIX) (Ohno, 2002) and spectral absorption coefficients (SAK) at wavelength of 210, 254, 280, 436 and 545 nm as well as discharge and assignment to geologic group according to Merk et al. (2020).

Table 4.1: Geographic coordinates of the selected sampling locations in the water catchment area of the upper Schönmünz River. (Coordinates in GK 3 reference frame, HW: "Hochwert", northing; RW: "Rechtswert", easting).

Spring	HW (m)	RW (m)	Elevation (m a.s.l.)	Group
D801	5381581	3443862	915	sandstone group
D802	5381967	3444088	911	sandstone group
D803	5381189	3448328	678	west granite group
D804	5381388	3448105	695	west granite group
D807	5381369	3447952	728	west granite group
D808	5381194	3447661	725	west granite group
D809	5381355	3446948	740	west granite group
D810	5381635	3446615	789	sandstone group
D811	5381520	3446299	734	west granite group
D812	5381568	3445913	738	west granite group
D813	5382427	3450357	695	east granite group
D814	5382692	3450617	688	east granite group
D816	5381186	3444539	898	sandstone group
D818	5381187	3444602	896	sandstone group
D820	5380502	3447918	829	sandstone group
D821	5382221	3450571	716	east granite group
Q01	5381653	3443774	958	sandstone group
Q02	5381731	3443941	920	sandstone group
Q03	5382053	3443859	955	sandstone group
S01	5382651	3449808	573	surface stream

Table 4.2: Summary of data by group and for all data.

			East granite group	Sandstone group	West granite group	Surface stream	All data
Elevation	m a.s.l	min; max	688; 716	789; 958	678; 740	573; 573	573; 958
		mean ± SD	700 ± 15	897 ± 55	720 ± 24	573 ± 0	789 ± 112
Temperature	°C	min; max	7.03; 8.57	4.83; 10.87	5.93; 10.93	4.90; 14.05	4.83; 14.05
		mean ± SD	7.68 ± 0.45	6.72 ± 1.18	7.80 ± 0.82	9.22 ± 3.29	7.44 ± 1.42
pH	-	min; max	6.0; 6.90	3.6; 5.12	4.7; 6.61	6.4; 7.42	3.6; 7.42
		mean ± SD	6.48 ± 0.27	4.33 ± 0.44	5.74 ± 0.40	6.95 ± 0.42	5.38 ± 1.02
SEC	µS/cm	min; max	43.9; 117.3	15.6; 61.0	19.2; 36.8	17.3; 34.7	15.6; 117.3
		mean ± SD	76.5 ± 24.1	29.0 ± 11.8	26.9 ± 3.9	25.3 ± 6.4	35.3 ± 21.5
O_2	%	min; max	83.9; 97.2	85.9; 102.3	63.8; 99.7	100.9; 104.3	63.8; 104.3
		mean ± SD	93.2 ± 3.2	96.6 ± 3.7	82.8 ± 10.7	102.3 ± 1.4	91.5 ± 9.7
EH	mV	min; max	522; 675	566; 755	494; 715	505; 600	494; 755
		mean ± SD	612 ± 41	684 ± 47	639 ± 63	558 ± 32	646 ± 63
HCO_3^-	meq/L	min; max	0.42; 1.10	0.00; 0.05	0.06; 0.28	0.04; 0.26	0.00; 1.10
		mean ± SD	0.69 ± 0.22	0.01 ± 0.01	0.14 ± 0.05	0.17 ± 0.08	0.17 ± 0.25
Ca^{2+}	mg/L	min; max	3.93; 12.41	0.02; 0.80	1.17; 2.55	1.42; 2.73	0.02; 12.41
		mean ± SD	7.14 ± 2.49	0.35 ± 0.21	1.66 ± 0.33	1.91 ± 0.50	1.99 ± 2.52
Mg^{2+}	mg/L	min; max	1.66; 6.33	0.02; 0.21	0.38; 1.35	0.56; 1.15	0.02; 6.33
		mean ± SD	3.48 ± 1.39	0.12 ± 0.05	0.67 ± 0.23	0.84 ± 0.24	0.89 ± 1.28
Na^+	mg/L	min; max	0.54; 0.82	0.32; 0.84	0.44; 1.69	0.66; 0.93	0.32; 1.69
		mean ± SD	0.69 ± 0.08	0.50 ± 0.10	0.73 ± 0.34	0.77 ± 0.11	0.63 ± 0.24
K^+	mg/L	min; max	0.97; 1.93	0.07; 1.60	0.58; 1.62	0.56; 1.12	0.07; 1.93
		mean ± SD	1.51 ± 0.27	0.67 ± 0.37	1.06 ± 0.25	0.81 ± 0.23	0.95 ± 0.42
Cl^-	mg/L	min; max	0.90; 1.29	0.37; 0.95	0.70; 1.08	0.77; 0.91	0.37; 1.29
		mean ± SD	1.04 ± 0.11	0.63 ± 0.13	0.85 ± 0.07	0.84 ± 0.05	0.79 ± 0.18
NO_3^-	mg/L	min; max	0.85; 1.97	0.25; 3.82	0.58; 2.65	0.39; 1.18	0.25; 3.82
		mean ± SD	1.33 ± 0.39	1.91 ± 0.98	1.66 ± 0.52	0.76 ± 0.29	1.66 ± 0.79
SO_4^{2-}	mg/L	min; max	2.52; 5.87	0.68; 2.61	1.06; 4.39	1.31; 1.99	0.68; 5.87
		mean ± SD	3.52 ± 0.94	1.38 ± 0.46	2.44 ± 0.93	1.73 ± 0.28	2.12 ± 1.05
TDS	mg/L	min; max	38.31; 93.04	2.74; 10.81	9.82; 26.65	8.64; 25.03	2.74; 93.04
		mean ± SD	60.8 ± 18.1	6.4 ± 2.3	17.5 ± 3.6	18.5 ± 6.0	19.7 ± 20.0
TOC	mg/L	min; max	0.40; 2.00	0.86; 27.53	0.25; 9.01	1.24; 11.43	0.25; 27.53
		mean ± SD	0.7 ± 0.4	11.6 ± 8.8	1.6 ± 2.2	5.8 ± 4.6	5.9 ± 7.7
DOC	mg/L	min; max	0.32; 2.26	0.76; 28.34	0.18; 9.54	1.20; 11.40	0.18; 28.34
		mean ± SD	0.74 ± 0.54	11.65 ± 8.86	1.53 ± 2.29	5.63 ± 4.43	5.88 ± 7.77
Si	mg/L	min; max	2.03; 3.50	0.98; 3.11	1.83; 4.71	2.02; 3.25	0.98; 4.71
		mean ± SD	2.93 ± 0.36	2.22 ± 0.50	3.02 ± 0.68	2.71 ± 0.43	2.65 ± 0.66
Al	mg/L	min; max	0.00; 0.08	0.00; 0.56	0.00; 0.25	0.00; 0.26	0.00; 0.56
		mean ± SD	0.02 ± 0.03	0.19 ± 0.19	0.02 ± 0.05	0.10 ± 0.11	0.10 ± 0.16
Fe	mg/L	min; max	0.00; 0.06	0.03; 0.39	0.00; 0.14	0.05; 0.15	0.00; 0.39
		mean ± SD	0.03 ± 0.02	0.13 ± 0.09	0.04 ± 0.03	0.09 ± 0.04	0.08 ± 0.08
Coliforms	MPN/100 ml	min; max	1.0; 770.1	1.0; 224.7	<1; 2419.6	115.3; 816.4	<1; 2419.6
		mean ± SD	118.3 ± 232.9	49.7 ± 49.8	296.2 ± 638.0	427.7 ± 260.0	174.6 ± 416.9
E. coli	MPN/100 ml	min; max	<1; 13.2	<1; 19.9	<1; 17.3	<1; 4.1	<1; 19.9
		mean ± SD	1.4 ± 3.8	1.9 ± 3.9	1.1 ± 3.3	2.2 ± 1.7	1.5 ± 3.6
Enterococci	MPN/100 ml	min; max	<1; 5.1	<1; 1.0	<1; 2.0	<1; 17.1	<1; 17.1
		mean ± SD	0.68 ± 1.52	0.06 ± 0.25	0.32 ± 0.67	4.64 ± 7.13	0.55 ± 2.10
HIX	-	min; max	0.06; 1.44	0.04; 0.08	0.04; 1.36	0.04; 0.10	0.04; 1.44
		mean ± SD	0.42 ± 0.41	0.06 ± 0.01	0.38 ± 0.40	0.07 ± 0.02	0.23 ± 0.33
BIX	-	min; max	0.53; 0.96	0.38; 0.50	0.40; 3.20	0.40; 0.44	0.38; 3.20
		mean ± SD	0.68 ± 0.14	0.43 ± 0.03	0.73 ± 0.54	0.42 ± 0.02	0.58 ± 0.36
Abs(254)	-	min; max	-0.01; 0.08	0.04; 1.38	-0.01; 0.44	0.05; 0.60	-0.01; 1.38
		mean ± SD	0.02 ± 0.02	0.62 ± 0.45	0.07 ± 0.12	0.33 ± 0.24	0.31 ± 0.41

4.2 EXPERIMENTAL DESIGN, MATERIALS, AND METHODS

4.2.1 *Field sampling*

Physicochemical parameters were determined in the field. Temperature, specific electrical conductivity (SEC), dissolved oxygen (DO), the redox potential and pH were taken using a WTW Multi 3430 and the respective probes.

A digital Sentix 82 probe was used during the first sampling campaign to measure pH. As this probe is not well suited for waters with low mineralization, these measurements did not pass quality control measures and could not be included in this dataset or used in data analysis. During the second sampling campaign, an analog Sentix HW probe in combination with an analog TetraCon 325 for temperature compensation and a WTW Multi 340i was used. A digital Sentix HW-T 900P probe was used during the other sampling campaigns, as this type is especially suitable for low mineralization waters.

The probe used for measurement of SEC was a TetraCon 925.

An optical probe of type FDO 925 was used to determine DO.

Redox potentials were not determined during the first sampling campaign. In campaigns two through five, a Sentix ORP-T 900 was used. Equilibration times of at least 20 minutes were observed before readings of redox were taken, as these probes are known to have long equilibration times. Measured values were converted into standard hydrogen electrode potentials by adding a temperature dependent reference voltage according to the documentation by the manufacturer. All probes – except the redox probe – had an integrated temperature sensor. Measured temperatures differed slightly between probes. For correction of redox potentials and data analysis, the mean was used.

Alkalinity was determined by titration of 100 mL of sample water with a solution of 25 mmol/L hydrochloric acid in the field.

Samples for anion and cation determination were filtered using 0.45 µm CA filters and stored in 30 mL PE bottles. Cation samples were acidified with 50 µL nitric acid (65%, suprapur). No chemical was added to samples for determination of anions. Silica samples were filtered using the same 0.45 µm CA filters and stored in 100 mL PE bottles.

Samples for determination of DOC were filtered using glass fibre filters with a mean pore size of 0.45 µm. These filters were heat treated at 450 °C for a minimum of 4 h to remove residual carbon from within the filter. Brown glass bottles with a volume of 50 mL were used for samples designated for DOC, TOC and fluorescence analysis. Samples for TOC were taken unfiltered. For inhibition of bacterial and algae growth and removal of inorganic carbon, pH of DOC and TOC samples was lowered using 250 mL of hydrochloric acid (37%, suprapur).

Samples for fluorescence spectroscopy were taken unfiltered and stored without addition of acid or any other stabilizing agents. No samples for TOC and fluorescence analysis were taken during the second sampling campaign.

All sample containers and sample taking equipment was rinsed several times and filters thoroughly flushed with sample water before taking the actual sample. Sample bottles were stored in a Styrofoam box, using cool packs as necessary and transported to the lab daily. All samples were subsequently stored in the dark at +8 °C and usually analysed within one week.

For microbial analysis of coliforms, *E. coli* and enterococci, two sterile PS-bottles (Idexx) were filled up to the 100 mL mark.

Discharge measurements were done using two different methods. The method used is listed next to discharge measurements in the supplemented data. Volumetric measurements were mainly done at the springs. Discharge from the spring was collected in a plastic bag that was pressed to the streambed. The time was measured using a stopwatch and the amount of water that was collected was subsequently measured using a measuring cylinder. In cases where the complete flow could not be retrieved, the proportion of the water that was missed was approximated. These measurements are marked as estimates.

The salt-dilution method (Hongve, 1987) was used for discharge measurements of the surface stream.

4.2.2   *Analysis*

Element concentrations of Mg^{2+}, K^+ and Na^+ were determined using ion chromatography (ICS-1100, Thermo Fisher Scientific). Ca^{2+} concentrations were determined by flame AAS (Perkin-Elmer 3030 B). Concentrations of Cl^-, SO_4^{2-} and NO_3^- were similarly determined using ion chromatography (ICS-2100, Thermo Fisher Scientific). TOC and DOC concentrations were determined by oxidative combustion at 850 °C and subsequent determination of carbon dioxide (Vario TOC cube, Elementar Analysesysteme GmbH).

Simultaneous measurement of absorbance spectra and fluorescence excitation-emission matrices (EEM) were done by fluorescence spectroscopy (Aqualog, Horiba Scientific). An integration time of two seconds was used for excitation wavelengths from 200 nm to 600 nm in steps of 3 nm. EEMs were corrected for inner filter effects and Raman scattering was removed in the software provided by the manufacturer. Measured intensities were used directly for further analysis without calibrating to any standard. Measured absorbance spectra have a resolution of 3 nm starting at 201 nm and ending at 600 nm, requiring absorbance at a specific wavelength to be interpolated linearly between its neighbours.

Dissolved silica was measured using the classical molybdenum blue method. Ammonium molybdate is added to the sample to form a complex of dissolved silica and molybdic acid. This complex is reduced by stannous chloride to molybdenum blue. Absorption measurements were done at 810 nm using a lab photometer (Photolab 6600 UV-Vis, WTW). Five mL of sample were diluted by 15 mL of distilled water to reduce equilibration times of the complex formation. Measured absorbance values were converted into Si-concentrations by use of calibration standards (prepared daily) and linear regression.

Aluminium was determined using a photometer and a sample kit (Spectroquant aluminum test, Merck). Al dissolved by organic complexation with humic substances or other organic molecules ($Al_{(org)}$) and Al that is dissolved inorganically as Al^{3+} or different Al-hydroxides ($Al_{(inorg)}$) have not been measured separately.

Total iron ($Fe^{2+/3+}$) was determined using a test kit (Aquaquant iron test, Merck).

Microbiological data was acquired by adding substrate powder directly to the designated 100 mL samples and shaking until dissolved. For determination of coliforms and *E. coli*, Colisure (Idexx) (IDEXX Laboratories) was used. For determination of enterococci, Enterolert (Idexx) (IDEXX Laboratories, Inc.) was used.

After adding a substrate powder, each sample was transferred to a Quanti-Tray/2000 within 12 hours after sampling, sealed and incubated for 24 hours at the specified temperature (Colisure: 35 °C, Enterolert: 42 °C). The number of positive indentations was then counted and the most probable number (MPN/100mL) calculated from the supplied conversion table.

5

PAIRED-CATCHMENT-STUDY IN THE WATER CATCHMENT AREAS OF THE SCHÖNMÜNZ AND THE LANGENBACH

A comprehensive understanding of the springs through time can only be achieved on the basis of continuous and long-term data. For this purpose, an observation network was conceptualized. It will allow for the documentation of the current state of the spring hydrochemistry and discharge dynamics and to identify changes in the response to different hydrometeorological events in the National Park. Based on the accumulated data, possible effects of climate change and land use changes on these ecosystems can be assessed in the future.

Further interests are in the influence of forest use on water quality and runoff dynamics. During a so-called paired-catchment study (PCS), a comparison between two contrasting forested catchments will allow to determine the influence of forest use on runoff characteristics (Brown et al., 2005; Suryatmojo et al., 2013). During the PCS, data is continuously collected at the monitoring points in the two catchment areas. The catchment areas have similar topographical and geographical locations, but different land and forest uses. A catchment area without (or at least very minimal) forest use is represented by the area around the Wildsee (Figure 5.1) at the heart of the National Park. This area has been established as a so called Bannwald over 100 years ago and was mainly left untouched to develop a natural structure during this time. For comparison, the valley of the Langenbach located to the north was chosen. It is a catchment area that has been intensively used by the Murgschifferschaft as a commercial forest for many years. The surface streams in both catchment areas, the Langenbach and the Schönmünz, have their origins within the area of the National Park. The locations of the monitoring points are chosen in such a way that a comparison between points can later be made (Figure 5.2).

The concept and initial setup of several monitoring stations in both catchment areas are presented in Appendix C.

Figure 5.1: Wildsee
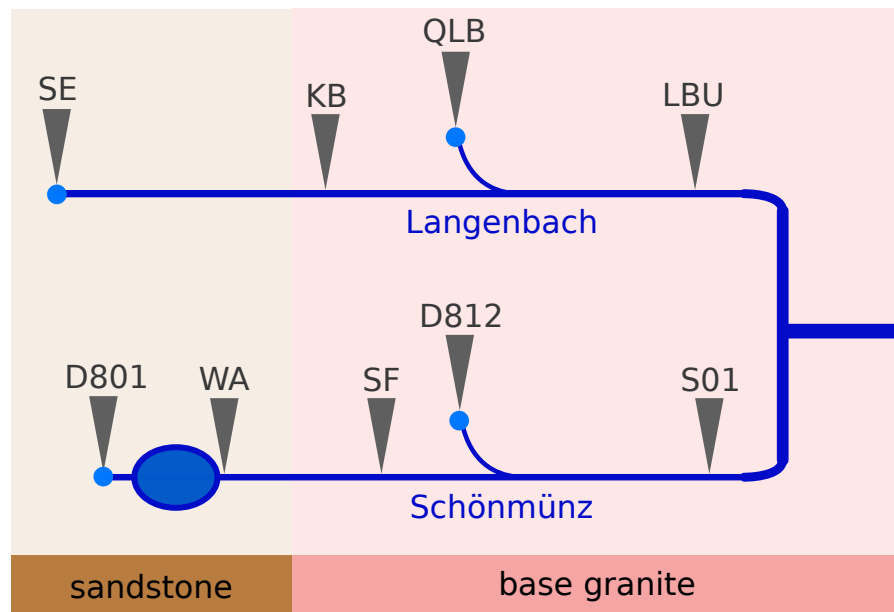
Figure 5.2: Basic concept and setup for the paired catchment study in the valleys of the Langenbach and the Schönmünz. Locations of monitoring points are also shown.

Part III

SYNSTHESIS

In this part, key findings obtained in the individual studies
are summarized in regard to the research objectives stated
in the Introduction (Chapter 1). Furthermore, aspects that
are important to future research are discussed and ap-
proaches to additional research opportunities proposed.

CONCLUSION AND OUTLOOK

In order to better understand hydrologic processes at steep hillslopes, they have been investigated at two distinct scales using relevant methods adopted to each. Both test sites offer unique research opportunities, allowing further insights into water movements in the unsaturated zone. Different scales of both test sites, and the different measurement techniques used, complement each other. The long term data series from the lysimeter site gives a temporal overview of past hydrometeorological conditions. Knowledge and understanding of these past variations helps in interpreting results from water sampling campaigns at specific dates. Several sampling campaigns were conducted during different seasons in the Black Forest National Park. They are like snapshots, only revealing a part of the underlying dynamics. For an in-depth understanding, the big picture is as important as the more detailed investigations.

The areas of research and methods used at the two test sites are quite different from each other. One study site is a forested catchment in the Black Forest National Park, the other is a large inclined lysimeter in the top cover of a municipal landfill site. Despite the different geologic setting of both test sites, they share a commonality: inclined hillslopes. The inclination of the steep slopes in the Black Forest are somewhat comparable to the slope of the test site near Karlsruhe.

The lysimeter site focused on soil moisture dynamics and water flux in the unsaturated zone. The study in the Black Forest was focused on water chemistry and discharge dynamics. In both cases, the water flow behavior was studied and a contribution to the current discussion was made.

Large Inclined Lysimeter

Based on a long-term time series of weekly soil moisture measurements at this test site, the moisture dynamics in the unsaturated zone could be studied. Main drivers of moisture dynamics are precipitation and evapotranspiration during the vegetation period. There is also a complex network of interactions between the different drivers of the water cycle at global, regional and local scales. Soil moisture measurements showed a clear seasonal pattern. Lowest values were measured at the end of the vegetation period after a gradual drying out of the soil during spring and summer. Highest values were measured after the vegetation period, following a sharp increase in soil moisture during the winter months. The seasonal response of soil moisture to

external influences driving the seasonal dynamics are delayed with depth.

The results further show an overall decline of soil moisture levels. This decline is not distributed evenly over the whole observation period. A step-change occurred during the exceptionally dry year 2003, after which soil moisture levels reached an alternate stable state at lower moisture content and with less seasonal variation. Furthermore, the decline does not affect measurements at all depths with the same intensity. It is most pronounced in the lower soil and at the beginning and end of the vegetation period. This has profound impacts on calculations of water balances, as storage loss due to deep desiccation of soils might be a significant flux that contributes significantly to the overall budget. This contribution can not be neglected. In recent years a further decrease in soil moisture levels was observed. This decrease has not yet reached a stable state. Some years even showed a complete lack of re-wetting during the winter months. This has implications for groundwater recharge. Therefore, this study into the past soil moisture variations at the test site provides necessary information needed for better predictions of future dynamics.

In a comparison with modeled soil moisture data published by the German weather service (DWD) a spatial heterogeneity was found. Not all locations experience this downward trend in soils moisture in the same way. It depends on the range of the regional water cycle. More precipitation leads to higher soil moisture, higher soil moisture to more evapotranspiration, and more evapotranspiration to more clouds and precipitation. The import and export of water to and from a catchment area determines the scale of the water cycle. This scale can not be described by a single number. It changes over time. Every local water cycle is driven by the global water cycle to a certain degree. But local feedback mechanisms may contribute significantly, depending on the regional setting. A concept for water ages in a catchment area is the mean residence time. Water of all possible ages is found in the catchment area, following a certain distribution. A similar concept should be applied to the scale of the water cycle. There are mechanisms on all scales influencing the local water cycle. The magnitude of these influences happening at different scales is different for each location. The distribution of these influences will probably also show seasonal variations. In winter, larger scale convection may provide precipitation distributed over large areas. In summer, local evapotranspiration and local thunderstorms and heavy rain indicate a much smaller scale of the water cycle.

Black Forest National Park

The water in the catchment area of the Schönmünz is characterized by its low pH and low specific electrical conductivities. The lack of soluble minerals in the host rock of the different fractured aquifers,

consisting mainly of granites, conglomerates and sandstones, leads to a generally very low overall solute budget of the spring waters. Water is weakly buffered by different buffer systems, mainly the ion exchange and silica buffer systems. In some waters with particularly low pH values, the contribution of aluminum to the overall buffer system is considerable. The carbonate buffer system is only of minor importance.

The springs and the surface stream in the catchment area can be divided into four groups, based on hydro-chemistry and geology. These groups can be clearly distinguished using Ca^{2+}-concentration and oxygen saturation. Based on these results, a conceptual model of the water catchment area was developed. It is presented in Figure 6.1. Springs discharge mainly at interfaces between geologic formations of differing hydraulic conductivity. Some springs discharge from glacial cirques or Quaternary sediments.

The different types of water flow being either parallel to the slope or along interfaces of geologic formations with differing hydraulic conductivities could be differentiated. This was achieved by the use of derived indices for the dissolved organic matter based on fluorescence measurements. They are indicative of the source of the dissolved organic carbon in spring waters.

Overall, the discharge behavior in the catchment area is highly dynamic. Following precipitation events, a rapid reaction of discharge was observed. This increase in discharge was accompanied by an increase in concentrations of dissolved organic carbon. Concentration of DOC is dependent on flow conditions. During the annual cycle, total mass of exported organic carbon with the water in the stream was lowest during the summer months. During this time discharge

Figure 6.1: Conceptual model of the Schönmünz water catchment area. Springs are mainly located at the interfaces between different geologic formations. (KB: glacial cirque; qum: quarternary sediments; sVgo: Upper pebble horizon; sVs: Building sandstone formation; suE: Eck-formation; zT: Tiger sandstone formation; GFO, GSE: base granite; pg: paragneiss.)

was very low and at the same time concentrations of DOC were also low. This is an important observation that has to be considered when calculating a carbon budget for this catchment area or other similar catchment areas in the Black Forest.

The data and discussion presented contribute to the general understanding of spatial and temporal dynamics of spring water chemistry in the newly established Black Forest National Park. They can further be used as baseline of hydrochemistry at springs located within the catchment area. They will aid to observe future changes due to land use variations or climate change.

Perspective and Outlook

When combining the findings from both study sites, there are several conclusions that can be drawn. Findings of the lysimeter study can be of help in the Black Forest, where deep desiccation of the soil may become an issue in the future. Especially at locations with shallow soils at hillslopes in the National Park.

Results from the lysimeter showed a clear seasonal asymmetry of soil moisture propagating downward through the soil column. Depth averaged soil moisture did not exhibit this strong seasonal asymmetry. This insight can also be applied to the Black Forest. There are currently no soil moisture measurements done within the catchment area. However, there are several remote sensing products offering time series raster data for soil moisture on different grid and time resolutions. This data is usually not depth resolved. While this depth averaged data is suitable to calculate water balances, it is not directly usable to describe discharge dynamics. Antecedent soil moisture conditions are known to have an impact on the generation of runoff. This might in part be due to the vertical distribution of soil moisture not contained in averaged data and should be considered. Different depths of the soil are affected differently by changes in climate and land use, resulting in changes to the vertical distribution patterns of soil moisture.

Work in the Black Forest National Park is still ongoing. Results and discussions presented here are only one small first step in gaining a more comprehensive understanding. The ongoing paired-catchment-study will reveal dynamics on a much smaller timescale than is possible with single sampling campaigns. Continued investigation into the spring related ecosystems in the Black Forest National Park are expected to greatly benefit from these results. They will reveal how water chemistry and discharge dynamics of the springs relate to the assemblage of flora and fauna in the vicinity of the springs and if there are certain species that are indicative of hydrochemical parameters. Furthermore, it will show how they are affected by changes.

Work on the large inclined lysimeter is also continued. It will be most interesting to see how the soil moisture will change in the future and what influences it will have. There are still even more things that can be learned from the already recorded and future data. Recently, an analytical solution of the Richards equation for constant rainfall intensity and gravity-driven infiltration was found by Baiamonte (2020). The data from the lysimeter are possibly suited to test this analytical solution for validity and derive further insights into soil water fluxes e.g. temporal changes to infiltration and seepage dynamics. Other models of the unsaturated zone are not beyond the realm of feasibility.

Part IV

APPENDIX

BIBLIOGRAPHY

Abichou, T., Liu, X., Tawfiq, K., 2006. Design Considerations for Lysimeters Used to Evaluate Alternative Earthen Final Covers. Journal of Geotechnical and Geoenvironmental Engineering 132, 1519–1525. doi:10.1061/(ASCE)1090-0241(2006)132:12(1519).

Ala-aho, P., Soulsby, C., Wang, H., Tetzlaff, D., 2017. Integrated surface-subsurface model to investigate the role of groundwater in headwater catchment runoff generation: A minimalist approach to parameterisation. Journal of Hydrology 547, 664–677. doi:10.1016/j.jhydrol.2017.02.023.

Albergel, C., Zheng, Y., Bonan, B., Dutra, E., Rodríguez-Fernández, N., Munier, S., Draper, C., Rosnay, P.d., Muñoz-Sabater, J., Balsamo, G., Fairbairn, D., Meurey, C., Calvet, J.C., 2019. Data assimilation for continuous global assessment of severe conditions over terrestrial surfaces. Hydrology and Earth System Sciences Discussions , 1–46doi:https://doi.org/10.5194/hess-2019-534.

Alfaro, C., Wallace, M., 1994. Origin and classification of springs and historical review with current applications. Environmental Geology 24, 112–124. doi:10.1007/BF00767884.

Allaire, S.E., Roulier, S., Cessna, A.J., 2009. Quantifying preferential flow in soils: A review of different techniques. Journal of Hydrology 378, 179–204. doi:10.1016/j.jhydrol.2009.08.013.

Aquaread, 2017. Instruction Manual for the Aquaprobe ® AP-5000 Multiparameter Water Quality Probe and associated Aquameter ®, Utilities & Accessories, Revision: L. URL: https://www.aquaread.com/aquaread-content/downloads/manuals/Aquaread-Aquaprobe-AP-5000-Instruction-Manual-Revision-L.pdf.

Armbruster, M., Abiy, M., Feger, K.H., 2003. The biogeochemistry of two forested catchments in the Black Forest and the eastern Ore Mountains (Germany). Biogeochemistry 65, 341–368.

Armbruster, M., Köhler, H., Feger, K.H., 2000. Chemische Zusammensetzung zweier quellnaher Waldbäche im Hochschwarzwald—Abflussabhängige Variabilität und Einfluss einer Bodenkalkung. Forstwissenschaftliches Centralblatt 119, 249–262. doi:10.1007/BF02769141.

Asano, Y., Uchida, T., Ohte, N., 2002. Residence times and flow paths of water in steep unchannelled catchments, Tanakami, Japan. Journal of Hydrology 261, 173–192.

Asano, Y., Uchida, T., Ohte, N., 2003. Hydrologic and geochemical influences on the dissolved silica concentration in natural water in a steep headwater catchment. Geochimica et Cosmochimica Acta 67, 1973–1989. doi:10.1016/S0016-7037(02)01342-X.

Augenstein, M., Goeppert, N., Goldscheider, N., 2015. Characterizing soil water dynamics on steep hillslopes from long-term lysimeter data. Journal of Hydrology 529, 795–804. doi:10.1016/j.jhydrol.2015.08.053.

Baiamonte, G., 2020. Analytical Solution of the Richards Equation under Gravity-Driven Infiltration and Constant Rainfall Intensity. Journal of Hydrologic Engineering 25, 04020031. doi:10.1061/(ASCE)HE.1943-5584.0001933.

Ball, J.W., Nordstrom, D.K., 1991. User's Manual for Wateq4f, with Revised Thermodynamic Data Base and Test Cases for Calculating Speciation of Major, Trace, and Redox Elements in Natural Waters. Technical Report Open-File Report 91-183. U.S. Geological Survey. Revised 2001.

Baur, S., Feger, K.H., 1992. Importance of natural soil processes relative to atmospheric deposition in the mobility of aluminium in forested watersheds of the Black Forest. Environmental Pollution 77, 99–105. doi:10.1016/0269-7491(92)90065-I.

Baur, S., Feger, K.H., Brahmer, G., 1988. Mobilität und Bindungsformen von Aluminium in Wassereinzugsgebieten des Schwarzwaldes. Mitteilgn. Dtsch. Bodenkundl. Gesellsch , 141–146.

Beck, H.E., Zimmermann, N.E., McVicar, T.R., Vergopolan, N., Berg, A., Wood, E.F., 2018. Present and future Köppen-Geiger climate classification maps at 1-km resolution. Scientific Data 5. doi:10.1038/sdata.2018.214.

Beierkuhnlein, C., 1996. Biomonitoring mit Quellen der silikatischen Mittelgebirge. Crunoecia 5, 141–151.

Bennett, P., Siegel, D.I., 1987. Increased solubility of quartz in water due to complexing by organic compounds. Nature 326, 684–686. doi:10.1038/326684a0.

Berger, K.U., 2015. On the current state of the Hydrologic Evaluation of Landfill Performance (HELP) model. Waste Management 38, 201–209. doi:10.1016/j.wasman.2015.01.013.

Bernal, S., Lupon, A., Catalán, N., Castelar, S., Martí, E., 2018. Decoupling of dissolved organic matter patterns between stream and riparian groundwater in a headwater forested catchment. Hydrology and Earth System Sciences 22, 1897–1910. doi:10.5194/hess-22-1897-2018.

Bertrand, G., Goldscheider, N., Gobat, J.M., Hunkeler, D., 2012. Review: From multiscale conceptualization to a classification system for inland groundwater-dependent ecosystems. Hydrogeology Journal 20, 5–25. doi:10.1007/s10040-011-0791-5.

Braden, H., 2012. The model AMBETI - A detailed description of a soil-plant-atmosphere model. Technical Report 195. DWD. Offenbach am Main.

Brantley, S.L., Lebedeva, M.I., Balashov, V.N., Singha, K., Sullivan, P.L., Stinchcomb, G., 2017. Toward a conceptual model relating chemical reaction fronts to water flow paths in hills. Geomorphology 277, 100–117. doi:10.1016/j.geomorph.2016.09.027.

Braukmann, U., 2000. Hydrochemische und biologische Merkmale regionaler Bachtypen in Baden-Württemberg. Dissertation. LfU. Karlsruhe. URL: http://www.gbv.de/dms/bs/toc/313067651.pdf.

Brown, A.E., Zhang, L., McMahon, T.A., Western, A.W., Vertessy, R.A., 2005. A review of paired catchment studies for determining changes in water yield resulting from alterations in vegetation. Journal of Hydrology 310, 28–61. doi:10.1016/j.jhydrol.2004.12.010.

Brune, G., 1975. Major and Historical Springs of Texas. Technical Report 189. Texas Water Development Board. Austin, Texas.

Bryan, K., 1919. Classification of Springs. The Journal of Geology 27, 522–561. doi:10.1086/622677.

Cantonati, M., Lange-Bertalot, H., 2011. Diatom monitors of close-to-pristine, very-low alkalinity habitats: three new Eunotia species from springs in Nature Parks of the south-eastern Alps. Journal of Limnology 70, 209–221. doi:10.4081/jlimnol.2011.209.

Cantonati, M., Stevens, L.E., Segadelli, S., Springer, A.E., Goldscheider, N., Celico, F., Filippini, M., Ogata, K., Gargini, A., 2020. Ecohydrogeology: The interdisciplinary convergence needed to improve the study and stewardship of springs and other groundwater-dependent habitats, biota, and ecosystems. Ecological Indicators 110, 105803. doi:10.1016/j.ecolind.2019.105803.

Casper, M.C., Volkmann, H.N., Waldenmeyer, G., Plate, E.J., 2003. The separation of flow pathways in a sandstone catchment of the Northern Black Forest using DOC and a nested Approach. Physics and Chemistry of the Earth, Parts A/B/C 28, 269–275. doi:10.1016/S1474-7065(03)00037-8.

Conant, B., Robinson, C.E., Hinton, M.J., Russell, H.A.J., 2019. A framework for conceptualizing groundwater-surface water interactions and identifying potential impacts on water quality, water quantity, and ecosystems. Journal of Hydrology 574, 609–627. doi:10.1016/j.jhydrol.2019.04.050.

Cumberland, S.A., Baker, A., 2007. The freshwater dissolved organic matter fluorescence–total organic carbon relationship. Hydrological Processes 21, 2093–2099. doi:10.1002/hyp.6371.

Darcy, H., 1856. Les fontaines publiques de la ville de Dijon: Exposition et application des principes à suivre et des formules à employer dans les questions de distribution d'eau : Ouvrage terminé par un appendice relatif aux fournitures d'eau de plusieurs villes, au filtrage des eaux et à la fabrication des tuyaux de fonte, de plomb, de tôle et de bitume. V. Dalmont. Google-Books-ID: 42EUAAAAQAAJ.

D'Odorico, P., Caylor, K., Okin, G.S., Scanlon, T.M., 2007. On soil moisture–vegetation feedbacks and their possible effects on the dynamics of dryland ecosystems. Journal of Geophysical Research: Biogeosciences 112. doi:10.1029/2006JG000379.

Dorigo, W., Wagner, W., Albergel, C., Albrecht, F., Balsamo, G., Brocca, L., Chung, D., Ertl, M., Forkel, M., Gruber, A., Haas, E., Hamer, P.D., Hirschi, M., Ikonen, J., de Jeu, R., Kidd, R., Lahoz, W., Liu, Y.Y., Miralles, D., Mistelbauer, T., Nicolai-Shaw, N., Parinussa, R., Pratola, C., Reimer, C., van der Schalie, R., Seneviratne, S.I., Smolander, T., Lecomte, P., 2017. ESA CCI Soil Moisture for improved Earth system understanding: State-of-the art and future directions. Remote Sensing of Environment 203, 185–215. doi:10.1016/j.rse.2017.07.001.

Drever, J.I., Zobrist, J., 1992. Chemical weathering of silicate rocks as a function of elevation in the southern Swiss Alps. Geochimica et Cosmochimica Acta 56, 3209–3216. doi:10.1016/0016-7037(92)90298-W.

Duethmann, D., Blöschl, G., 2018. Why has catchment evaporation increased in the past 40 years? A data-based study in Austria. Hydrology and Earth System Sciences 22, 5143–5158. doi:https://doi.org/10.5194/hess-22-5143-2018.

DWD Climate Data Center, 2020. Calculated daily values for different characteristic elements of soil and crops. URL: ftp://opendata.dwd.de/climate_environment/CDC/derived_germany/soil/daily/historical/.

DWD Climate Data Center (CDC), 2020. Historical daily precipitation observations for Germany. URL: ftp://opendata.dwd.de/climate_environment/CDC/observations_germany/climate/daily/more_precip/historical/.

Evett, S.R., Schwartz, R.C., Howell, T.A., Louis Baumhardt, R., Copeland, K.S., 2012. Can weighing lysimeter ET represent surrounding field ET well enough to test flux station measurements of daily and sub-daily ET? Advances in Water Resources 50, 79–90. doi:10.1016/j.advwatres.2012.07.023.

Evett, S.R., Steiner, J.L., 1995. Precision of Neutron Scattering and Capacitance Type Soil Water Content Gauges from Field Calibration. Soil Science Society of America Journal 59, 961–968. doi:10.2136/sssaj1995.03615995005900040001x.

Feger, K.H., Brahmer, G., 1986. Factors affecting snowmelt streamwater chemistry in the black forest (West Germany). Water, Air, and Soil Pollution 31, 257–265. doi:10.1007/BF00630841.

Feger, K.H., Brahmer, G., Zöttl, H.W., 1990. Element budgets of two contrasting catchments in the Black Forest (Federal Republic of Germany). Journal of Hydrology 116, 85–99. doi:10.1016/0022-1694(90)90117-G.

Feger, K.H., Martin, D., Zöttl, H.W., 1995. Entwicklung der Gewässeracidität im Schwarzwald — sind depositionsbedingte Veränderungen erkennbar? Naturwissenschaften 82, 420–423. doi:10.1007/BF01133676.

Gabrielli, C.P., McDonnell, J.J., Jarvis, W.T., 2012. The role of bedrock groundwater in rainfall–runoff response at hillslope and catchment scales. Journal of Hydrology 450-451, 117–133. doi:10.1016/j.jhydrol.2012.05.023.

Garcia, R.D., Reissig, M., Queimaliños, C.P., Garcia, P.E., Dieguez, M.C., 2015. Climate-driven terrestrial inputs in ultraoligotrophic mountain streams of Andean Patagonia revealed through chromophoric and fluorescent dissolved organic matter. Science of The Total Environment 521–522, 280–292. doi:10.1016/j.scitotenv.2015.03.102.

Gattinoni, P., Scesi, L., 2018. Short review of some methods for groundwater flow assessment in fractured rock masses. Acque Sotterranee - Italian Journal of Groundwater 7, 7–17. doi:10.7343/as-2018-342.

Gerecke, R., Cantonati, M., Spitale, D., Stur, E., Wiedenbrug, S., 2011. The challenges of long-term ecological research in springs in the northern and southern Alps: indicator groups, habitat diversity, and medium-term change. Journal of Limnology , 168–187doi:10.4081/jlimnol.2011.s1.168.

Gerlach, A., 2007. Wasserbilanzierung der Oberflächen-Abdichtung von Deponien unter Verwendung mathematischer Bilanzierungsmodelle. Dissertation. Universität Karlsruhe. Karlsruhe. URL: https://publikationen.bibliothek.kit.edu/1000006087, doi:10.5445/IR/1000006087.

Gibbs, R.J., 1970. Mechanisms Controlling World Water Chemistry. Science, New Series 170, 1088–1090.

Goldscheider, N., Klute, M., Sturm, S., Hötzl, H., 2000. The PI method - A GIS-based approach to mapping groundwater vulnerability with special consideration of karst aquifers. Zeitschrift fur Angewandte Geologie 46, 157–166.

Goss, M.J., Ehlers, W., Unc, A., 2010. The role of lysimeters in the development of our understanding of processes in the vadose zone relevant to contamination of groundwater aquifers. Physics and Chemistry of the Earth, Parts A/B/C 35, 913–926. doi:10.1016/j.pce.2010.06.004.

Groh, J., Slawitsch, V., Herndl, M., Graf, A., Vereecken, H., Pütz, T., 2018. Determining dew and hoar frost formation for a low mountain range and alpine grassland site by weighable lysimeter. Journal of Hydrology 563, 372–381. doi:10.1016/j.jhydrol.2018.06.009.

Hangen, E., Lindenlaub, M., Leibundgut, C., von Wilpert, K., 2001. Investigating mechanisms of stormflow generation by natural tracers and hydrometric data: a small catchment study in the Black Forest, Germany. Hydrological Processes 15, 183–199. doi:10.1002/hyp.142.

Hartmann, J., Jansen, N., Dürr, H.H., Kempe, S., Köhler, P., 2009. Global CO_2-consumption by chemical weathering: What is the contribution of highly active weathering regions? Global and Planetary Change 69, 185–194. doi:10.1016/j.gloplacha.2009.07.007.

Hinderer, M., Einsele, G., 1998. Grundwasserversauerung in Baden-Württemberg / Hrsg. von der Landesanstalt für Umweltschutz, [Abteilung 4 - Wasser und Altlasten. Verf.: M. Hinderer ; G. Einsele.].

Hinderer, M., Jüttner, I., Winkler, R., Steinberg, C.E.W., Kettrup, A., 1998. Comparing trends in lake acidification using hydrochemical modelling and paleolimnology: The case of the Herrenwieser See, Black Forest, Germany. Science of The Total Environment 218, 113–121. doi:10.1016/S0048-9697(98)00187-9.

Hirschi, M., Seneviratne, S.I., Alexandrov, V., Boberg, F., Boroneant, C., Christensen, O.B., Formayer, H., Orlowsky, B., Stepanek, P., 2011. Observational evidence for soil-moisture impact on hot extremes in southeastern Europe. Nature Geoscience 4, 17–21. doi:10.1038/ngeo1032.

Hodnett, M.G., 1986. The Neutron Probe for Soil Moisture Measurement, in: Gensler, W.G. (Ed.), Advanced Agricultural Instrumentation: Design and Use. Springer Netherlands, Dordrecht. NATO ASI Series, pp. 148–192. URL: `https://doi.org/10.1007/978-94-009-4404-6_7`, doi:10.1007/978-94-009-4404-6_7.

Hongve, D., 1987. A revised procedure for discharge measurement by means of the salt dilution method. Hydrological Processes 1, 267–270. doi:10.1002/hyp.3360010305.

Hothorn, T., Hornik, K., Zeileis, A., 2006. Unbiased Recursive Partitioning: A Conditional Inference Framework. Journal of Computational and Graphical Statistics 15, 651–674. doi:10.1198/106186006X133933.

Hothorn, T., Zeileis, A., 2015. partykit: A Modular Toolkit for Recursive Partytioning in R. Journal of Machine Learning Research 16, 3905–3909.

IDEXX Laboratories, I., . Colisure procedure 06-14048-06. URL: `https://www.idexx.com/files/colisure-procedure-en.pdf`.

IDEXX Laboratories, Inc., . Enterolert procedure 06-02150-15. URL: `https://www.idexx.com/files/enterolert-procedure-en.pdf`.

Ionita, M., Nagavciuc, V., Kumar, R., Rakovec, O., 2020. On the curious case of the recent decade, mid-spring precipitation deficit in central Europe. npj Climate and Atmospheric Science 3, 1–10. doi:10.1038/s41612-020-00153-8.

IPCC, 2020. Working Group I – The Physical Science Basis. URL: `https://www.ipcc.ch/working-group/wg1/`.

Jackisch, C., Germer, K., Graeff, T., Andrä, I., Schulz, K., Schiedung, M., Haller-Jans, J., Schneider, J., Jaquemotte, J., Helmer, P., Lotz, L., Bauer, A., Hahn, I., Šanda, M., Kumpan, M., Dorner, J., Rooij, G.d., Wessel-Bothe, S., Kottmann, L., Schittenhelm, S., Durner, W., 2020. Soil moisture and matric potential – an open field comparison of sensor systems. Earth System Science Data 12, 683–697. doi:https://doi.org/10.5194/essd-12-683-2020.

Kędzior, M., Zawadzki, J., 2016. Comparative study of soil moisture estimations from SMOS satellite mission, GLDAS database, and cosmic-ray neutrons measurements at COSMOS station in Eastern Poland. Geoderma 283, 21–31. doi:10.1016/j.geoderma.2016.07.023.

Kløve, B., Ala-aho, P., Bertrand, G., Boukalova, Z., Ertürk, A., Goldscheider, N., Ilmonen, J., Karakaya, N., Kupfersberger, H., Kværner, J., Lundberg, A., Mileusnić, M., Moszczynska, A., Muotka, T., Preda, E., Rossi, P., Siergieiev, D., Šimek, J., Wachniew, P., Angheluta, V., Widerlund, A., 2011. Groundwater dependent ecosystems. Part I: Hydroecological status and trends. Environmental Science & Policy 14, 770–781. doi:10.1016/j.envsci.2011.04.002.

Kløve, B., Ala-Aho, P., Bertrand, G., Gurdak, J.J., Kupfersberger, H., Kværner, J., Muotka, T., Mykrä, H., Preda, E., Rossi, P., Uvo, C.B., Velasco, E., Pulido-Velazquez, M., 2014. Climate change impacts on groundwater and dependent ecosystems. Journal of Hydrology 518, 250–266. doi:10.1016/j.jhydrol.2013.06.037.

Knauss, K.G., Wolery, T.J., 1988. The dissolution kinetics of quartz as a function of pH and time at 70°C. Geochimica et Cosmochimica Acta 52, 43–53. doi:10.1016/0016-7037(88)90055-5.

Kolusu, S.R., Shamsudduha, M., Todd, M.C., Taylor, R.G., Seddon, D., Kashaigili, J.J., Ebrahim, G.Y., Cuthbert, M.O., Sorensen, J.P.R., Villholth, K.G., MacDonald, A.M., MacLeod, D.A., 2019. The El Niño event of 2015–2016: climate anomalies and their impact on groundwater resources in East and Southern Africa. Hydrology and Earth System Sciences 23, 1751–1762. doi:https://doi.org/10.5194/hess-23-1751-2019.

Kottek, M., Grieser, J., Beck, C., Rudolf, B., Rubel, F., 2006. World Map of the Köppen-Geiger climate classification updated. Meteorologische Zeitschrift , 259–263doi:10.1127/0941-2948/2006/0130.

Lanen, H.A.J.V., Laaha, G., Kingston, D.G., Gauster, T., Ionita, M., Vidal, J.P., Vlnas, R., Tallaksen, L.M., Stahl, K., Hannaford, J., Delus, C., Fendekova, M., Mediero, L., Prudhomme, C., Rets, E., Romanowicz, R.J., Gailliez, S., Wong, W.K., Adler, M.J., Blauhut, V., Caillouet, L., Chelcea, S., Frolova, N., Gudmundsson, L., Hanel, M., Haslinger, K., Kireeva, M., Osuch, M., Sauquet, E., Stagge, J.H., Loon, A.F.V., 2016. Hydrology needed to manage droughts: the 2015 European case. Hydrological Processes 30, 3097–3104. doi:10.1002/hyp.10838.

Leibundgut, C., Abraham, V., Landesanstalt für Umwelt, M.u.N.B.W., Landesanstalt für Umweltschutz Baden-Württemberg, 2001. WaBoA Wasser- und Bodenatlas Baden-Württemberg. OCLC: 723617895.

Li, B., Pales, A.R., Clifford, H.M., Kupis, S., Hennessy, S., Liang, W.Z., Moysey, S., Powell, B., Finneran, K.T., Darnault, C.J.G., 2018. Preferential flow in the vadose zone and interface dynamics: Impact of microbial exudates. Journal of Hydrology 558, 72–89. doi:10.1016/j.jhydrol.2017.12.065.

Li, J., Xu, R., Tiwari, D., Ji, G., 2006. Mechanism of aluminum release from variable charge soils induced by low-molecular-weight organic acids: Kinetic study. Geochimica et Cosmochimica Acta 70, 2755–2764. doi:10.1016/j.gca.2006.03.017.

Li, Z., Liu, H., Zhao, W., Yang, Q., Yang, R., Liu, J., 2019. Quantification of soil water balance components based on continuous soil moisture measurement and the Richards equation in an irrigated agricultural field of a desert oasis. Hydrology and Earth System Sciences 23, 4685–4706. doi:https://doi.org/10.5194/hess-23-4685-2019.

Liancourt, P., Sharkhuu, A., Ariuntsetseg, L., Boldgiv, B., Helliker, B.R., Plante, A.F., Petraitis, P.S., Casper, B.B., 2012. Temporal and spatial variation in how vegetation alters the soil moisture response to climate manipulation. Plant and Soil 351, 249–261. doi:10.1007/s11104-011-0956-y.

Liesch, T., Wunsch, A., 2019. Aquifer responses to long-term climatic periodicities. Journal of Hydrology 572, 226–242. doi:10.1016/j.jhydrol.2019.02.060.

Lin, H., 2010. Earth's Critical Zone and hydropedology: concepts, characteristics, and advances. Hydrology and Earth System Sciences 14, 25–45. doi:https://doi.org/10.5194/hess-14-25-2010.

Long, D., Bai, L., Yan, L., Zhang, C., Yang, W., Lei, H., Quan, J., Meng, X., Shi, C., 2019. Generation of spatially complete and daily continuous surface soil moisture of high spatial resolution. Remote Sensing of Environment 233, 111364. doi:10.1016/j.rse.2019.111364.

Maher, K., Druhan, J., 2014. Relationships between the Transit Time of Water and the Fluxes of Weathered Elements through the Critical Zone. Procedia Earth and Planetary Science 10, 16–22. doi:10.1016/j.proeps.2014.08.004.

Mahmood, R., Littell, A., Hubbard, K.G., You, J., 2012. Observed data-based assessment of relationships among soil moisture at various depths, precipitation, and temperature. Applied Geography 34, 255–264. doi:10.1016/j.apgeog.2011.11.009.

Mälicke, M., Hassler, S.K., Blume, T., Weiler, M., Zehe, E., 2019. Soil moisture: variable in space but redundant in time. Hydrology and Earth System Sciences Discussions , 1–28doi:10.5194/hess-2019-574.

Mälicke, M., Hassler, S.K., Blume, T., Weiler, M., Zehe, E., 2020. Soil moisture: variable in space but redundant in time. Hydrology and Earth System Sciences 24, 2633–2653. doi:https://doi.org/10.5194/hess-24-2633-2020.

McGuire, K.J., McDonnell, J.J., 2006. A review and evaluation of catchment transit time modeling. Journal of Hydrology 330, 543–563. doi:10.1016/j.jhydrol.2006.04.020.

Meinzer, O.E., 1927. Large springs in the United States. USGS Numbered Series 557. U.S. Government Printing Office. Washington, D.C. URL: http://pubs.er.usgs.gov/publication/wsp557, doi:10.3133/wsp557. code Number: 557 Code: Large springs in the United States Publication Title: Large springs in the United States Reporter: Large springs in the United States Series: Water Supply Paper.

Menzel, L., 1999. Flächenhafte Modellierung der Evapotranspiration mit TRAIN. Technical Report. Potsdam-Institut für Klimafolgenforschung e.V.

Merk, M., Goeppert, N., Goldscheider, N., 2020. Processes controlling spatial and temporal dynamics of spring water chemistry in the Black Forest National Park. Science of The Total Environment 723, Article: 137742. doi:10.1016/j.scitotenv.2020.137742.

Murtagh, F., Legendre, P., 2014. Ward's Hierarchical Agglomerative Clustering Method: Which Algorithms Implement Ward's Criterion? Journal of Classification 31, 274–295. doi:10.1007/s00357-014-9161-z.

Neukum, C., Azzam, R., 2012. Impact of climate change on groundwater recharge in a small catchment in the Black Forest, Germany. Hydrogeology Journal 20, 547–560. doi:10.1007/s10040-011-0827-x.

Ohno, T., 2002. Fluorescence Inner-Filtering Correction for Determining the Humification Index of Dissolved Organic Matter. Environmental Science & Technology 36, 742–746. doi:10.1021/es0155276.

Otkin, J.A., Anderson, M.C., Hain, C., Svoboda, M., Johnson, D., Mueller, R., Tadesse, T., Wardlow, B., Brown, J., 2016. Assessing the evolution of soil moisture and vegetation conditions during the 2012 United States flash drought. Agricultural and Forest Meteorology 218-219, 230–242. doi:10.1016/j.agrformet.2015.12.065.

OTT, 2010. OTT CTD Grundwasser-Datensammler. URL: http://www.ott.com/de-de/produkte/download/prospekt-grundwasser-datensammler-mit-leitfahigkeitsmesszelle-ott-ctd/.

Parkhurst, D.L., Appelo, C., 2013. Description of input and examples for PHREEQC version 3: a computer program for speciation, batch-reaction, one-dimensional transport, and inverse geochemical calculations. USGS Numbered Series 6-A43. U.S. Geological Survey. Reston, VA. URL: http://pubs.er.usgs.gov/publication/tm6A43.

Pellenq, J., Kalma, J., Boulet, G., Saulnier, G.M., Wooldridge, S., Kerr, Y., Chehbouni, A., 2003. A disaggregation scheme for soil moisture based on topography and soil depth. Journal of Hydrology 276, 112–127. doi:10.1016/S0022-1694(03)00066-0.

Penna, D., Borga, M., Norbiato, D., Dalla Fontana, G., 2009. Hillslope scale soil moisture variability in a steep alpine terrain. Journal of Hydrology 364, 311–327. doi:10.1016/j.jhydrol.2008.11.009.

Perkins, S.E., 2015. A review on the scientific understanding of heatwaves—Their measurement, driving mechanisms, and changes at the global scale. Atmospheric Research 164-165, 242–267. doi:10.1016/j.atmosres.2015.05.014.

Pflanz, D., Hornung, J., Hinderer, M., 2014. Dreidimensionale Hydrostratigrafie eines Tal-Hang-Aquifers: Kombination von Georadar, Geoelektrik, Bodenkunde und Sedimentologie am Beispiel des Seebachs, Nordschwarzwald [Three-dimensional hydrostratigraphy of a hillslope valley aquifer: combination of GPR, geoelectrics, pedology and sedimentology using the example of the Seebach, northern Black Forest]. Zeitschrift der Deutschen Gesellschaft für Geowissenschaften 165, 425–438. doi:10.1127/1860-1804/2014/0073.

Piper, A.M., 1944. A graphic procedure in the geochemical interpretation of water-analyses. Transactions, American Geophysical Union 25, 914. doi:10.1029/TR025i006p00914.

Prédélus, D., Coutinho, A.P., Lassabatere, L., Bien, L.B., Winiarski, T., Angulo-Jaramillo, R., 2015. Combined effect of capillary barrier and layered slope on water, solute and nanoparticle transfer in an unsaturated soil at lysimeter scale. Journal of Contaminant Hydrology 181, 69–81. doi:10.1016/j.jconhyd.2015.06.008.

Probst, A., Fritz, B., Ambroise, B., Viville, D., 1987. Forest influence on the surface water chemistry of granitic basins receiving acid precipitation in the Vosges massif, France. Forest Hydrology and Watershed Management , 109–120.

Qin, M., Giménez, D., Miskewitz, R., 2018. Temporal dynamics of subsurface soil water content estimated from surface measurement using wavelet transform. Journal of Hydrology 563, 834–850. doi:10.1016/j.jhydrol.2018.06.023.

Quadflieg, A., 1990. Zur Geohydrochemie der Kluftgrundwasserleiter des nord- und osthessischen Buntsandsteingebietes und deren Beeinflussung durch saure Depositionen. volume 90 of *Geologische Abhandlungen Hessen*. Hess. Landesamt für Bodenforschung, Wiesbaden.

R Core Team, 2017. R: A Language and Environment for Statistical Computing. URL: https://www.R-project.org.

R Core Team, 2020. R: A Language and Environment for Statistical Computing. URL: https://www.R-project.org.

Richards, L.A., 1931. Capillary conduction of liquids through porous mediums. Physics 1, 318–333. doi:10.1063/1.1745010.

Rimstidt, J.D., 1997. Quartz solubility at low temperatures. Geochimica et Cosmochimica Acta 61, 2553–2558. doi:10.1016/S0016-7037(97)00103-8.

Rivera Villarreyes, C.A., Baroni, G., Oswald, S.E., 2011. Integral quantification of seasonal soil moisture changes in farmland by cosmic-ray neutrons. Hydrology and Earth System Sciences 15, 3843–3859. doi:https://doi.org/10.5194/hess-15-3843-2011.

Robinson, D.A., Jones, S.B., Lebron, I., Reinsch, S., Domínguez, M.T., Smith, A.R., Jones, D.L., Marshall, M.R., Emmett, B.A., 2016. Experimental evidence for drought induced alternative stable states of soil moisture. Scientific Reports 6, 20018. doi:10.1038/srep20018.

Ross, D.S., G., M., U., S., 2008. Cation exchange in forest soils: the need for a new perspective. European Journal of Soil Science 59, 1141–1159. doi:10.1111/j.1365-2389.2008.01069.x.

Roth, V.N., Lange, M., Simon, C., Hertkorn, N., Bucher, S., Goodall, T., Griffiths, R.I., Mellado-Vázquez, P.G., Mommer, L., Oram, N.J., Weigelt, A., Dittmar, T., Gleixner, G., 2019. Persistence of dissolved organic matter explained by molecular changes during its passage through soil. Nature Geoscience 12, 755–761. doi:10.1038/s41561-019-0417-4.

Samaniego, L., Kumar, R., Zink, M., 2012. Implications of Parameter Uncertainty on Soil Moisture Drought Analysis in Germany. Journal of Hydrometeorology 14, 47–68. doi:10.1175/JHM-D-12-075.1.

Samaniego, L., Thober, S., Kumar, R., Wanders, N., Rakovec, O., Pan, M., Zink, M., Sheffield, J., Wood, E.F., Marx, A., 2018. Anthropogenic warming exacerbates European soil moisture droughts. Nature Climate Change 8, 421–426. doi:10.1038/s41558-018-0138-5.

Scheliga, B., Tetzlaff, D., Nuetzmann, G., Soulsby, C., 2018. Groundwater dynamics at the hillslope–riparian interface in a year with extreme winter rainfall. Journal of Hydrology 564, 509–528. doi:10.1016/j.jhydrol.2018.06.082.

Schenk, E.R., O'Donnell, F., Springer, A.E., Stevens, L.E., 2020. The impacts of tree stand thinning on groundwater recharge in aridland forests. Ecological Engineering 145, 105701. doi:10.1016/j.ecoleng.2019.105701.

Schneider, J., Groh, J., Pütz, T., Helmig, R., Rothfuss, Y., Vereecken, H., Vanderborght, J., 2021. Prediction of soil evaporation measured with weighable lysimeters using the FAO Penman–Monteith method in combination with Richards' equation. Vadose Zone Journal 20, e20102. doi:https://doi.org/10.1002/vzj2.20102.

Schnellmann, R., Busslinger, M., Schneider, H.R., Rahardjo, H., 2010. Effect of rising water table in an unsaturated slope. Engineering Geology 114, 71–83. doi:10.1016/j.enggeo.2010.04.005.

Schnetzer, F., 2017. The Interaction of Water and 2:1 Layer Silicates. PhD Thesis. Karlsruher Institut für Technologie (KIT). doi:10.5445/IR/1000067415.

Schoen, R., Gaudet, J.P., Bariac, T., 1999. Preferential flow and solute transport in a large lysimeter, under controlled boundary conditions. Journal of Hydrology 215, 70–81. doi:10.1016/S0022-1694(98)00262-5.

Seneviratne, S.I., Corti, T., Davin, E.L., Hirschi, M., Jaeger, E.B., Lehner, I., Orlowsky, B., Teuling, A.J., 2010. Investigating soil moisture–climate interactions in a changing climate: A review. Earth-Science Reviews 99, 125–161. doi:10.1016/j.earscirev.2010.02.004.

Siegel, D., Glaser, P., So, J., Janecky, D., 2006. The dynamic balance between organic acids and circumneutral groundwater in a large boreal peat basin. Journal of Hydrology 320, 421–431. doi:10.1016/j.jhydrol.2005.07.046.

Šimůnek, J., Jarvis, N.J., van Genuchten, M., Gärdenäs, A., 2003. Review and comparison of models for describing non-equilibrium and preferential flow and transport in the vadose zone. Journal of Hydrology 272, 14–35. doi:10.1016/S0022-1694(02)00252-4.

Singh, G., Kaur, G., Williard, K., Schoonover, J., Kang, J., 2018. Monitoring of Water and Solute Transport in the Vadose Zone: A Review. Vadose Zone Journal 17, 160058. doi:10.2136/vzj2016.07.0058.

Solander, K.C., Newman, B.D., Carioca de Araujo, A., Barnard, H.R., Berry, Z.C., Bonal, D., Bretfeld, M., Burban, B., Antonio Candido, L., Célleri, R., Chambers, J.Q., Christoffersen, B.O., Detto, M., Dorigo, W.A., Ewers, B.E., José Filgueiras Ferreira, S., Knohl, A., Leung, L.R., McDowell, N.G., Miller, G.R., Terezinha Ferreira Monteiro, M., Moore, G.W., Negron-Juarez, R., Saleska, S.R., Stiegler, C., Tomasella, J., Xu, C., 2020. The pantropical response of soil moisture to El Niño. Hydrology and Earth System Sciences 24, 2303–2322. doi:https://doi.org/10.5194/hess-24-2303-2020.

Sołtysiak, M., Rakoczy, M., 2019. An overview of the experimental research use of lysimeters. Environmental & Socio-economic Studies 7, 49–56. doi:10.2478/environ-2019-0012.

Sommer, M., Thies, H., Kolb, E., Bächle, H., Stahr, K., 1997. Biogeochemistry of a cirque-lake landscape: An interdisciplinary study in a catchment of the northern Black Forest, Germany. Water Resources Research 33, 2129–2142. doi:10.1029/97WR01501.

Springer, A.E., Stevens, L.E., 2008. Spheres of discharge of springs. Hydrogeology Journal 17, 83. doi:10.1007/s10040-008-0341-y.

Stober, I., 1996. Hydrogeological investigations in crystalline rocks of the Black Forest, Germany. Terra Nova 8, 255–258. doi:10.1111/j.1365-3121.1996.tb00754.x.

Stober, I., Bucher, K., 1999. Deep groundwater in the crystalline basement of the Black Forest Region. Applied Geochemistry 14, 237–254. doi:10.1016/S0883-2927(98)00045-6.

Sucker, C., Puhlmann, H., Zirlewagen, D., Wilpert, K., Feger, K.H., 2009. Bodenschutzkalkungen in Wäldern zur Verbesserung der Wasserqualität – Vergleichende Untersuchungen auf Einzugsgebietsebene. Hydrologie und Wasserbewirtschaftung 53, 250–262.

Suryatmojo, H., Masamitsu, F., Kosugi, K., Mizuyama, T., 2013. Effects of Selective Logging Methods on Runoff Characteristics in Paired Small Headwater Catchment. Procedia Environmental Sciences 17, 221–229. doi:10.1016/j.proenv.2013.02.032.

Terajima, T., Moriizumi, M., 2013. Temporal and spatial changes in dissolved organic carbon concentration and fluorescence intensity of fulvic acid like materials in mountainous headwater catchments. Journal of Hydrology 479, 1–12. doi:10.1016/j.jhydrol.2012.10.023.

Tetzlaff, D., Malcolm, I.A., Soulsby, C., 2007. Influence of forestry, environmental change and climatic variability on the hydrology, hydrochemistry and residence times of upland catchments. Journal of Hydrology 346, 93–111. doi:10.1016/j.jhydrol.2007.08.016.

Thies, H., 1994. Chemical properties of an acidified humic headwater lake with respect to reducing acidic depositions and expected climate change. Hydrobiologia 274, 143–154. doi:10.1007/BF00014637.

Tunaley, C., Tetzlaff, D., Lessels, J., Soulsby, C., 2016. Linking high-frequency DOC dynamics to the age of connected water sources. Water Resources Research 52, 5232–5247. doi:10.1002/2015WR018419.

Van Tol, J., Le Roux, P., Hensley, M., Lorentz, S., 2010. Soil as indicator of hillslope hydrological behaviour in the Weatherley Catchment, Eastern Cape, South Africa. Water SA 36. doi:10.4314/wsa.v36i5.61985.

Vanderborght, J., Fetzer, T., Mosthaf, K., Smits, K.M., Helmig, R., 2017. Heat and water transport in soils and across the soil-atmosphere interface: 1. Theory and different model concepts. Water Resources Research 53, 1057–1079. doi:https://doi.org/10.1002/2016WR019982.

Volkmann, H.N., 2002. Gelöste organische Kohlenstoffverbindungen (DOC) im Dürreychbachtal (Nordschwarzwald). Dissertation. Universität Fridericiana zu Karlsruhe (TH). Karlsruhe. URL: `http://www.duerreych.de/Literatur/volkmann.pdf`.

Waldenmeyer, G., 2003. Abflussbildung und Regionalisierung in einem forstlich genutzten Einzugsgebiet (Dürreychtal, Nordschwarzwald). volume 20 of *Karlsruher Schriften zur Geographie und Geoökologie*. Institut für Geographie und Geoökologie der Universität Karlsruhe (TH), Karlsruhe. OCLC: 231977953 Dissertation, genehmigt von der Fakultät für Bio- und Geowissenschaften der Universität Fridericiana zu Karlsruhe (TH), 2002.

Walker, J.P., Houser, P.R., 2002. Evaluation of the OhmMapper Instrument for Soil Moisture Measurement. Soil Science Society of America 66, 728–734. doi:http://dx.doi.org/10.2136/sssaj2002.0728.

Wang, H., Tetzlaff, D., Soulsby, C., 2018. Modelling the effects of land cover and climate change on soil water partitioning in a boreal headwater catchment. Journal of Hydrology 558, 520–531. doi:10.1016/j.jhydrol.2018.02.002.

Wenninger, J., Uhlenbrook, S., Tilch, N., Leibundgut, C., 2004. Experimental evidence of fast groundwater responses in a hillslope/floodplain area in the Black Forest Mountains, Germany. Hydrological Processes 18, 3305–3322. doi:10.1002/hyp.5686.

Willey, J.D., Kieber, R.J., Eyman, M.S., Avery, G.B., 2000. Rainwater dissolved organic carbon: Concentrations and global flux. Global Biogeochemical Cycles 14, 139–148. doi:10.1029/1999GB900036.

Wisotzky, F., 2011. Angewandte Grundwasserchemie, Hydrogeologie und hydrogeochemische Modellierung: Grundlagen, Anwendungen und Problemlösungen. Springer, Berlin.

Yang, Y., Guan, H., Long, D., Liu, B., Qin, G., Qin, J., Batelaan, O., 2015. Estimation of Surface Soil Moisture from Thermal Infrared Remote Sensing Using an Improved Trapezoid Method. Remote Sensing 7, 8250–8270. doi:10.3390/rs70708250.

Zehe, E., Loritz, R., Jackisch, C., Westhoff, M., Kleidon, A., Blume, T., Hassler, S.K., Savenije, H.H., 2019. Energy states of soil water – a thermodynamic perspective on soil water dynamics and storage-controlled streamflow generation in different landscapes. Hydrology and Earth System Sciences 23, 971–987. doi:https://doi.org/10.5194/hess-23-971-2019.

Zhao, K., Hu, T., Li, Y., 2019a. Rbeast: Bayesian Change-Point Detection and Time Series Decomposition. URL: `https://CRAN.R-project.org/package=Rbeast`.

Zhao, K., Wulder, M.A., Hu, T., Bright, R., Wu, Q., Qin, H., Li, Y., Toman, E., Mallick, B., Zhang, X., Brown, M., 2019b. Detecting change-point, trend, and seasonality in satellite time series data to track abrupt changes and nonlinear dynamics: A Bayesian ensemble algorithm. Remote Sensing of Environment 232, 111181. doi:10.1016/j.rse.2019.04.034.

Zhou, Z., Guo, L., Osburn, C.L., 2015. Fluorescence EEMs and PARAFAC Techniques in the Analysis of Petroleum Components in the Water Column, in: McGenity, T.J., Timmis, K.N., Nogales, B. (Eds.), Hydrocarbon and Lipid Microbiology Protocols. Springer Berlin Heidelberg, Berlin, Heidelberg, pp. 179–200.

Zischak, R., 1997. Alternatives Oberflächenabdichtungssystem "Verstärkte mineralische Abdichtung mit untenliegender Kapillarsperre". Wasserbilanz und Gleichwertigkeit. Dissertation. Universität Karlsruhe. Karlsruhe.

Zöttl, H.W., Feger, K.H., Brahmer, G., 1985. Chemismus von Schwarzwaldgewässern während der Schneeschmelze 1984. Naturwissenschaften 72, 268–270. doi:10.1007/BF00448688.

SUPPLEMENTAL FIGURES FOR CHAPTER 2
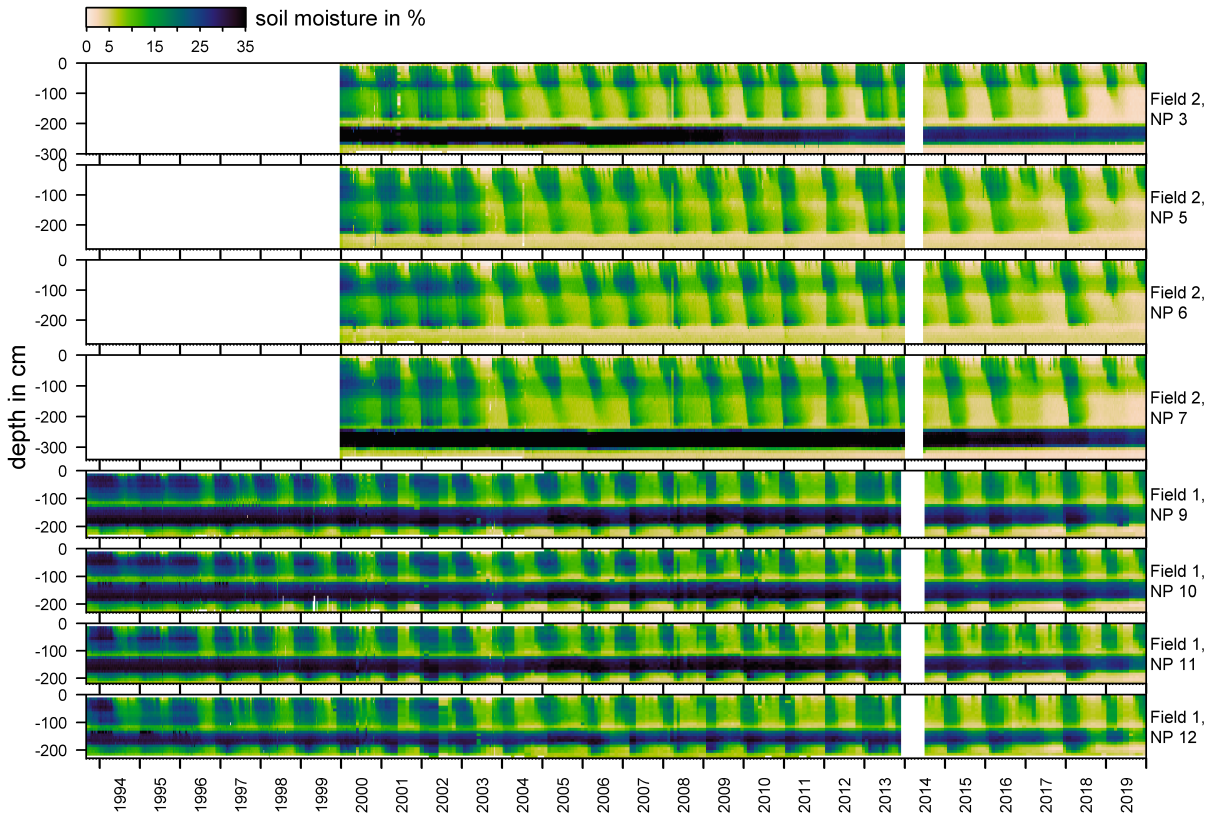
Figure A.1: Time series of soil moisture measurements at the test site near Karlsruhe, Germany. Measurements on Field 2 are available from 2000 onward. No measurements were taken during the first half of the year 2014.
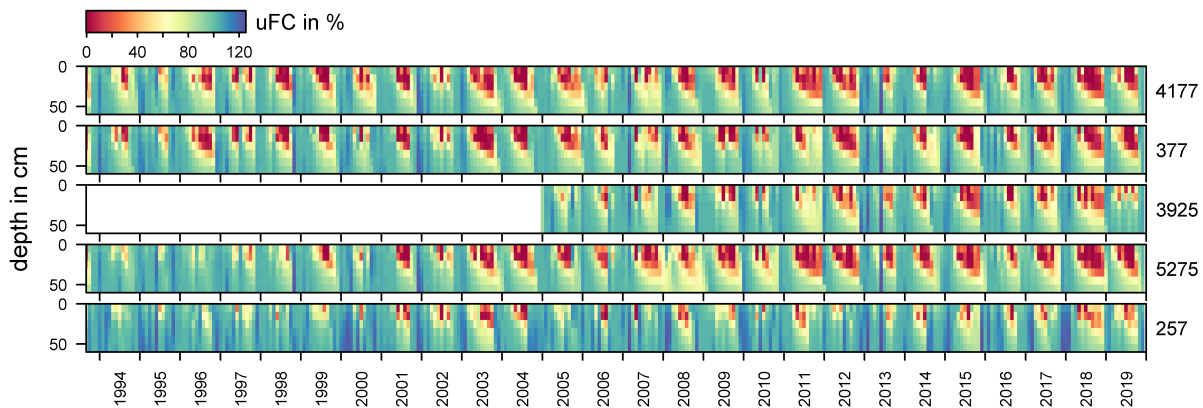
Figure A.2: Monthly averages of usable field capacity calculated at five selected weather stations (DWD Climate Data Center, 2020). Values were computed by the agrometeorological model AMBAV. The model calculates soil moisture under grass with sandy loam. The soil sandy loam has a wilting point of 13 volumic% and a field capacity of 37 volumic%. Further model input parameters are hourly values of temperature, dew point, wind speed, precipitation, global radiation and reflected long-wave radiation.
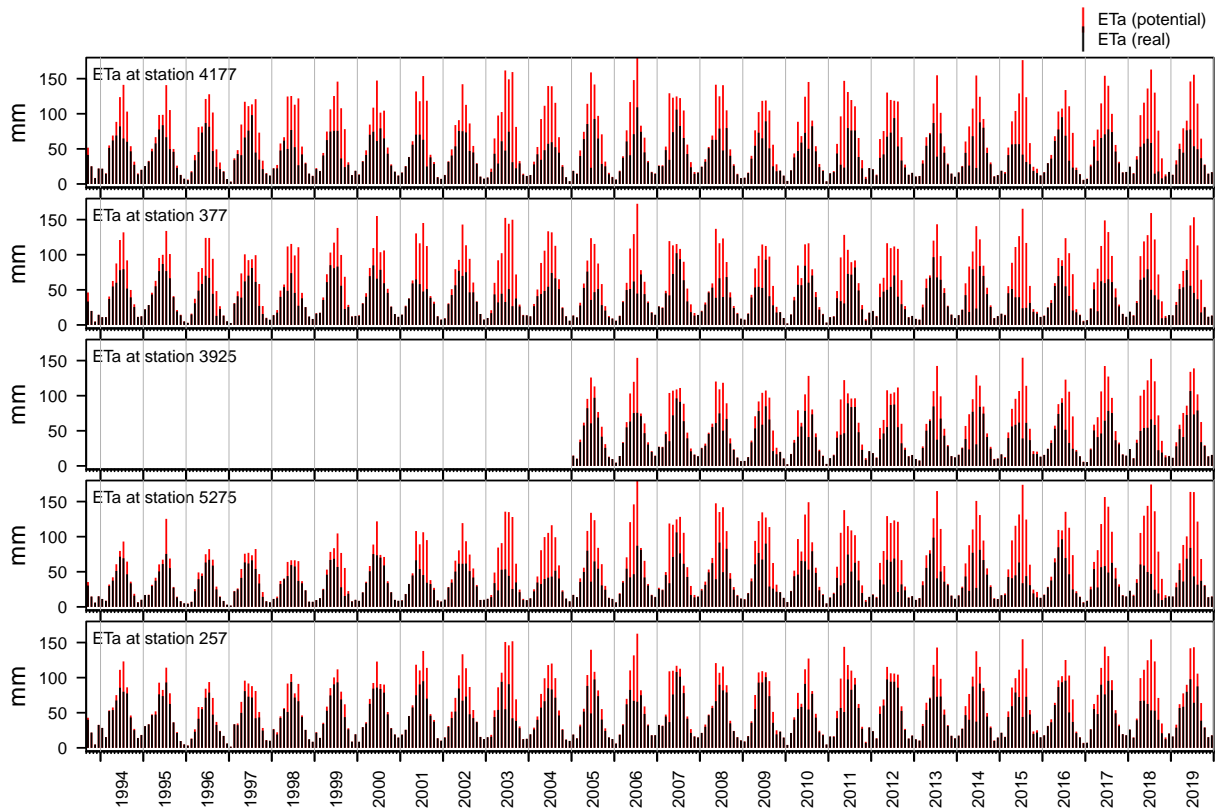
Figure A.3: Potential and real evapotranspiration at five selected weather stations (DWD Climate Data Center, 2020).
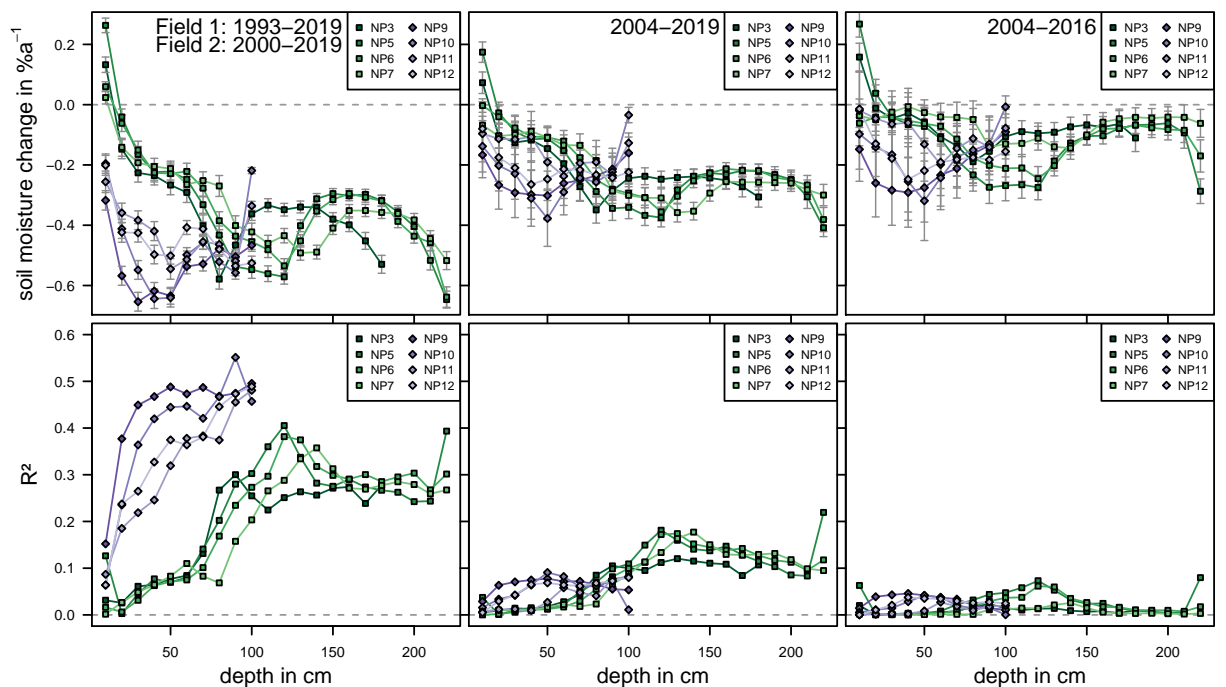
Figure A.4: Results of individual linear regressions for soil moisture measurements in the recultivation layer, expressed as change in soil moisture content $\left[\%a^{-1}\right]$.
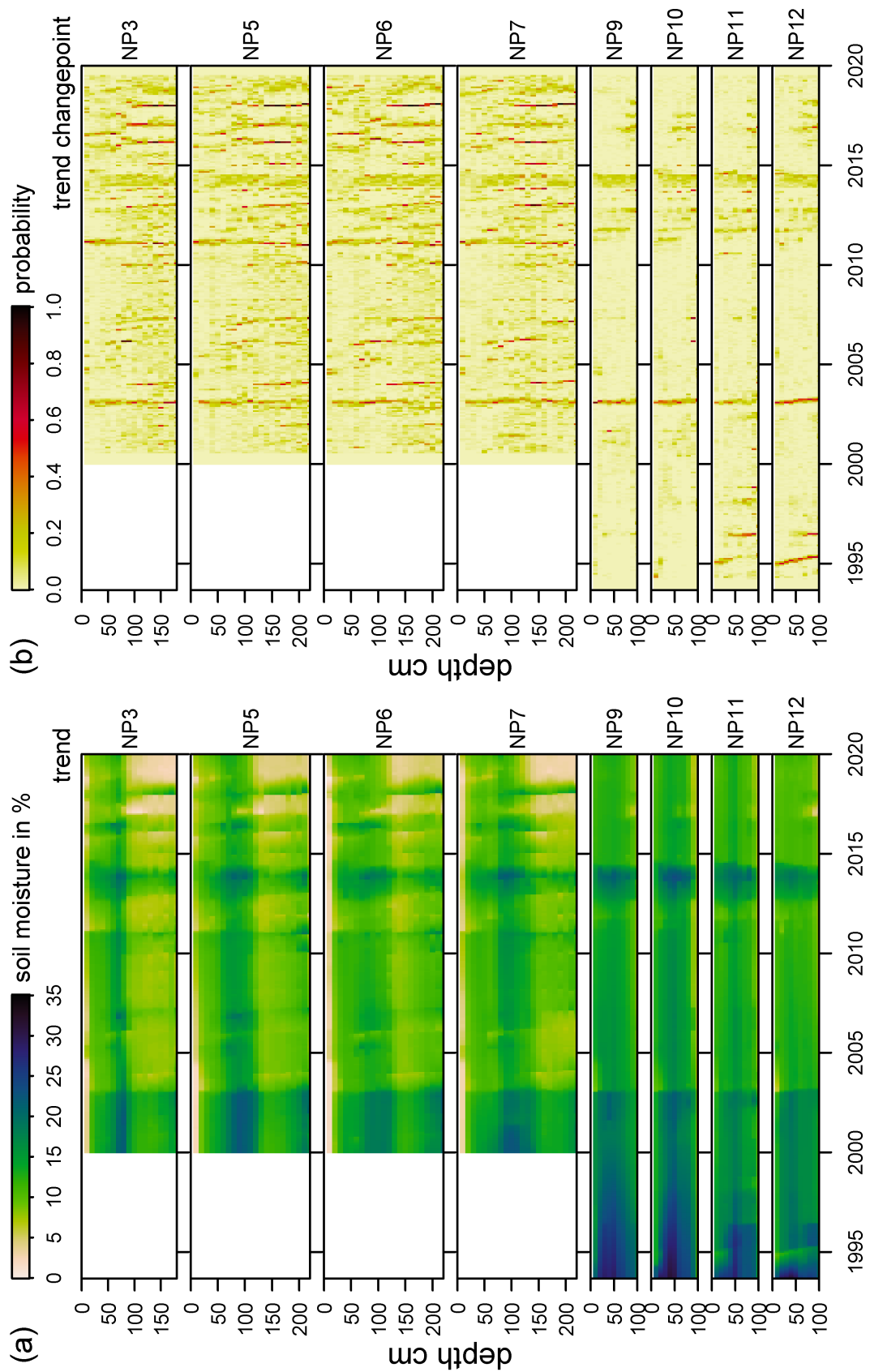
Figure A.5: Results of modeling soil moisture with Rbeast. a) Trend component of soil moisture time series. b) Probability of change point in trend component.
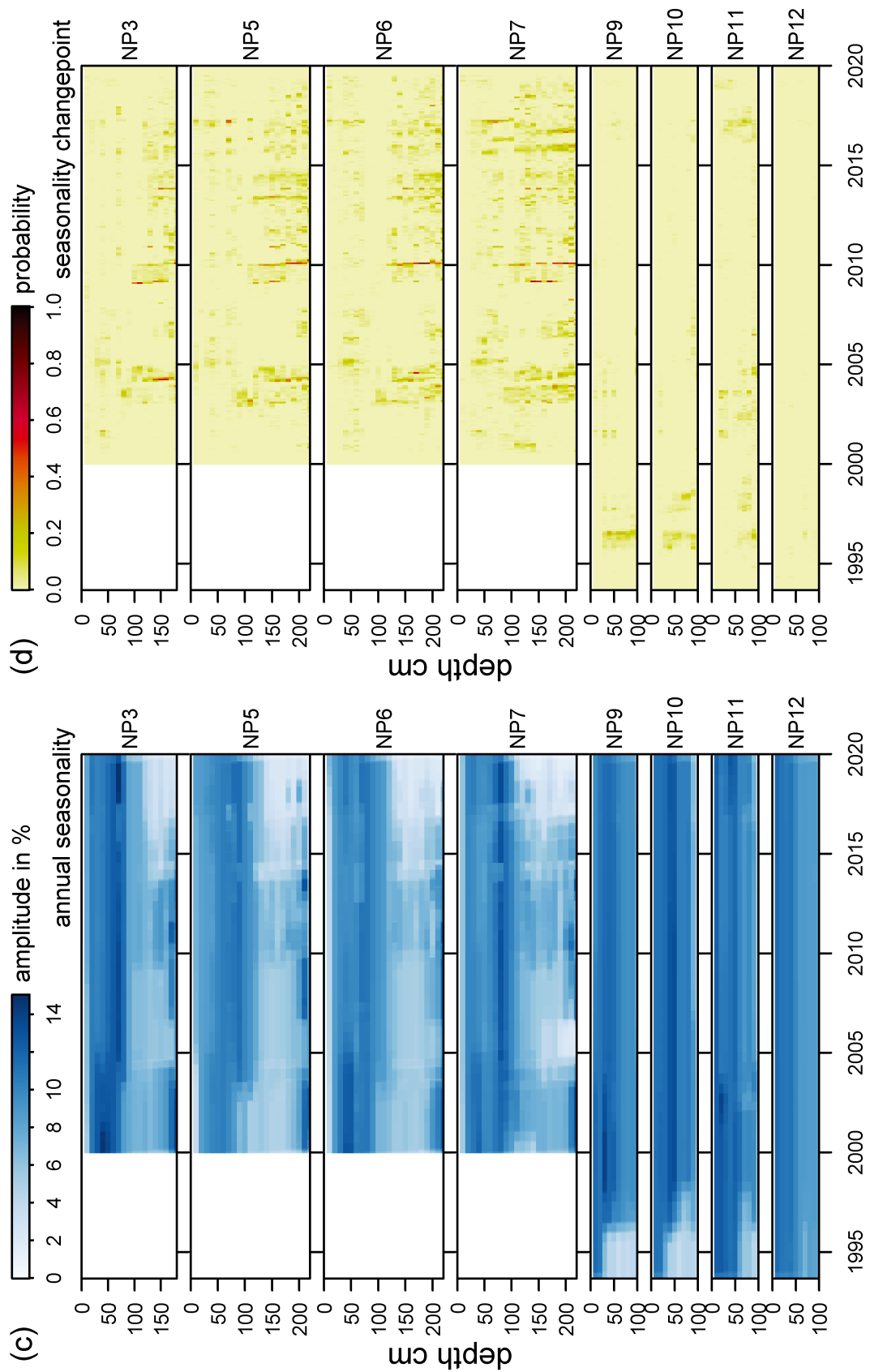
Figure A.6: Results of modeling soil moisture with Rbeast. c) Amplitude of annual seasonality derived from seasonal component. d) Probability of change point in seasonality component.
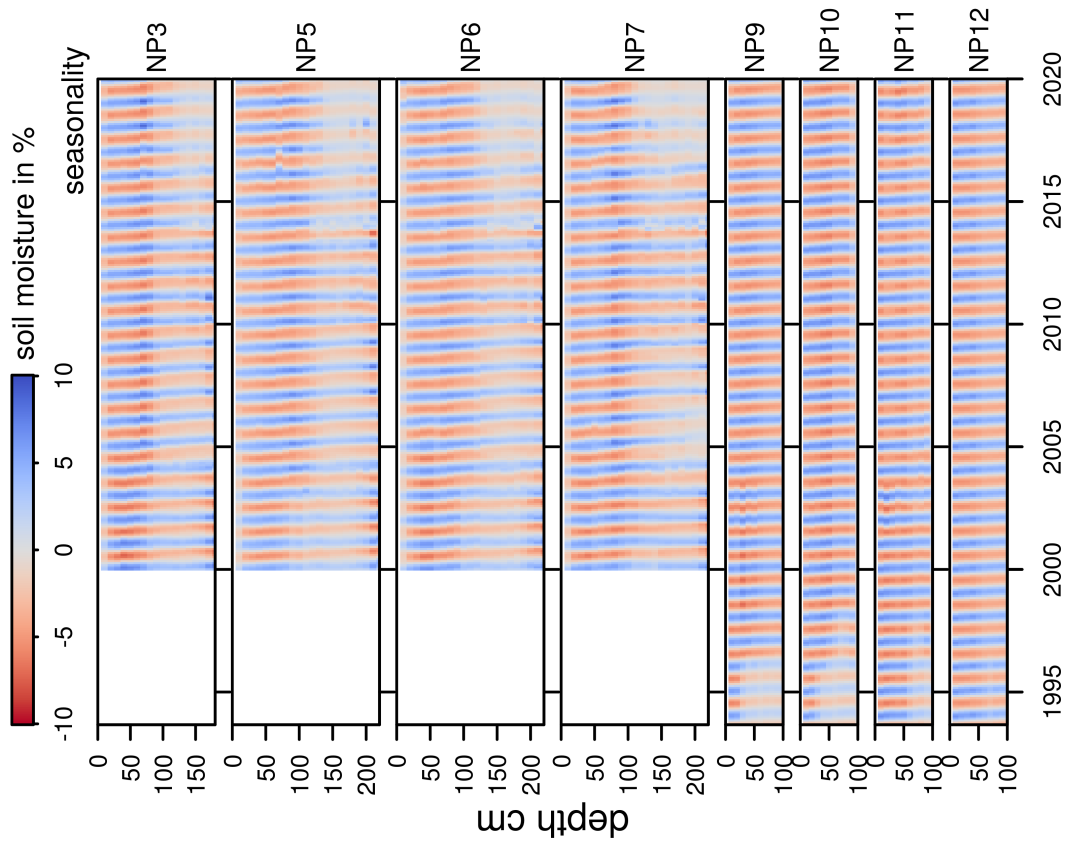
Figure A.7: Results of modeling soil moisture with Rbeast. Seasonal component of soil moisture time series.

B

SUPPLEMENTARY DATA FOR CHAPTER 4

Water Chemistry Data

https://ars.els-cdn.com/content/image/1-s2.0-S2352340920305394-mmc2.xlsx

Absorption

https://ars.els-cdn.com/content/image/1-s2.0-S2352340920305394-mmc3.zip

Fluorescence

https://ars.els-cdn.com/content/image/1-s2.0-S2352340920305394-mmc4.zip

Locations (shp-file)

https://ars.els-cdn.com/content/image/1-s2.0-S2352340920305394-mmc1.zip

Locations (kml-file)

https://ars.els-cdn.com/content/image/1-s2.0-S2352340920305394-mmc5.zip

PAIRED CATCHMENT STUDY

In order to achieve a more comprehensive understanding of the spring ecosystems in the water catchment area of the Schönmünz in the Black Forest National Park, a continuous monitoring network was established.

Hydrogeological sampling had already been carried out at some selected springs in the water catchment area of the Schönmünz (Chapter 3). The field parameters (pH-value, conductivity, temperature, oxygen content, hydrogen carbonate) were determined and water samples were taken for further laboratory analyses. These included the quantification of main cations and ~anions, total organic carbon (TOC) and dissolved organic carbon (DOC) content and dissolved silicate. The fluorescence properties of the water were also measured. As microbiological parameters the number of total coliform bacteria and *E. coli*, as well as the number of enterococci were determined. Sampling was carried out on consecutive days under the same hydrological conditions. The aim of the investigations was and is to better understand the hydrochemical and microbiological characteristics of the individual sources and to identify commonalities and distinguishing features of the individual sources.

C.1 LOCATION OF THE WATER CATCHMENT AREAS

The location of the water catchment areas of the Schönmünz and Langenbach rivers are shown in Figure C.1. The area of the National Park is also shown. The water catchment area of the Schönmünz covers an area of 16.46 km², the water catchment area of the Langenbach covers an area of 16.73 km². In Zwickgabel the Langenbach flows into the Schönmünz, which finally drains into the Rhine via the Murg.

C.2 DESCRIPTION OF UTILIZED MEASUREMENT EQUIPMENT

Two different types of monitoring probes were used. The OTT-CTD (OTT HydroMet GmbH) and AP-5000 multi-parameter probes (Aquaread Ltd.).

OTT-CTD probes measure and record water level, specific electrical conductivity and temperature. The technical specifications are given in Table C.1.

The AP-5000 multi-parameter probes (Aquaread Ltd.) can measure a wide range of field parameters, depending on which of the available sensors are screwed into the probe. Water level, temperature, specific
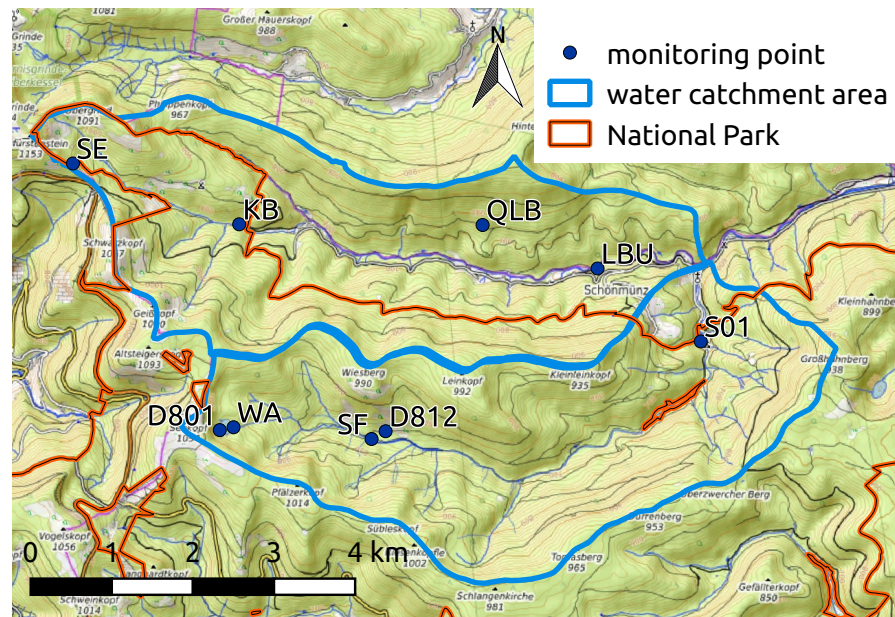
Figure C.1: Location of the water catchment areas of the Schönmünz and Langenbach rivers as well as the area of the Black Forest National Park and the location of the observation points. Basemap: © OpenStreetMap contributors, SRTM. Map display: © OpenTopoMap (CC-BY-SA). cactchment areas Leibundgut et al. (2001).

electrical conductivity and dissolved oxygen is measured by default without additional sensors. For the monitoring system, sensors for pH, redox potential, turbidity and chromophoric dissolved organic carbon (CDOM) were added. The technical specifications of the sensors used are given in Table C.2. For recording of data, a separate data logger of type Aqualogger-7000 (Aquaread Ltd.) was installed.

Due to the poor coverage of cellphone services in the catchment areas, the possibility of remote data connection was abandoned. The installed data loggers must be read out in the field at regular intervals.

C.3 DESCRIPTION OF MONITORING POINTS

In the water catchment area of the Schönmünz, five observation points along the flow path of the water were selected. The observation point situated at the highest altitude is spring D801. This spring discharges into into the Wildsee. The second observation point is at the outlet of the Wildsee. The third observation point is located in the Schönmünz near the weather station installed by the National Park. The fourth observation point is located at the bridge near the youth campground Hahnenbrunnenwiese, where the Schönmünz flows out of the area of the National Park. In addition, an observation point is at spring D812.

Previous investigations have shown a clear difference in water chemistry between springs at higher altitudes around the Wildsee (e.g. D801) and springs at lower altitudes in the Schönmünz valley (e.g.

Table C.1: Technical specifications of OTT-CTD (OTT, 2010).

Depth	Range	0 ... 4 m, 0 ... 10 m, 0 ... 20 m, 0 ... 40 m, 0 ... 100 m
	Resolution	0,001 m / 0,1 cm
	Accuracy	±0,05 % of reading
Specific Electrical Conductivity	Range	0,001 ... 2,000 mS
	Resolution	0,001 mS/cm
	Accuracy	±0,5 % of reading (min. ±0,001 mS/cm)
Temperature	Range	− 25 °C ... +70 °C
	Resolution	0,01 °C
	Accuracy	±0,1 °C

D812) (Merk et al., 2020). For a future comparison of these two groups of springs based on continuous measurement data, both springs were included in the monitoring program.

A total of five monitoring sites in the Schönmünz valley and four monitoring sites in the Langenbach valley were selected. Locations are shown in Figure C.1. Exact coordinates and elevations are given in Table C.3.

C.3.1 *Schönmünz*

The two springs D801 and D812, and three locations in the Schönmünz stream (WA, SF, S01) were selected.

S01   The measuring station at lowest altitude is located in the Schönmünz near the youth campground Hahnenbrunnenwiese. A multi-parameter probe of the type AP-5000 was installed. It measures air pressure, water level, temperature, pH-value, redox potential, dissolved oxygen, electrical conductivity, turbidity and CDOM. The position after installation on 4 April 2018 is shown in Figure C.2.

SF   A probe of the type OTT-CTD was installed on 4 April 2018 under the bridge near the weather station (F) operated by the National Park in the Schönmünz valley (Figure C.3). It records water level, specific electrical conductivity and water temperature.

WA   A probe of the type OTT CTD is installed at the outlet of the Wildsee (Figure C.4). The installation took place on 19 April 2018. It records water level, specific electrical conductivity and water temperature.

Table C.2: Technical specifications of sensors in the AP-5000 multi-parameter probes (Aquaread, 2017).

Optical Dissolved Oxygen	Range	0 – 500.0% / 0 – 50.00 mg/L
	Resolution	0.1% / 0.01mg/L
	Accuracy	0 - 200%: ± 1% of reading. 200% - 500%: ± 10%
Specific Electrical Conductivity	Range	0 – 200 mS/cm (0 - 200,000 µS/cm)
	Resolution	3 Auto-range scales: 0 – 9999 µS/cm, 10.00 – 99.99 mS/cm, 100.0 – 200.0mS/cm
	Accuracy	± 1% of reading or ± 1µS/cm if greater
pH	Range	0 – 14 pH / ± 625mV
	Resolution	0.01 pH / ± 0.1mV
	Accuracy	± 0.1 pH / ± 5mV
ORP	Range	± 2000mV
	Resolution	0.1mV
	Accuracy	± 5mV
Depth	Range	± 0 – 60.00 m
	Resolution	1cm
	Accuracy	± 0.2% FS
Temperature	Range	-5˚C – +50˚C (23˚F – 122˚F)
	Resolution	0.01˚ C/F
	Accuracy	± 0.1˚ C
Turbidity	Range	0 – 3000 NTU
	Resolution	2 Auto-range scales: 0.0 - 99.9 NTU, 100 - 3000 NTU
	Accuracy	± 5% of auto-ranged scale
CDOM/FDOM	Range	0 – 20,000 µg/L (ppb) (Quinine Sulphate)
	Resolution	2 Auto-range scales: 0.0 – 9,999.9 µg/L, 10,000 – 20,000 µg/L
	Accuracy	± 10% of reading

Table C.3: Location of the selected monitoring points in the water catchment areas of the Schönmünz and the Langenbach (Coordinates in GK 3 reference frame, HW: "Hochwert", northing; RW: "Rechtswert", easting).

	Descriptor	HW	RW	Elevation
Schönmünz	D801	5381582	3443868	915 m a.s.l.
	D812	5381568	3445913	738 m a.s.l.
	WA	5381617	3444038	910 m a.s.l.
	SF	5381472	3445740	735 m a.s.l.
	S01	5382675	3449799	573 m a.s.l.
Langenbach	SE	5384875	3442058	1015 m a.s.l.
	QLB	5384114	3447108	760 m a.s.l.
	KB	5384124	3444107	740 m a.s.l.
	LBU	5383574	3448526	600 m a.s.l.

D801   The measuring station at highest altitude is located at spring D801. This spring discharges into the Wildsee. A multi-parameter probe of the type AP-5000 was installed. It measures air pressure, water level, temperature, pH-value, redox potential, dissolved oxygen, electrical conductivity, turbidity and CDOM. The position after installation on 19 April 2018 is shown in Figure C.5.

D812   A probe of type OTT-CTD was installed at spring D812 (Figure C.6). Due to the shallow water depth directly at the springs' outlet, the probe was installed about four meters downstream where there was sufficient water depth. Water temperatures are especially affected by this as they change very fast and over a short distance in water flowing openly. This has to be taken into account during the data evaluation.

C.3.2 *Langenbach*

The two springs QLB and SE, and two locations in the Langenbach stream (KB, QLB) were selected.

LBU   This is the measuring station at lowest altitude in the Langenbach. A multi-parameter probe of the type AP-5000 was installed. It measures air pressure, water level, temperature, pH-value, redox potential, dissolved oxygen, electrical conductivity, turbidity and CDOM. The position is shown in Figure C.7. The location is comparable to S01 in the Schönmünz valley.

KB   A probe of the type OTT-CTD was installed at this location in the surface stream (Figure C.8). The location in the stream is comparable to location SF in the Schönmünz valley.

QLB   A probe of the type OTT-CTD was installed in this spring (Figure C.9). It records water level, specific electrical conductivity and water temperature. Location of the spring is comparable to spring D812 in the Schönmünz valley.

SE   A multi-parameter probe of the type AP-5000 was installed inside the the spring catchment (Figure C.10). It measures air pressure, water level, temperature, pH-value, redox potential, dissolved oxygen, electrical conductivity, turbidity and CDOM. Location of the spring is comparable to spring D801 in the Schönmünz valley.

Figure C.2: Position after first installation of the probe on 4 April 2018 in the Schönmünz near the youth campground Hahnenbrunnenwiese (S01).

Figure C.3: Position of the probe installed in the Schönmünz stream at location SF.

Figure C.4: Position of the probe installed at the starting point of the Schönmünz stream at the outlet of the Wildsee (WA).
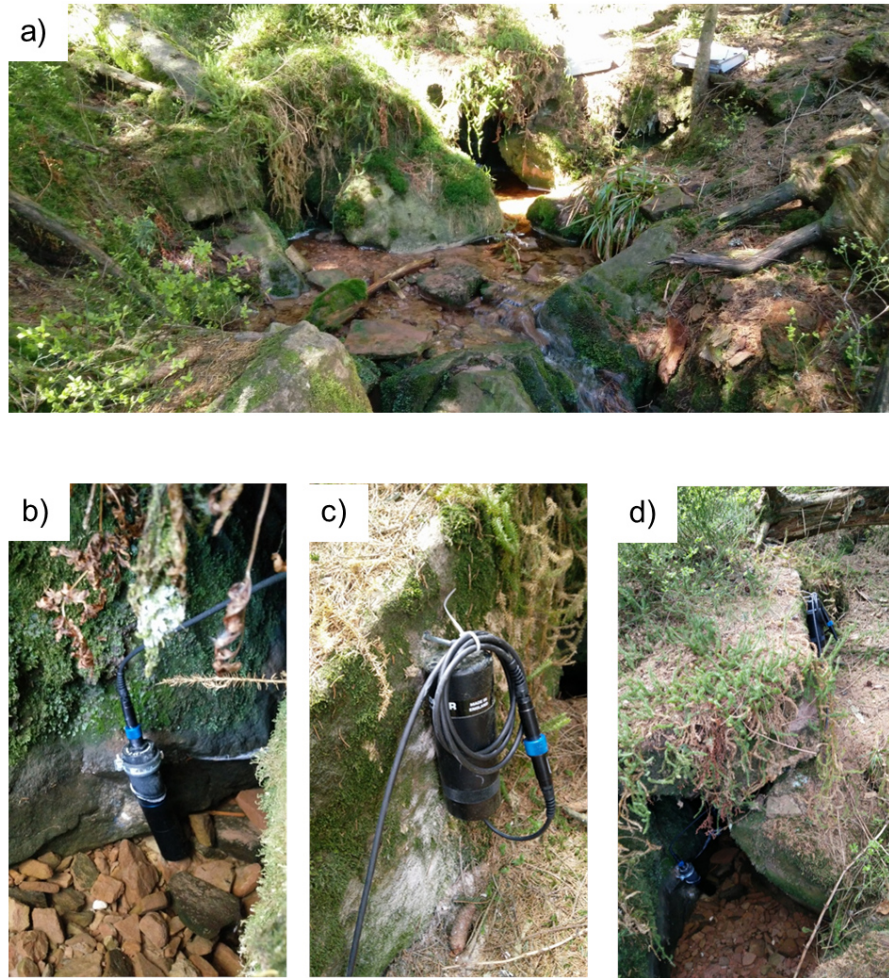
Figure C.5: Position of the probe installed at spring D801; a) Overview of the spring; b) Position of the probe; c) Position of the logger; d) Position of probe and logger.

Figure C.6: Position of the probe installed at spring D812

Figure C.7: Position of the probe installed in the Langenbach (LBU)

Figure C.8: Position of the probe installed in the Kesselbach (KB), which drains into the Langenbach (KB).

Figure C.9: Position of the probe installed at spring QLB.

Figure C.10: Position of the probe installed inside the spring catchment at the Seibleseckle (SE).

D801
sandstone
group

HW: 5381581, RW: 3443862, 915 m a.s.l.

D802
sandstone
group
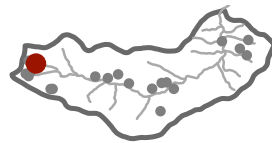
HW: 5381967, RW: 3444088, 911 m a.s.l.

D803

west granite
group
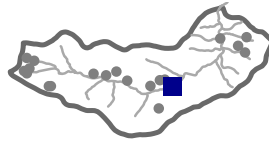
HW: 5381189, RW: 3448328, 678 m a.s.l.

D804

west granite
group
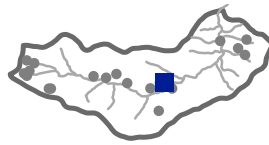
HW: 5381388, RW: 3448105, 695 m a.s.l.

D807

west granite
group
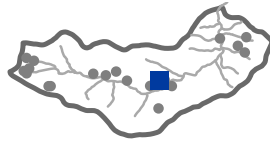
HW: 5381369, RW: 3447952, 728 m a.s.l.

D808

west granite
group

HW: 5381194, RW: 3447661, 725 m a.s.l.

D809

west granite
group
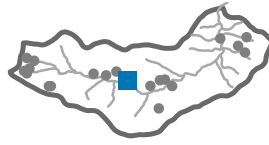
HW: 5381355, RW: 3446948, 740 m a.s.l.

D810

sandstone
group
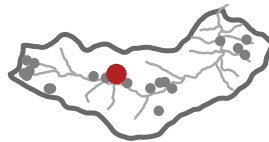
HW: 5381635, RW: 3446615, 789 m a.s.l.

D811

west granite
group

HW: 5381520, RW: 3446299, 734 m a.s.l.

D812

west granite
group

HW: 5381568, RW: 3445913, 738 m a.s.l.

D813

east granite
group
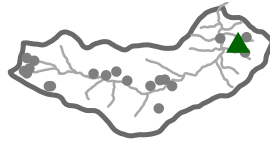
HW: 5382427, RW: 3450357, 695 m a.s.l.

D814

east granite
group
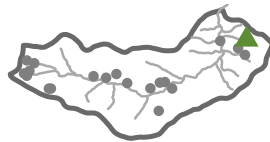
HW: 5382692, RW: 3450617, 688 m a.s.l.

D816
sandstone
group
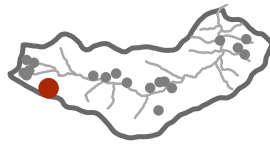
HW: 5381186, RW: 3444539, 898 m a.s.l.

D818
sandstone
group
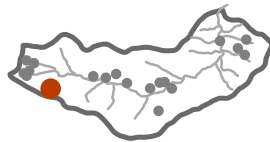
HW: 5381187, RW: 3444602, 896 m a.s.l.

D820

sandstone
group
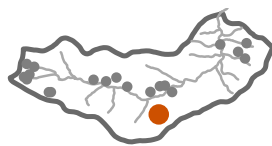
HW: 5380502, RW: 3447918, 829 m a.s.l.

D821

east granite
group
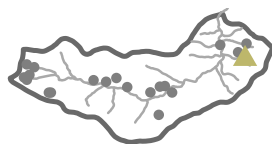
HW: 5382221, RW: 3450571, 716 m a.s.l.

Q01

sandstone
group
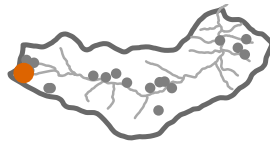
HW: 5381653, RW: 3443774, 958 m a.s.l.

Q02

sandstone
group
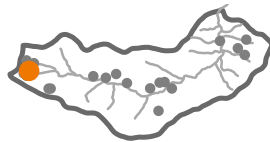
HW: 5381731, RW: 3443941, 920 m a.s.l.

Q03
sandstone
group
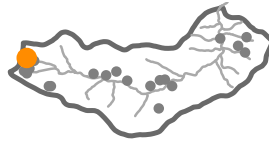
HW: 5382053, RW: 3443859, 955 m a.s.l.

S01
surface stream
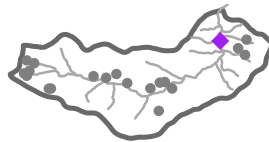
HW: 5382651, RW: 3449808, 573 m a.s.l.

ACKNOWLEDGMENTS

Der Mensch empfängt unendlich mehr als er gibt.
Dankbarkeit macht das Leben erst reich.

Dietrich Bonhoeffer

This work would not have been possible without the help of the numerous people involved at different times and in different ways over the past years. When I started the endeavor of writing this thesis some four and a half years ago, I had no idea of where it might lead me. But now I can look back with a thankful heart, filled with plenty experiences and memories of people that I will surely remember. The time, for sure, had its ups and downs. It was not always as easy as I had anticipated, but I learned a lot about the scientific subject at hand and not least about myself. And because I could not have done all this by myself alone, I want to specifically acknowledge the help of some people:

First, I want to thank Prof. Dr. Nico Goldscheider for all the scientific discussions, his ideas, comments, and suggestions, supervision and support during my work on this thesis, and for entrusting different projects to me and for giving me the opportunity to work on this thesis.

I thank Prof. Dr. Lucas Menzel for his willingness to be on the committee and additionally for being the second reviewer.

I thank the other members of the committee: Prof. Zehe, Prof. Eiff, and Prof. Neumann for their time and interest in this work.

I thank Prof. Tim Bechtel fruitful discussions and for instructing me in the ways of SP-measurements.

I thank Nadine Göppert for her valuable contribution to my work, for her feedback on the numerous reports I had to write, for scientific discussions and instructions regarding field and laboratory work.

I thank Frank Schilling for his support and encouragement when I needed them the most.

I thank Mario Schirmer for his openness, uncomplicated personality and that I was welcome to stay with his group at the Eawag for three months during an ongoing pandemic. This allowed me to finish writing my thesis in a very pleasant and stimulating environment. I would also like to thank the members of his working group for helpful feedback and discussions and their welcoming attitude.

I further thank the laboratory team, consisting of Daniela Blank, Chris Buschhaus, and Christine Roske-Stegemann for their help with all kinds of laboratory work and their dedication to analyze the numerous water samples brought back from the field. For the support

I thank all colleagues from my working group, past and present: M. Augenstein, F. Grimmeisen, S. Frank, A. Ender, Z. Chen, J. Xanke, N. Fahrmeier, M. Ohmer, A. Wunsch, D. Richter, Diep.

I thank all colleagues who spent some of their time for discussions during lunch breaks or the Thursday coffee break: H. Steger, T. Mutschler, T. Kling, S. Hale, L. Makni, L. Bienstein, S. Schüppler, S. Wilke, C. Tissen, C. Butscher, P. Fleuchaus, D. Schweizer, G. Rau, I. Stein.

And of course I thank all those who I have forgotten to mention in this list. Sorry!

The support by the Graduate School for Climate and Environment (GRACE) is acknowledged, with special thanks to A. Schenk and E. Engelmann. I thank T. Liesch for being part of my personal steering group, organized by GRACE.

Furthermore, I acknowledge the help I received from deepl.com during the writing process.

A special thanks goes to Simon Breuer, with whom I spent some time while doing the masters degree at university and who became a close friend during the time we spent at the same institute both doing our doctorate. Thank you for all the support, the coffee, and the encouragement you provided.

My last and biggest thank goes to my family, my parents and my two brothers, for everything!

That's all for now. And if you have been, thanks for reading!

DECLARATION OF AUTHORSHIP

Peer reviewed publications:

Citation: MERK M, GOEPPERT N, GOLDSCHEIDER N (2021) *Deep desiccation of soils observed by long-term high-resolution measurements on a large inclined lysimeter*, Hydrol. Earth Syst. Sci., 25, 3519–3538.
Declaration of authorship: MM together with NG and NG developed the concept of the study, formulated research questions and discussed methods of data evaluation. MM supervised the fieldwork, which was mainly done by students. Formal analysis of the data and visualization of the results was done by MM and discussed by all authors. The structure of the study was discussed by all authors and the manuscript written by MM. The manuscript was reviewed, edited and finally approved by all authors.
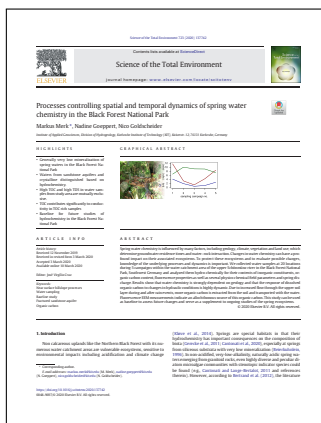
Citation: MERK M, GOEPPERT N, GOLDSCHEIDER N (2020) *Processes Controlling Spatial and Temporal Dynamics of Spring Water Chemistry in the Black Forest National Park*, Science of the Total Environment, 723, Article: 137742
Declaration of authorship: MM together with NG and NG developed the concept of the study, formulated research questions and discussed methods of data evaluation. MM did fieldwork (supported by students), formal analysis of the data and visualization of the results. Work was supervised by NG and NG. The structure of the study was discussed by all authors and the manuscript written by MM. The manuscript was reviewed, edited and finally approved by all authors.

Citation: MERK M, GOEPPERT N, GOLDSCHEIDER N (2020) *Physicochemical and major ion data for springs in the Black Forest National Park, Germany*, Data in Brief, 30C, Article: 105645
Declaration of authorship: MM did fieldwork, formal analysis of the data, visualization of the results and wrote the manuscript. The manuscript was reviewed, edited and finally approved by all authors.